UNCLASSIFIED

AD NUMBER		
AD504391		
CLASSIFICATION CHANGES		
TO:	**UNCLASSIFIED**	
FROM:	**CONFIDENTIAL**	
LIMITATION CHANGES		
TO:		
Approved for public release; distribution is unlimited.		
FROM:		
Distribution authorized to U.S. Gov't. agencies and their contractors; Critical Technology; MAY 1968. Other requests shall be referred to Air Force Armament Laboratory, Attn: ATWT, Eglin AFB, FL 32542. This document contains export-controlled technical data.		
AUTHORITY		
USADTC ltr, 3 Jul 1979; USADTC ltr, 3 Jul 1979		

THIS PAGE IS UNCLASSIFIED

SECURITY

MARKING

The classified or limited status of this report applies to each page, unless otherwise marked.

Separate page printouts MUST be marked accordingly.

AFATL-TR-68-60

AD504391

STUDY AND APPLICATION OF
MACH WAVE TECHNIQUES (U)

N. A. Louie
A. L. Mottet, Jr.
I. Lieberman
Shock Hydrodynamics, Inc.

TECHNICAL REPORT AFATL-TR-68-60

MAY 1968

In addition to security requirements which must be met, this document is subject to special export controls and each transmittal to foreign governments or foreign nationals may be made only with prior approval of the Air Force Armament Laboratory (ATWT), Eglin AFB, Florida 32542.

SEP 26 1969

AIR FORCE ARMAMENT LABORATORY

AIR FORCE SYSTEMS COMMAND • UNITED STATES AIR FORCE

EGLIN AIR FORCE BASE, FLORIDA

CONFIDENTIAL

STUDY AND APPLICATION OF
MACH WAVE TECHNIQUES (U)

N. A. Louie
A. L. Mottet, Jr.
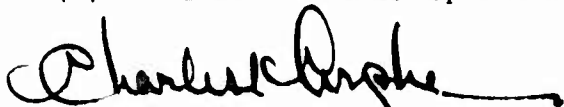I. Lieberman, et al

CONFIDENTIAL

FOREWORD

(U) This report summarizes the work performed on the "Study and Application of Mach Wave Techniques" under Air Force Contract AF08(635)-5999, between June 1966 and December 1967. This program was administered by the Air Force Armament Laboratory (ATWT), Eglin AFB, Florida 32542. The program was originally monitored by Mr. R. Lenton Hill and subsequently by Mr. Walter Dittrich (ATWT) of the Air Force Armament Laboratory. The Contractor's Report Number is SHI C-1016.

(U) The program was carried out by members of the scientific staff of Shock Hydrodynamics, Inc., 15010 Ventura Boulevard, Sherman Oaks, California 91403. The work was performed under the general technical supervision of Dr. Louis Zernow. The theoretical studies were carried out by N. A. Louie. The experimental effort was carried out by N. A. Louie, A. L. Mottet, Jr., I. Lieberman and R. R. Randall.

(U) This report contains no classified information extracted from other classified documents.

(U) Information in this report is embargoed under the Department of State International Traffic In Arms Regulations. This report may be released to foreign governments by departments or agencies of the U.S. Government subject to approval of the Air Force Armament Laboratory (ATWT), Eglin AFB, Florida 32542, or higher authority within the Department of the Air Force. Private individuals or firms require a Department of State export license.

(U) This technical report has been reviewed and is approved.

CHARLES K. ARPKE, Lt. Colonel, USAF
Acting Chief, Weapons Division

UNCLASSIFIED ABSTRACT

(U)   A theoretical and experimental study of convergent wave initiation and detonation techniques has been carried out. This included analytical and experimental studies of wave shapes and Mach discs in cylindrical explosive charges overdriven by concentric external faster explosives. The techniques were also applied to shaped charge systems. The results indicate that it is possible to overdrive TNT loaded shaped charges so that they perform as well as Composition B loaded charges. A depressurization disruption mechanism has been postulated to explain the jet breakup seen in flash X-ray and penetration observations, made when similar overdriving methods were applied to more energetic explosive systems like Composition B overdriven by PBX-9404.

(The reverse of this page is blank)

TABLE OF CONTENTS

LIST OF FIGURES

LIST OF FIGURES (Cont'd.)

LIST OF FIGURES (Cont'd.)

SECTION I

INTRODUCTION

(U)   The purpose of this program was to carry out theoretical and experimental studies of convergent wave phenomena which can lead to Mach waves, and to apply the results to shaped charge systems. The program was divided into three parts.

(U)   The first portion of the program involved a theoretical study of convergent waves accompanied by an experimental program of wave shape observations related to the theoretical work.

(U)   The second portion of the program involved a screening study of the effects of convergent waves when applied to shaped charge systems. The screening study was carried out with normal precision metal parts as used in the fabrication of production shaped charges.

(U)   The third portion of the program was a specific experimental application of the convergent wave techniques to precision metal parts and precision assemblies of shaped charges.

(U)   The three portions of the study are discussed separately in the following sections II, III and IV.

(U)   Convergent wave systems arising from external explosive drivers can be expected to contribute in at least two ways to the modified behavior of the interior receptor explosives.

> (1) The additional increased pressures generated by the convergent wave system can be expected to result in the initiation and detonation of explosive systems whose diameters are sub-critical, so that under the stimulus of normal end initiation, they would not be capable of propagating a detonation without having it fade out.
>
> (2) The formation of a Mach disc, in the central region where the convergent waves interact very strongly, generates still higher pressures, which can also be expected to affect increases in the performance of the metal systems with which they interact.

(U)   In the present study, the applications to sub-critical or marginally critical systems were primarily for the purpose of illustrating the beneficial effects that can arise. Thus, TNT was used under conditions which were either sub-critical or marginally critical. While the intrinsic interest is not in TNT loaded explosives, the beneficial effects could be dramatically

1

illustrated. Furthermore, it was expected that the principles involved could logically be extended to other explosive systems of interest.

(U) The shaped charge system represents only one specific potential application of the beneficial effects of convergent wave systems generated by external explosive overdrivers.

2

SECTION II

THEORETICAL STUDY OF CONVERGENT WAVES

1. INTRODUCTION

(U)   The theory of Mach reflection in planar geometry has been developed so that it is capable of analytic solution only for very special and simplified cases. A review of the hydrodynamic theory including comparisons with experiments, for gases, is given in reference 1. Much less theory appears in the open literature for the case of conically convergent shocks, i.e., Mach reflection in cylindrical geometry. However, enough work has been done to point out significant differences between Mach waves in planar and cylindrical geometry. In planar geometry there is a distinct critical collision angle for two shocks at which the normal reflection cannot occur and the Mach reflection results. However, in cylindrical geometry, it has been shown in reference 2, that irregular reflection must always occur in conically convergent flow of a material with a "normal" equation of state. A "normal" equation of state can be defined as one in which the first and second partial derivatives, of the pressure with respect to the density, in isentropic hydrodynamic flow, are positive quantities. Another important aspect of convergent flow in cylindrical geometry is that the strength of a shock wave increases as the wave converges towards the axis. Generally, a variation of shock pressure inversely with some power of the radius can be fitted to the experimental data reported in the literature. Some modification of such a relation is necessary very close to the axis, since for a real fluid, the viscosity and thermal effects cause the pressure to remain finite, even on the axis, where the radial distance is zero.

(U)   These factors, led to consideration of approximate methods for treating the case of a conically converging shock without the necessity of obtaining direct solutions to the hydrodynamic equations of fluid flow which would require expensive machine computations which were not possible within the present program scope.

(U)   It was hoped that such a simplified analysis could provide reasonable guidance in making theoretical predictions of the phenomena in much the way that Huygens principle provides reasonably accurate predictions of the propagation properties of optical rays without the necessity for solving Maxwell's Equations.

(U)   Accordingly, a theory has been developed which provides a model for the steady state propagation of a Mach wave formed by converging conical shocks. The model has been extended to include converging conical shocks in both inert and explosive material.

3

a.   Derivation of Mach Parameters in Inert Cylinders

(U)   In the model, to be described, the following assumptions are made:

(1) The pressure (P) of a conically convergent shock wave is an inverse function of some power (K) of the radius, i.e.,

$$P = P_O \left(\frac{r}{r_O}\right)^{-K} = P_O \left(\frac{r_O}{r}\right)^{K} \tag{1}$$

where the subscript zero denotes initial values. K will be called the pressure convergence magnification exponent.

(2) Equation (1) applies only at points where the wave is converging and for any particular radius, the differential increase in pressure is proportional to the differential decrease in radius, i.e.,

$$dP = - \left| F(r) \right| \, dr \tag{2}$$

where $F(r)$ is the appropriate function of the radius. Thus, no pressure increase would be obtained from point to point along a portion of the wave front that was moving in a direction parallel to the axis.

(3) All geometrical factors are taken into account by the first two assumptions, and the usual (planar) Rankine-Hugoniot discontinuity relations are assumed to be valid at any point of the shock front. A derivation of the discontinuity relations is given in reference 3 which shows the geometrical invariance of the discontinuity relations. Under the assumptions, listed above, as a differential portion of the conically convergent shock front moves inward, its velocity vector is turned in a direction away from the axis, resulting eventually, in a wave front moving in a direction parallel to the axis. The details of this turning action are derived below. Reference is made to Figure 1.

(U)   Compare the movement of two points on the wave front initially at B and C in Figure 1. Let the point at B have a wave velocity D. Now because point C is closer to the axis, by an amound dr, C will have a wave velocity of $D + dD$. The term dD is a small differential of velocity and is a function of r. In a small increment of time, dt, point C on the wave front will travel a distance dD dt further than B. This

4
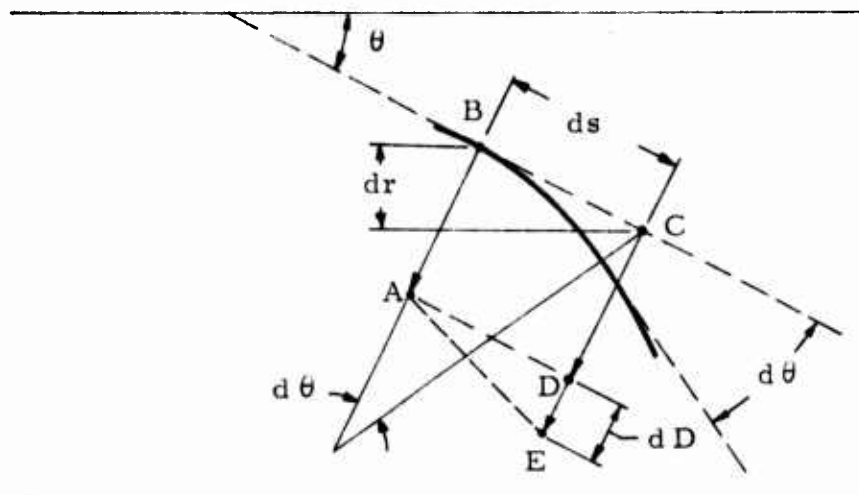
As the converging wave approaches the axis, its pressure increases in accordance with Equation (1) causing a corresponding velocity increase which results in turning of the wave as shown.

Figure 1. The Geometrical Relations for a Converging Wave, Showing the Differential Turning as it Approaches the Axis.

results in turning the portion of the wave front between them by the small differential angle dθ. If ds is the initial small differential distance along the wave front between B and C, then from the existing geometrical relations

$$\tan (d\theta) \cong d\theta = \frac{dD\, dt}{ds} \tag{3}$$

From Figure 1, one also finds that

$$\frac{dr}{ds} = \sin\theta \tag{4}$$

Likewise,

$$\frac{dr}{dt} = D \cos\theta \tag{5}$$

5

Hence, from Eqns. (3), (4), and (5) we obtain

$$\frac{d\theta}{\tan \theta} = \frac{dD}{D}$$ (6)

On integrating Eqn. (6), we obtain

$$\frac{D}{D_O} = \frac{\sin \theta}{\sin \theta_O}$$ (7)

where the subscript zeros again indicate initial values.

(U)   The variation of the shock velocity (D) with the radius (r) can be derived as follows.

(U)   The Rankine-Hugoniot relation for conservation of momentum across a shock discontinuity is,

$$P = \rho_O D u$$ (8)

where

    u   is the mass velocity behind the wave front

    ρ_O is the density of the material ahead of the
            wave front, where the pressure is negligible
            with respect to P.

Many solids and liquids under strong shock compression behave in accordance with the relationship

$$u = AD + B$$ (9)

where A and B are constants. In addition, A is positive and B is negative. Equations (1), (8), and (9) when combined, yield the relationship

$$P_O \left(\frac{r_O}{r}\right)^K = \rho_O D (AD + B)$$ (10)

Solving for the shock velocity D, we obtain the relationship

$$D = \left(\left[\alpha^2 + \beta \left(\frac{r_O}{r}\right)^K\right]^{1/2} - \alpha\right)$$ (11)

where

$$\alpha = \frac{B}{2A} \qquad \text{and,} \qquad (12)$$

$$\beta = \frac{P_O}{\rho_O A} \qquad (13)$$

Substituting in Eqn. (7) we obtain the relationship

$$\frac{\sin \theta}{\sin \theta_O} = \frac{([\alpha^2 + \beta (\frac{r_O}{r})^K]^{1/2} - \alpha)}{([\alpha^2 + \beta]^{1/2} - \alpha)} \qquad (14)$$

A "Mach" wave is formed when θ becomes equal to 90°. This occurs at a radius given by

$$([\alpha^2 + \beta (\frac{r_O}{r})^K]^{1/2} - \alpha) = \frac{([\alpha^2 + \beta]^{1/2} - \alpha)}{\sin \theta_O} \qquad (15)$$

The above equation shows that a "Mach" wave must occur, at $r > 0$, for any convergent shock inclined with respect to the axis at an angle greater than zero, in conformance with the conclusions in reference 2.

(U)   The axial velocity of the Mach region is given by

$$D = \frac{D_O}{\sin \theta_O} \qquad (16)$$

Thus, if the Hugoniot of the material is known in a form as shown in Eqn. (9), then substitution into Eqn. (8) and evaluation of the "Mach" velocity by Eqn. (16) yields the dynamic pressure just behind the "Mach" front.

(U)   A cross section of a typical wave front for "Mach" formation, in the case of a converging conical shock is shown in Figure 2.

(U)   Since the model is based on a continuous turning of the wave front, the transition to the "Mach" front is not abrupt in this model although the turn is evidently made in a comparatively short distance.

(U)   An important element of the theory with respect to its utilization is the specific value of the exponent K in Eqn. (1). There have been several studies on converging shocks in cylindrical geometry. However, most of the work has been in terms of an ideal gas with γ the ratio of

7
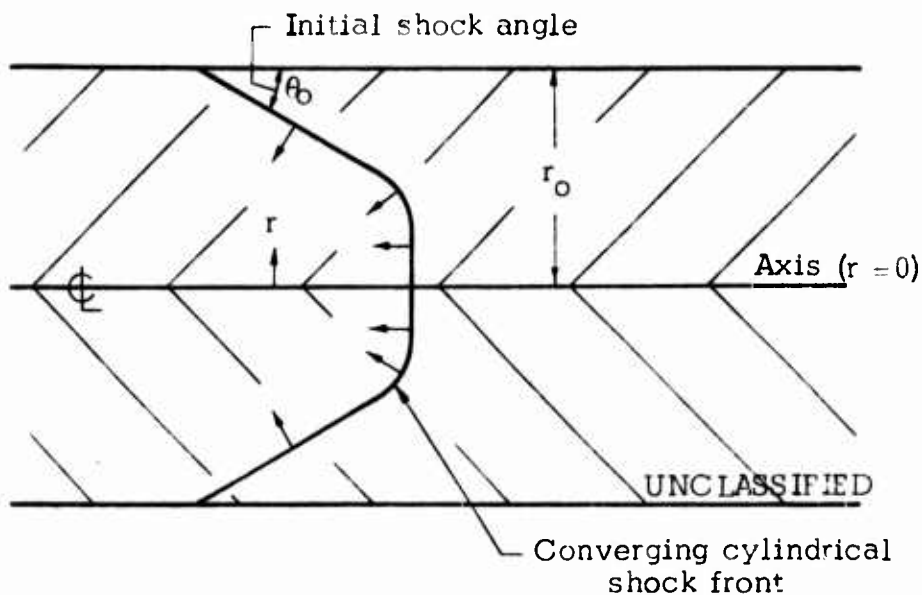
Figure 2. Cross Section of Wave Front

specific heats, ranging from approximately 1.4 (air) to a value of 3 (detonation products). The research reported in reference 5 indicated that for a γ of 1.4, K has a value of .4. For a γ of 1.4, reference 6 gives a K of .5. For a γ of 3, reference 7 gives a K equal to .47 at points close to the axis of the cylinder. It appears therefore that K is a slowly varying function of γ.

(U)   The solid analog to the polytropic gas equation of state is given by the Murnaghan equation of state

$$P = A (\rho^\gamma - \rho_o^\gamma) \tag{17}$$

where

A and γ are constants.

(U)   K can be calculated from the known Hugoniot of a material and is generally of the order of .3 to .5 in magnitude. If on the basis of this evidence, it is assumed that K is indeed a slowly varying function of γ even in the extension to the case of solids or liquids, then as a first approximation, a value of K = .5 seems to be reasonable.

      b. Derivation of Mach Parameters in Cylinders of Explosive Material

8

(U)   Much of the analysis given above for inert material, also applies to the treatment of the case for explosive (reactive) materials. The principle difference is that, for the case of an explosive, the properties of the detonation wave must be considered, as differentiated from the ordinary shock wave. When an axially converging shock wave enters a cylinder having an explosive interior medium rather than an inert one, there are two different reactions that can occur, depending upon the shock strength and the explosive sensitivity. These two different reactions are as follows:

(1)   The explosive may detonate immediately upon the arrival of a sufficiently strong shock at the outer interface.

(2)   The explosive may sustain a weaker conical shock converging inwards until the shock strength increases sufficiently to bring about the initiation of a detonation wave.

(U)   In the first case, the initial wave, inclined at an angle of θ_0, has a pressure equal to P_{cj}, and a wave velocity, D_{cj}, where the subscript cj indicates the Chapman-Jouguet values associated with the particular explosive. As the wave propagates inward, the intensity increases and the equations describing an overdriven detonation wave, as derived by Skidmore and Hart[8], must now be used in place of Eqn. (9), i.e.,

$$\frac{D_{cj}}{D} = [\frac{P_{cj}}{P} (2-\frac{P_{cj}}{P})]^{1/2} \tag{18}$$

This equation, together with Eqn. (1) gives the following relationship for the overdriven wave,

$$\frac{\sin \theta}{\sin \theta_0} = \frac{1}{[\delta_{cj} (2 - \delta_{cj})]^{1/2}} \tag{19}$$

where

$$\delta_{cj} = (\frac{r}{r_0})^K \tag{20}$$

The equation giving the radius of the Mach disc is,

$$\delta_{cj} = 1 - (1-\sin^2\theta_0)^{1/2} = 1 - \cos \theta_0 \tag{21}$$

9

Equation (21) suggests that the radius of the Mach disc in a cylindrical explosive core is independent of the properties of the explosive, for a given convergence angle, θ_0. Constraints on the incident convergence angle may exist however, which are related to the explosive's dynamic physical properties such as the shock Hugoniot.

(U)   The extension of this first case under strong shock conditions, can be made to the second case in which the shock is initially too weak to initiate the explosive, but grows in strength so that the detonation is initiated after the converging conical wave has moved inward some distance from the outer interface. Once criteria are provided for determining the conditions for a shift from unreactive shock propagation to detonation, the previous strong shock analysis can be used to obtain the conditions for the transition to Mach disc formation.

(U)   The criteria for the shift from shock wave to detonation wave are not simple, since this is a complicated process for which the threshold pressure levels are strongly dependent on the geometry. For example, it has been reported in the literature that shocks of relatively low intensity (appreciably lower than the Chapman-Jouguet pressure) will initiate a solid explosive if the geometry is favorable and a sufficient build up time is available. On the other hand, any time the shock strength becomes comparable to that of the appropriate von Neumann spike, there certainly would be a detonation wave present. Neither of these criteria seem applicable to the case of a conically convergent shock. The first appears inappropriate because the process is too slow and the second because partial chemical decomposition can occur even at low pressure levels. As soon as any decomposition occurs behind the shock, the effective Hugoniot of the material changes. The critical transition pressure should lie between the two above mentioned extremes. In the following calculations, the Chapman-Jouguet pressure will be used as the critical transition pressure since it is intermediate between the two extremes and is a convenient value to work with. No pretense is made that this criterion has been derived rigorously.

(U)   Under the conditions given, the shock Hugoniot of the unreacted explosive is used until the pressure reaches the Chapman-Jouguet value (P_{cj}). The corresponding shock velocity (D_{cj}) can be calculated from Eqns. (8) and (9). Then Eqns. (7) and (14) can be used to find the radius (r_{cj}) at which this occurs. From this point inward, the equations describing an overdriven detonation wave (Eqn. (18)) must be used and the result is the same as Eqn. (19) with the exception that now Eqn. (20) becomes:

$$\delta_{cj} = (\frac{r}{r_{cj}})^{K} \tag{22}$$

10

Since the Chapman-Jouguet point does not lie on the Hugoniot of the unreacted explosive, for the case of a critical transition pressure there will be a discontinuous increase in the slope of the wave front at r_{cj}. In the actual case the change in slope would be expected to be abrupt but not discontinuous.

c. Sample Calculations

(U)   In order to specifically illustrate the application of this theoretical model several sample calculations are carried out.

(1) Inert Inner Cylinder

(U)   A sample calculation for an inert inner cylinder, in this case copper, surrounded by an annulus of an explosive, Comp B, will be given first. The explosive is circumferentially initiated at one end, and the detonation wave propagates axially to the opposite end. The explosive parameters are,

> Initial density = 1.7 gm/cc
> Detonation velocity = 8.0 mm/μsec
> Chapman-Jouguet pressure = 292 kilobars

The copper parameters are,

> Initial density = 8.9 gm/cc
> Hugoniot equation: $D = 1.5u + 4.0$ mm/μsec
>
> where D is the shock velocity, and
>   u is the particle velocity.

(U)   To obtain the inputs for Eqn. (15), it is necessary to calculate θ_o. The method given in Appendix A, which is applicable to planar geometry, can be used to good approximation for the cylindrical case, since only the initial angle is desired. The results of the calculation are as follows:

> γ for the detonation products is taken to be 3
> Induced peak pressure in copper - 230 kilobars
> Initial shock velocity - 4.8 mm/μsec.

Thus, following the procedure described in Appendix A we obtain $\theta_o = 37^o$.

(U)   From the sample calculation shown above, we obtain the following:

11

$$A = .667, \quad B = -2.667, \text{ then}$$

$$\alpha = -2, \quad \alpha^2 = 4, \quad \beta = 3.88$$

let
$$\delta = (\frac{r_O}{r})^K$$

then from Eqn. (15),

$$\delta = \frac{1}{\beta} \{ [\; \frac{(\alpha^2 + \beta)^{1/2} - \alpha}{\sin \theta_O} + \alpha]^2 - \alpha^2 \} \tag{23}$$

giving,

$$\delta = 1.91 = (\frac{r_O}{r})^K \tag{24}$$

$$\therefore \qquad \frac{r_O}{r} = (1.91)^{1/K} \tag{25}$$

and
$$\ln (\frac{r_O}{r}) = \frac{1}{K} \ln (1.91) \tag{26}$$

(U)   A graph of $(\frac{r_O}{r})$ as a function of K is given in Figure 3. If the value of K is taken as .5 then the expected Mach disc diameter would be .274 times the diameter of the copper rod. Likewise an experimental determination of $(\frac{r_O}{r})$ provides an estimate of the effective value for K.

(2) Explosive Inner Cylinder

(U)   The next sample calculation is given for the case of an explosive inner cylinder surrounded by an annulus of another explosive, where the outer explosive has a faster detonation velocity and initiates the inner explosive at the interface. This calculation is simpler than the previous case.

(U)   Let the detonation velocity of the inner explosive be D_I and the detonation velocity of the outer explosive be D_O. Then,

$$\theta_O = \text{Arc sin} (\frac{D_I}{D_O}) \tag{27}$$

If this relationship is substituted into Eqn. (21) then,

$$\delta_{cj} = (\frac{r_O}{r})^K = 1 - [1 - (\frac{D_I}{D_O})^2]^{1/2} \tag{28}$$

12
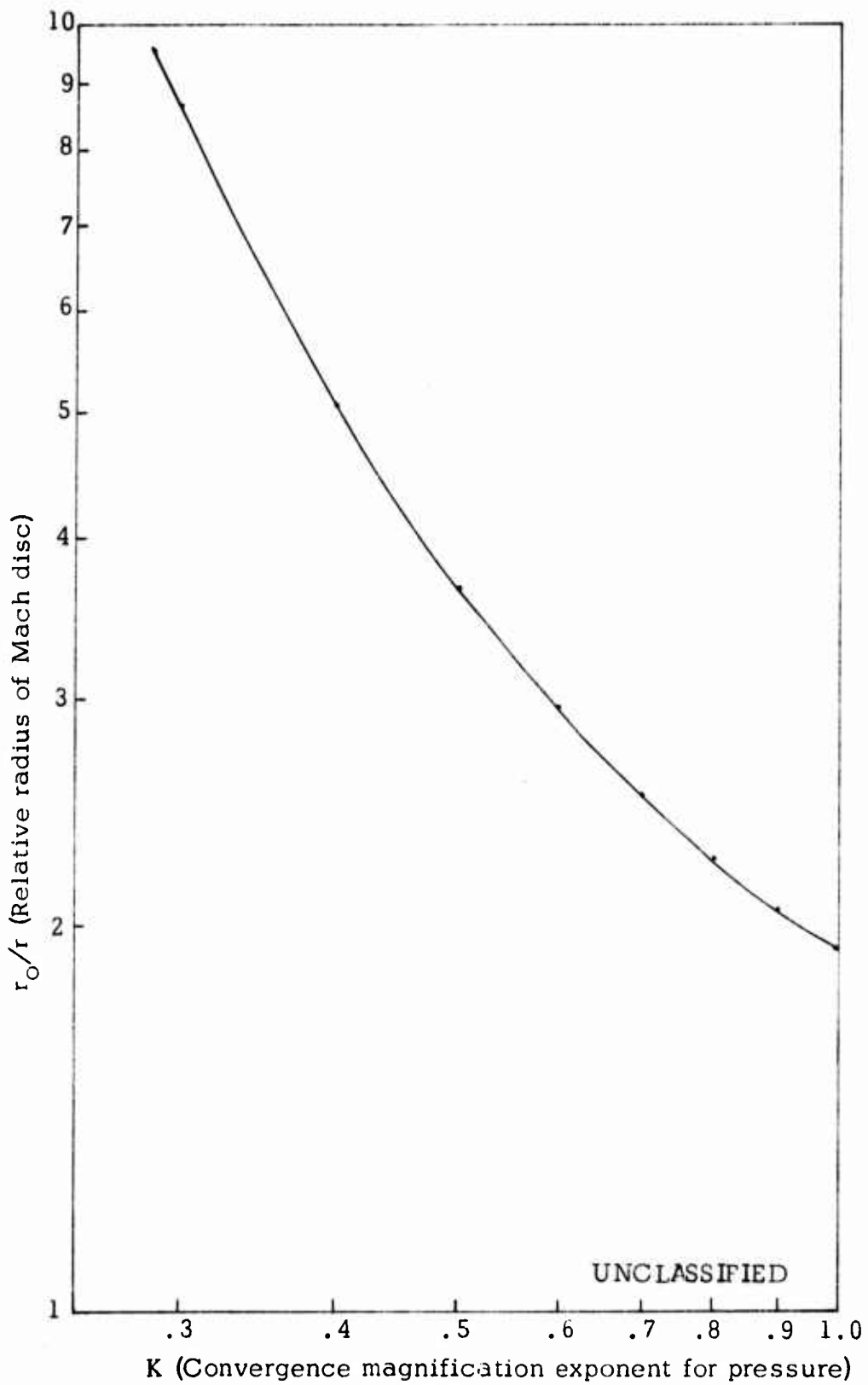
Figure 3. Graph Showing How the Relative Mach Disc Radius (r_O/r) Varies as a Function of K, the Convergence Magnification Exponent For Pressure.

13

Once the values for D_I and D_O are known, then a graph can be drawn for $(\frac{r_o}{r})$ vs K as in the previous section.

(U)   If the two explosives are Comp B and TNT and the respective detonation velocities are 8.0 mm/μsec and 7.0 mm/μsec , then

$$\theta_o = \text{Arc sin} \left(\frac{7.0}{8.0}\right) = 61^o \qquad (29)$$

Equation (28) then yields the result

$$\ln\left(\frac{r_o}{r}\right) = \frac{1}{K} \, \ln 1.94 \qquad (29a)$$

This equation is plotted in Figure 4.

(U)   If K is taken to be .5 the expected Mach disc diameter in TNT would be .270 times the diameter of the TNT charge.

d. Computation of the Distance Needed to Form a Mach Interaction

(U)   It is useful to be able to estimate the length of charge necessary to be certain of the formation of a Mach wave. From a theoretical standpoint, the solution is quite complex since, besides all the geometrical problems, the desired solution is a transient rather than a steady state phenomena. For this reason the analysis of Section 1. is not applicable. An approximate method for tracing the wave progression to Mach interaction has been devised which is based on a planar model. The results obtained from this method can be considered as representing an upper limit to the length of charge needed to generate a Mach interaction since, in cylindrical geometry, the wave velocity increases as the wave moves inward. This decreases the formation time of the Mach wave. A rough estimate for the cylindrical case suggests that a formation distance of about 2/3 the value derived, would be sufficient.

(U)   The case in which the charge is initiated on one end at the center of the inner explosive is shown , together with the wave progression, in Figure 5.

(U)   Let L be the length of charge needed to achieve Mach interaction, L_1 the distance the wave travels in the inner charge before it reaches the outer explosive, (A to B) , L_2 the distance from B to the point where the lateral waves intersect (B to C) and L_3 the distance from the interaction point to the line corresponding to the front of the detonation wave in the outer explosive (C to D). Let r_o be the distance from A to the outer explosive, D_I and D_O be the detonation velocities of the inner and outer

14
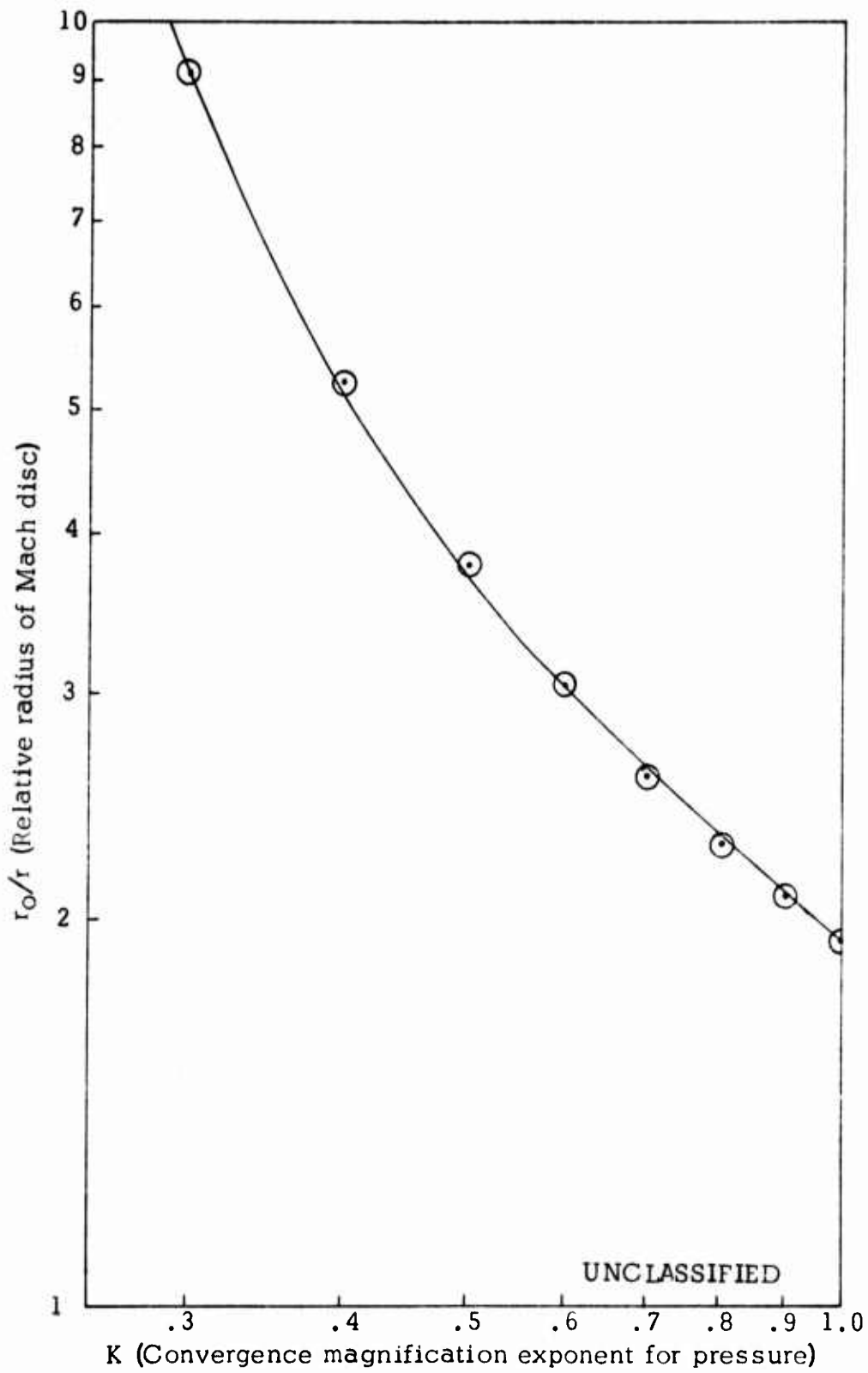
Figure 4. Graph of r_o/r versus K for TNT – Comp B Mach System
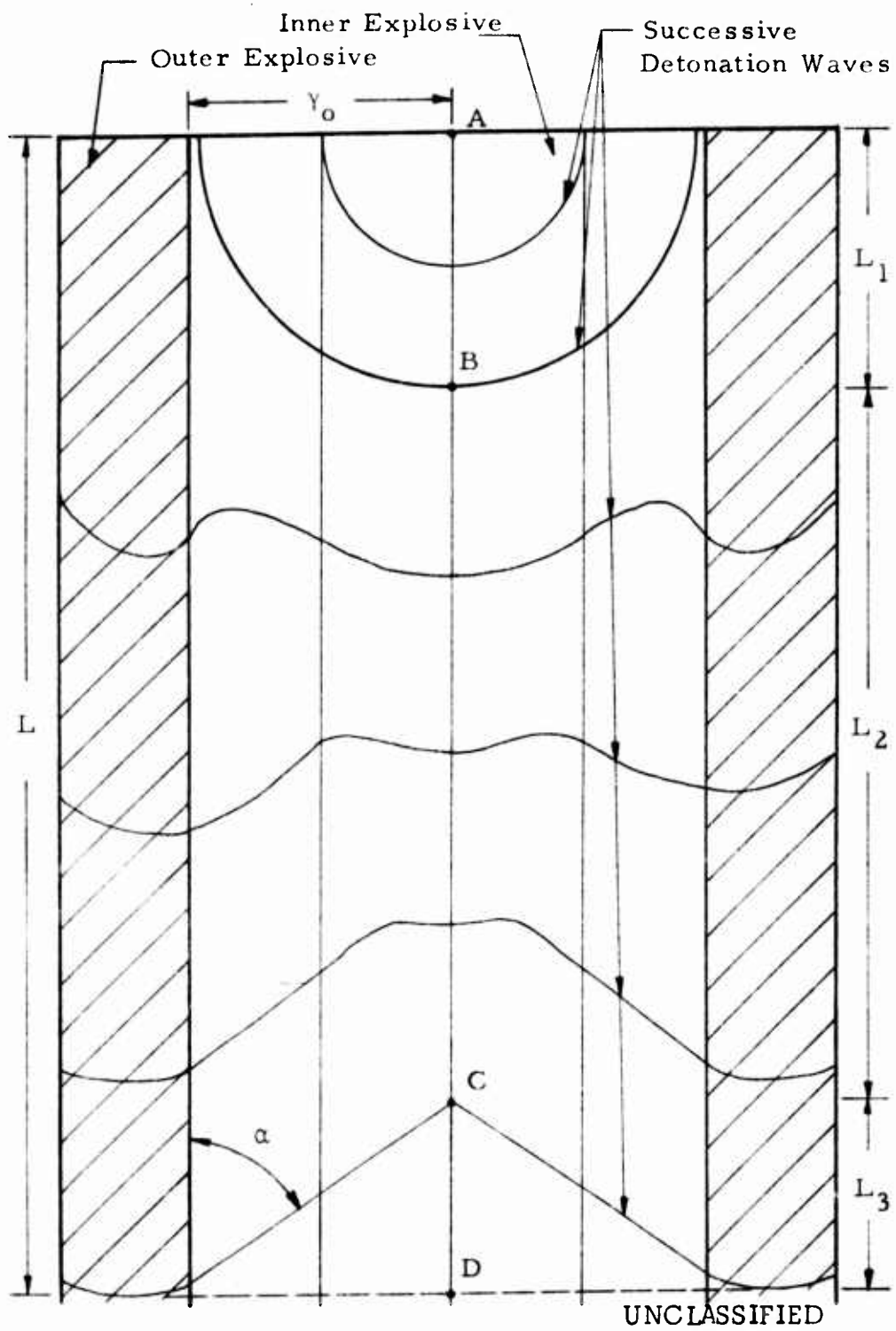
Figure 5.   Wave Progression to Mach Interaction
            Case A

16

explosives respectively. Then $L = L_1 + L_2 + L_3$. If α is the angle between the original interface in the explosive and the lateral detonation wave, then

$$\sin \alpha = \frac{D_I}{D_O} \qquad (30)$$

The following relations also hold

$$L_1 = r_O \qquad (31)$$

$$L_2 = L \left(\frac{D_I}{D_O}\right) \qquad (32)$$

$$L_3 = L - (L_1 + L_2) \qquad (33)$$

Equations (1) through (5) then give

$$L = r_O \left[\frac{R + \sqrt{1-R^2}}{R(1-R)}\right]^{1/2} \qquad (34)$$

where

$$R = \left(\frac{V_I}{V_O}\right) \qquad (35)$$

It is evident from Eqn. (6) that no Mach wave is possible for $R = 1$.

(U)   The length of charge needed to form a Mach wave, when the end of the charge is covered by a thickness (T) of explosive with the same detonation velocity as the outer explosive, can be calculated in a similar manner. The result is,

$$L = \frac{r_O}{R(1-R)} \left\{\sqrt{1-R^2} + \frac{R^2}{r_O}\left[(r_O^2 + T^2)^{1/2} - T\right]\right\}^{1/2} \qquad (36)$$

Note that L does not include T.

(U)   The length of charge needed to form a Mach wave, when the same end of both charges is detonated simultaneously is given by

$$L = r_O \frac{\sqrt{1-R^2}}{R(1-R)}^{1/2} \qquad (37)$$

(U)   This formula comes directly from Eqn. (36) for $T \to \infty$. Equations (34) and (37) are drawn in Figure 6 for L/r_O as a function of R. Equation (36) is also plotted in the same figure with T arbitrarily set equal to $3/4\, r_O$ for illustrative purposes. The graphs show that of the three initiation processes, case C gives the shortest charge length for Mach wave formation.

17
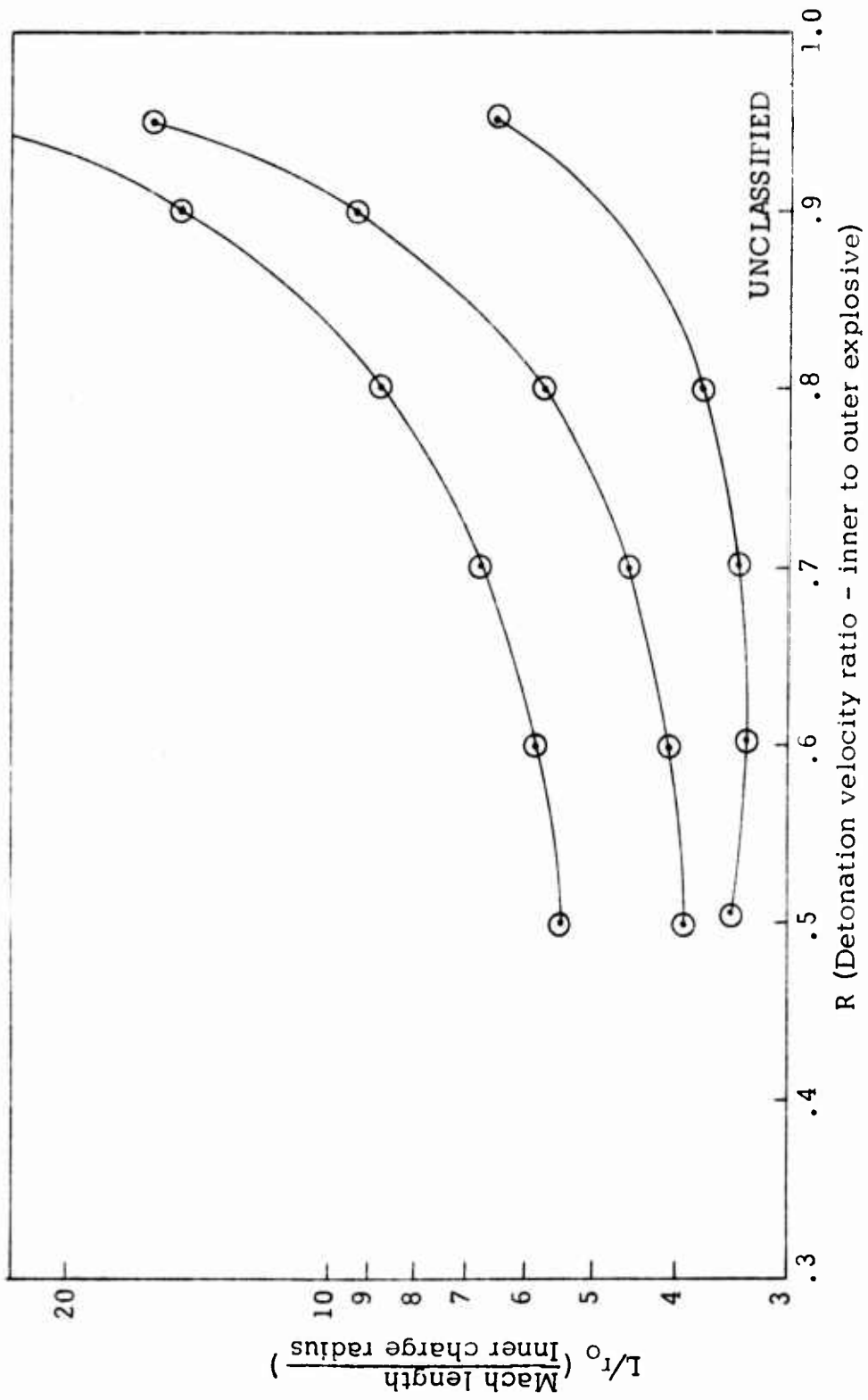
Figure 6.   Graph of Ratio of Charge Length for Forming Mach Wave to Inner Charge Radius (L/r_O) vs Detonation Velocity Ratio – Inner to Outer Explosive (R)

(U)   The derivative of Eqn. (37) can be taken and set equal to zero. This gives R for the minimum value of L/r_0. At this minimum, R = .618 and L/r_0 = 3.33.

2.   WAVE PROFILE EXPERIMENTS

    a. Introduction

(U)   The profile of the detonation wave in the cylindrical Mach wave experiments is an important experimental parameter. It's observation should provide information about the phenomena involved that is detailed enough to permit comparison with the theoretical estimates.

(U)   The measurement is complicated by the fact that the experimental geometry is cylindrical and that the test fixture is by its nature opaque to visible light. The experimental method used to obtain the wave profiles is fully described later in this section. Briefly the method consists of observing the emerging wave profile in a cylindrical body, as the wave arrives at the flat end opposite the initiation point, by recording the shock which passes from the end, through a thin sheet of aluminum and across an argon gap, causing the argon to flash. The shock pressures generated in these experiments are high enough to give a complete record over the area of interest. From these flash records, which are recorded by means of a high speed streak camera, the effects of varying experimental parameters can be examined.

        (1) Inner and Outer Explosive Material

(U)   In general the outer explosive must have a higher detonation velocity than the inner explosive for Mach wave formation to be possible. The assumption in all the measurements is that steady state has been reached sometime before the wave reaches the end of the charge. The amount by which the detonation velocity of the outer explosive exceeds that of the inner explosive determines how long it will take before the Mach wave forms. Similarly, the detonation pressure and velocity of the outer explosive is an important factor in determining the characteristics of the Mach wave which is formed.

        (2) Physical Dimensions of the Composite Charge

(U)   The physical dimensions of the composite charge, besides determining whether the Mach wave has formed and whether it is in a steady state, also determines the extent of the Mach wave region. The approximate theory as given in Section 1. predicts that this is a factor that scales linearly as the diameter. However, since the correlation between theory and experiment is one of the pieces of information to be determined, the relation between Mach wave diameter and charge diameter must be determined.

19

(3) Barrier Material and Thickness

(U)   In a practical application of the composite charge generation of Mach configurations, it is likely that the inner charge will be enclosed in a cylindrical sleeve and separated from the outer explosive by the thickness of this sleeve or barrier. A practical approach to the problems associated with the generation of Mach waves with composite charges will include an examination of the effects due to barrier both as it relates to the constituent material and its thickness. A representative selection of barrier materials was made that would cover the variation in material properties likely to be encountered in a practical situation. In addition, the selection was also diverse enough with respect to shock properties to provide some basis for understanding of the fundamental principles involved. The three materials chosen were: (1) phenolic tubing, representing a heterogeneous plastic material of moderate strength; (2) aluminum, a light metal of high relative shock impedance; and (3) steel, a heavy metal with moderate relative shock impedance with wide structural application.

b. Experimental Plan

(U)   An experimental plan was formulated to examine all of these parameters. The test matrix appears in Table I. TNT, as the inner explosive, represents the standard for which all the variations are examined since it is easily cast and X-rayed, it's properties are well known, and it has a moderately low detonation velocity. Therefore, many common explosives with higher detonation velocities, are available for use as an outer explosive. Composition B is an important military explosive which is also easily cast and X-rayed, however, only a limited number of standard explosives are available which have an appreciable higher detonation velocity. A limited number of experiments were planned with baratol. However, as it turned out, the properties of baratol are not as well documented. Furthermore, casting and X-ray examination of baratol charges was much more difficult than with TNT and Comp B.

(1) Experimental Procedure

(U)   The experimental configuration is shown in Figure 7. The cylindrical charge is set upright in the center of a .125-inch thick, 5" x 5" 2024-T3 aluminum plate. A set of location lines are marked on top of the plate so that the center of the charge can be precisely aligned. A small amount of silicone oil is put between the end of the cylinder and plate to eliminate any air cavities. An air cavity could significantly retard the shock passage into the aluminum. On the bottom of the aluminum plate on the opposite side from the explosive charge, a .250-inch thick, 5" x 5" plexiglas plate is fastened.

TABLE I. EXPERIMENTAL PLAN FOR MACH WAVE PROFILE EXPERIMENTS

	Barrier Material	Barrier Thickness (inches)	Inner Explosive Diam. (inches)	Inner Explosive Length (inches)
Inner: TNT	None	----	1/2	6
	None	----	1	2
	None	----	1	4
	None	----	1	6
	None	----	2	6
Outer: A2	Phenolic	1/16	1	6
	Phenolic	1/8	1	4
	Phenolic	1/8	1	6
	Phenolic	1/4	1	6
	Aluminum	.133	1	6
	Steel	.120	1	6
Inner: TNT	None	----	1	6
Outer: Octol	Phenolic	1/8	2	6
Inner: Comp B	None	----	1	6
Outer: Octol	Phenolic	1/16	1	6
	Phenolic	1/8	1	6
	Phenolic	1/4	1	6
	Aluminum	.133	1	6
	Steel	.120	1	6
Inner: Baratol	Phenolic	1/16	1	4
	Phenolic	1/8	1	4
Outer: A2	Phenolic	1/4	1	4

21

(U)   The surface of the plexiglas is separated from the aluminum by a gap of 10 mils. This gap is obtained by means of a 10 mil lead shim between the two plates. A fiducial mark is put on the outside surface of the plexiglas by means of two strips of black tape which are put on the plexiglas with a spacing between them just a little larger than the overall diameter of the explosive charge. The spacing between the strips of tape is accurately measured with vernier calipers. Small strips of white drafting tape are positioned on the sides of the plexiglas plate to accurately locate the center corresponding to the center locator on the top surface of the aluminum plate.

Detonator

Detonator Centering Fixture

Test Charge

.125-in. Thick
2024-T3 Aluminum Plate
10 Mil Lead Shim

.250-in. Thick Clear
Plexiglas Plate

Argon
Gas
Supply

Fiducial
Tapes

To Streak
Camera Lens

Mirror

UNCLASSIFIED
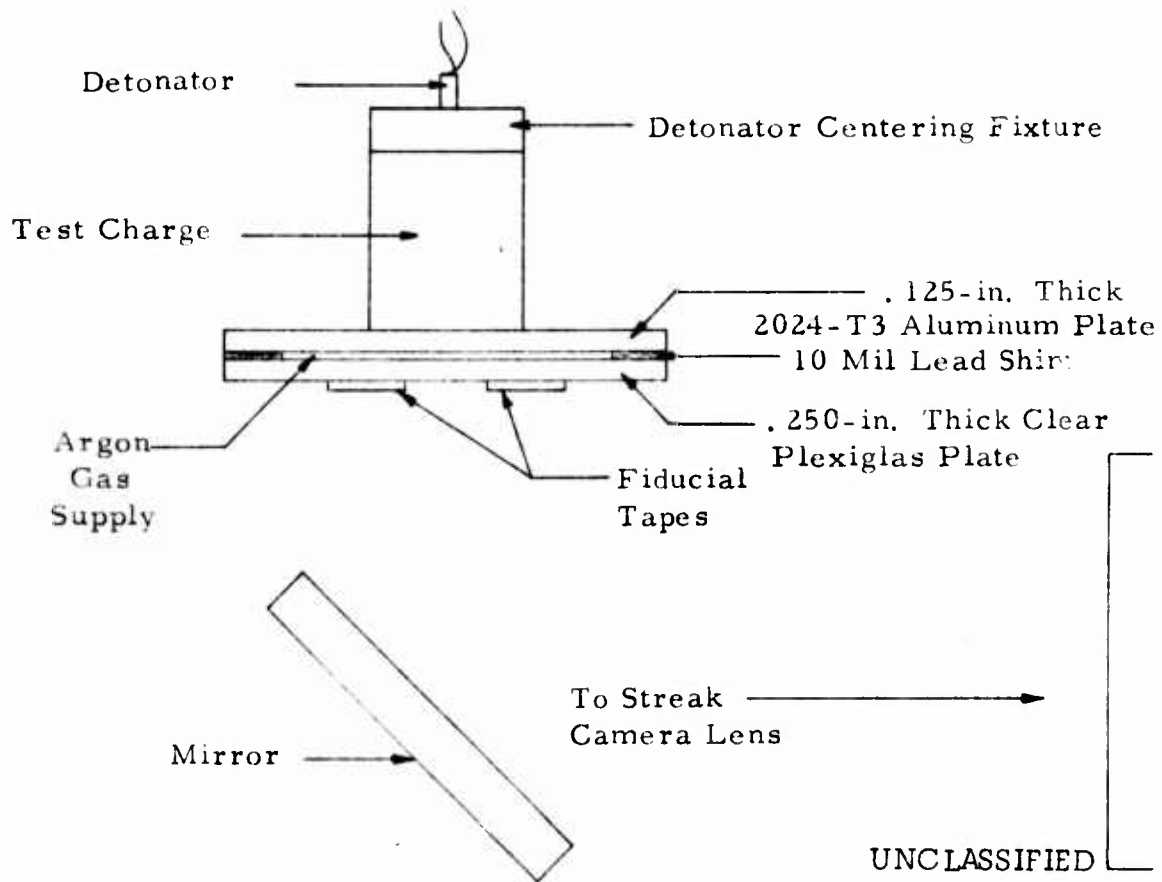
Figure 7.   Experimental Configurations of Argon Gap
Plates for Wave Profile Determinations

22

(U)   When the slit of the streak camera is aligned with respect to the locating points the resulting streak image on the film will record the detonation profile of the emerging wave along a diameter across the end of the explosive charge. The streak record results from the flashing of argon gas, which fills the gap volume. The argon gas is flashed by the shock wave transmitted through the aluminum by the detonation wave. The thin gap and the aluminum plate provide a record consisting of a thin sharp easily measured line without any spurious light from the explosive gases. Representative streak camera pictures are shown in section 2c.

(U)   All the charges were X-rayed after fabrication and those with excessive voids or heterogeneities were discarded. In cases where the defects were small and located at relatively uncritical positions in the charge, the charges were used but the defects were oriented with respect to the streak camera slit so as not to affect the streak record.

(2) Sources of Asymmetry

(U)   The two principle external sources for asymmetry in the Mach wave are variations in the uniformity of the outer charge and deviation of the center line of the detonator from the axis of the explosive charge. An experiment was therefore set up to evaluate these possible external sources of Mach wave asymmetry.

(U)   In order to eliminate internal explosive effects, magnesium rods 1.0-inch in diameter, 4.0-inch long were used to simulate the TNT charges. EL506A2 sheet explosive was wrapped around them as the external shock wave source. The sheet explosive in this configuration produces a Mach shock wave in magnesium that is strong enough to leave a distinct impression in a steel witness plate.

(U)   Non-uniformity in the outer charge was simulated in two ways. The first method involved leaving a 3/16-inch wide gap along the length of the sheet explosive. The second method involved the use of a .250-inch overlap of the sheet explosive along its length. Non-alignment of the detonator and explosive charge center lines was achieved by moving the detonator .250-inch from the center. Replicate tests were fired of the three cases listed above as well as a "control" case where the outer sheet explosive had no gaps or overlaps and the detonator was centered.

(U)   The results of the gap and overlap tests, as determined by the deviation of the Mach identation from where the center of the charge was located showed that movement of the Mach wave due to these specific non-uniformities of the outer charge, was negligible. The results were surprisingly indistinguishable from the control tests and suggest an unexpected lack of sensitivity to small perturbations of this type.

23

(U)   Off center alignment of the detonator however did cause signifi-
cant deviation of the Mach impression from the center line. For the
geometry used, the deviation averaged .16-inch or approximately 2/3 of
the displacement of the detonator from the centerline.

(U)   These test results were not interpreted to mean that one could
relax in maintaining symmetry. In fact, the results obtained with the
.25" off center detonator were considered to be of sufficient concern
that more than the usual careful centering was undertaken, even though
the normal centering procedure did not permit deviations even 1/10th as
large as the .250" extreme used in the evaluation experiments.

(U)   The results of the gap and overlap test indicate that at least for
inert interiors and perhaps for those cases where initiation of the interior
explosive does not occur, until the Mach disc region is reached, there is
a lower than expected sensitivity to exterior charge defects of the type
studied. This is less likely to be true with reactive explosive interiors
which are initiated quickly by the converging shock. The net effect of
these experiments was a further tightening of constraints on assembly
asymmetries of all kinds.

(3) Explosive Properties

(U)   Important parameters which must be determined for the data reduc-
tion and comparison with theory, are the detonation velocities of the
inner and outer explosive used. The detonation velocity of the inner
explosive is also important for making the comparisons between theory
and experiment. Most of the detonation velocities were measured
directly, but that of baratol was measured indirectly since its critical
diameter was such that it could not be conveniently and economically
fabricated and fired. An indirect check of the measured detonation
velocities was made by also measuring the density of the cast explosives
using known detonation velocity-density relations to calculate the deto-
nation velocity. The velocity of TNT was obtained in this way since it's
data is well documented.

(U)   The detonation velocity was measured directly by means of
special probes that were pushed against the outer surface of the explo-
sive along the direction of the detonation. When the detonation wave
reached the probe, the pressure wave pushed a piece of brass foil into
a pointed brass pin positioned less than a mil behind it. The resultant
electrical contact caused the discharge of an R-C circuit. The pulses
from this circuit were recorded on a rasteroscilloscope with very accurate
time markers on the trace. Since the distance between the pin points
was previously measured, the time interval data from the rasteroscillo-
scope records permitted the computation of the required detonation
velocity. The detonation velocities of A2, Comp B, and Octol explosives
were measured in this way.

24

(U)   The detonation velocity of baratol was measured indirectly by means of the experimental set up illustrated in Figure 8. A slab of baratol is positioned next to a slab of Comp B which is detonated simultaneously along the top edge by a line wave generator. Two slabs of .75-inch thick steel are placed around the explosive. The detonation wave front is recorded by means of an argon shock plate described previously. Measurement of the angle (θ) of the detonation wave in the baratol at the interface between the two explosives provides a means for estimating the unknown detonation velocity (D_x) in terms of the detonation velocity of Comp B, D_{CB}, from the relation,

$$D_x = D_{CB} \sin \theta$$

(U)   A table of detonation velocities as estimated by the specifically applicable methods, is given in Table II.

3.   DATA REDUCTION

(U)   Representative streak camera records from each of the different experimental categories studied in the argon gap plate tests are shown in Figure 9.

(U)   The data analysis procedure for records of this type was carried out in the manner described below.

(U)   Large scale tracings were drawn by hand from the streak camera films through an optical enlarging apparatus. The scale distance corresponding to one-half inch on the films was indicated on the tracings as well.

(U)   Descriptive measurements were taken from the tracings using calipers and drafting apparatus. Figure 10 shows the critical measurements made at this time. They were recorded in tabular form.

(U)   Measurement (in inches) in the time direction, were denoted as A and H. The vertical slope components were also measured. Measurements (in inches) in the distance direction were denoted as B, C, D, E, F, and G. The horizontal slope components were also measured. D is the distance between the center of C and the center of B. The slope component measurements were tabulated as related pairs of distance and time components. Some of the distances measured were used as indicators of symmetry and were not used directly in calculations.

(U)   The following experimental constants were also tabulated for each case.

> 1. Camera streak speed in inches per usec is denoted as CTIME.

25
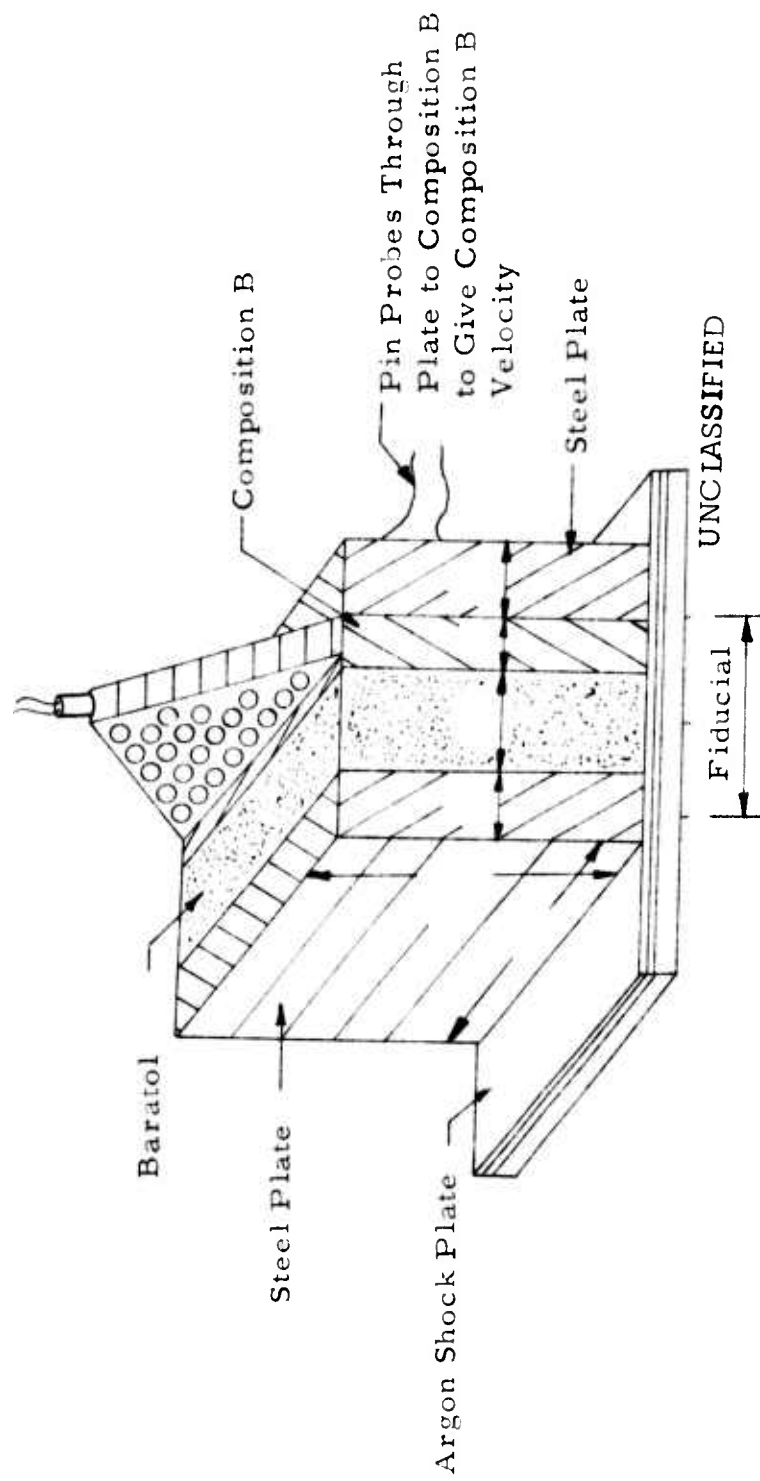
Figure 8. Fixture for Indirect Measurement of Baratol Detonation Velocity

26

TABLE II. DETONATION VELOCITY OF EXPLOSIVES
USED IN MACH WAVE TESTS

Explosive	Measured Density (gms/cc)	Measured Detonation Velocity (m/sec)	Detonation Velocity Computed From Density (m/sec)
TNT	1.54	- - - -	6750
Comp B	1.68	7860	7790
Octol	1.76	8460	8370
A-2	1.48*	7630	- - - -
PBHMX	1.86	8940	9000
Baratol	2.30	5260**	- - - -
			UNCLASSIFIED

* Obtained by measuring dimension of sample and then weighing it.

**Measured indirectly as indicated in Figure 8.

2. The fiducial length in inches as measured on the test picture is denoted as FPOL.

3. The actual distances in inches corresponding to the fiducial distance on the test picture is denoted as FCHART.

4. The scaled distance in inches on the tracings corresponding to .500 inches on the test film is denoted as CINT.

5. The detonation velocity of the outer explosive, in meters/sec is denoted as VEL.

a. Computations For Data Reduction

(U) The actual experimental distances describing the features of the shock wave were computed on an IBM 1108 computer in the following manner:

27
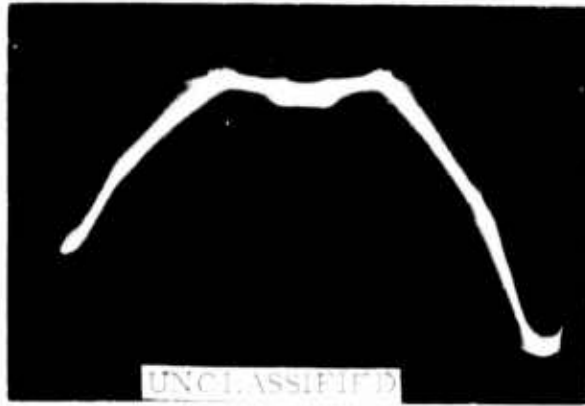
TNT-A2
1" Dia x 4" Long
Phenolic Barrier
1/8" Thick
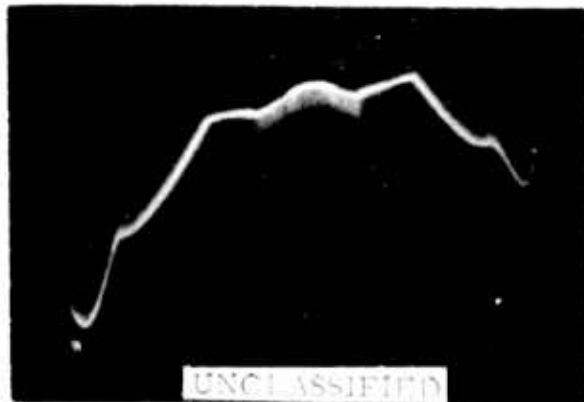
TNT-A2
1" Dia x 6" Long
Phenolic Barrier
1/16" Thick
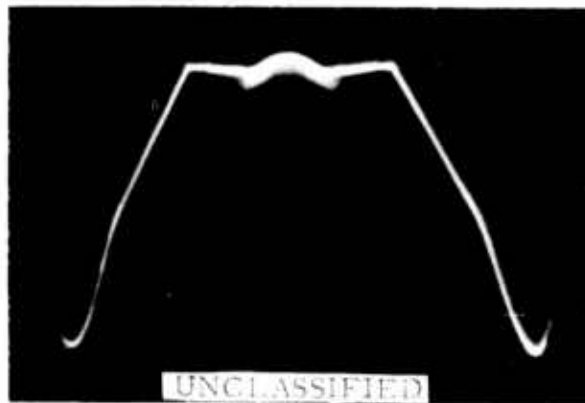
TNT-A2
1" Dia x 6" Long
Phenolic Barrier
1/8" Thick

Figure 9.   Representative Streak Camera Records for Each of
Explosive Configuration in Mach Wave Tests

28
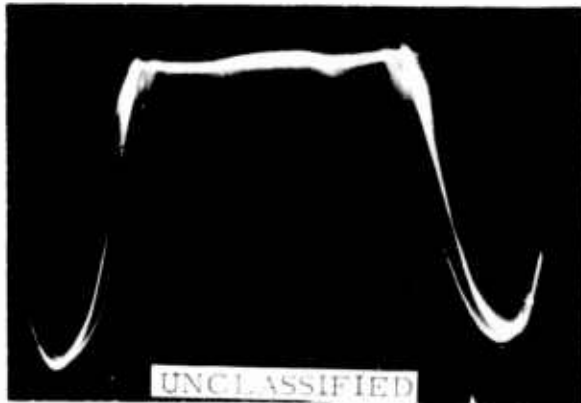
TNT-A2
1" Dia x 6" Long
Aluminum Barrier
1/8" Thick

TNT-A2
1" Dia x 6" Long
Phenolic Barrier
1/4" Thick

Figure 9.   (Continued)

29

TNT-A2
1" Dia x 6" Long
Steel Barrier
3/32" Thick
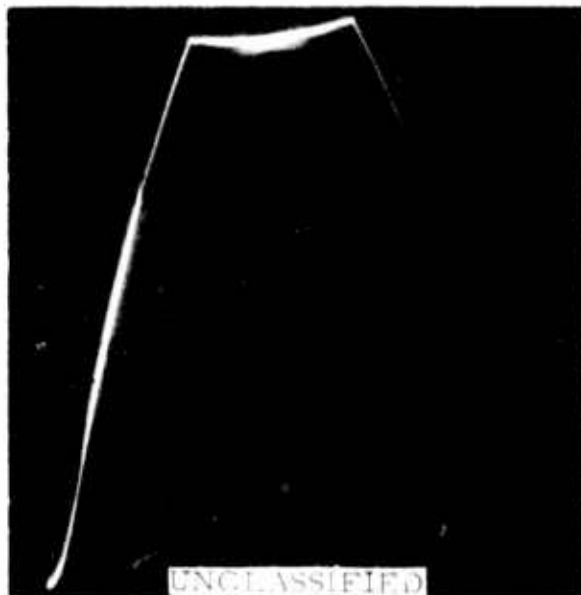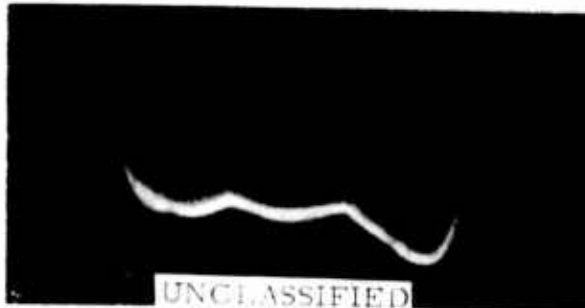
TNT-A2
1/2" Dia x 6" Long
No Barrier
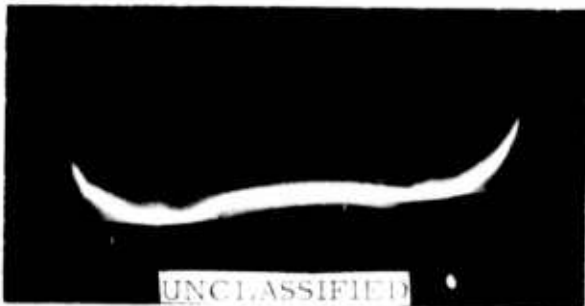
TNT-A2
1" Dia x 2" Long
No Barrier

Figure 9.   (Continued)
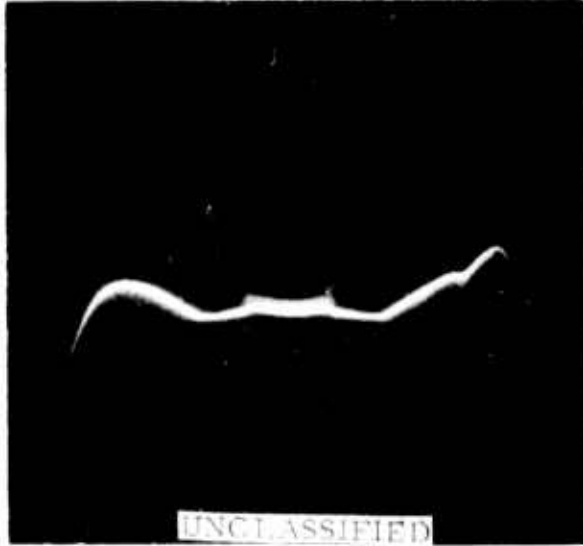
TNT-A2
1" Dia x 6" Long
No Barrier
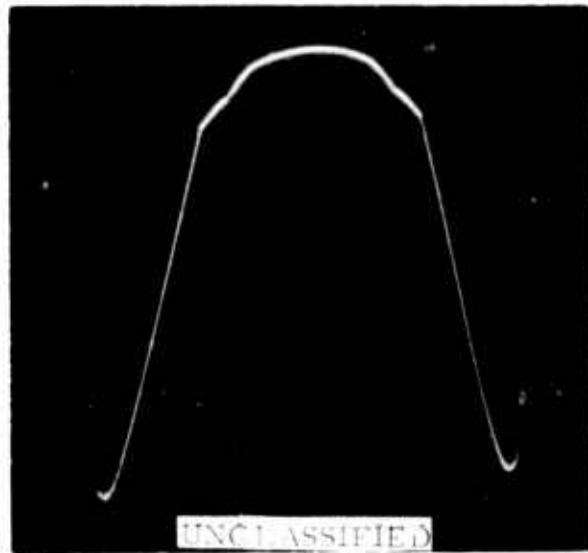
TNT-A2
2" Dia x 6" Long
No Barrier
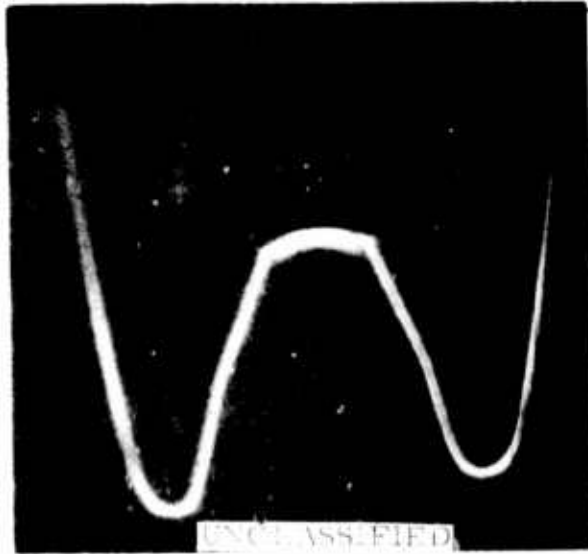
Figure 9. (Continued)

TNT-Octol
1" Dia x 6" Long
Phenolic Barrier
1/8" Thick
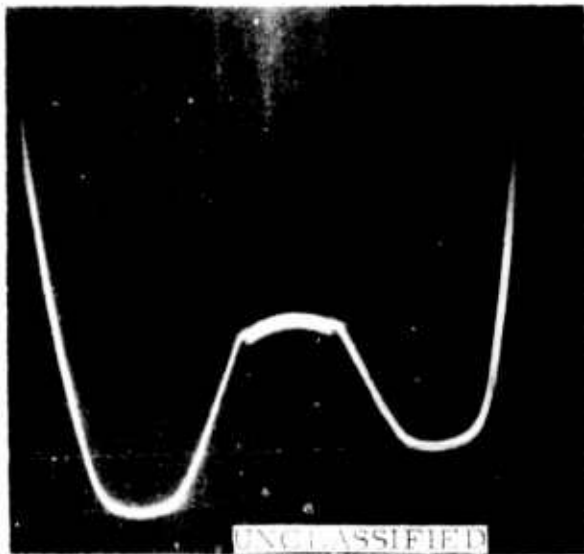
TNT-Octol
1" Dia x 6" Long
No Barrier

Figure 9.   (Continued)

32

Composition B-Octol
1" Dia x 6" Long
Phenolic Barrier
1/16" Thick
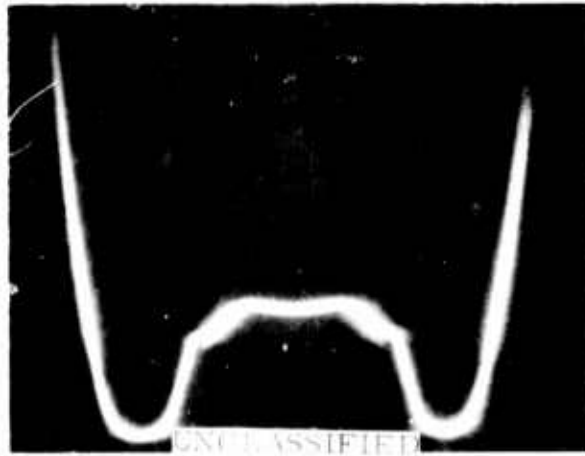
Composition B-Octol
1" Dia x 6" Long
Phenolic Barrier
1/8" Thick
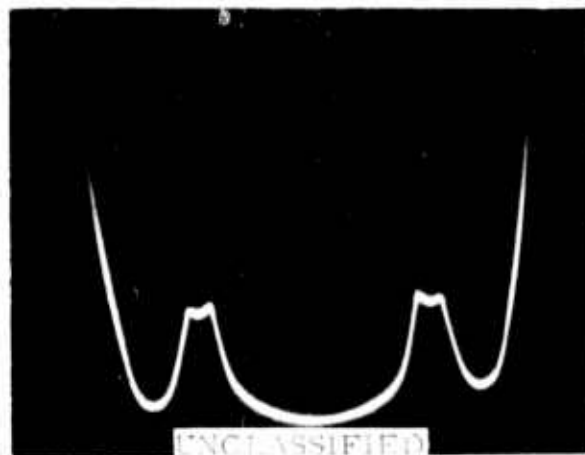
Composition B-Octol
1" Dia x 6" Long
Phenolic Barrier
1/4" Thick

Figure 9.   (Continued)

33
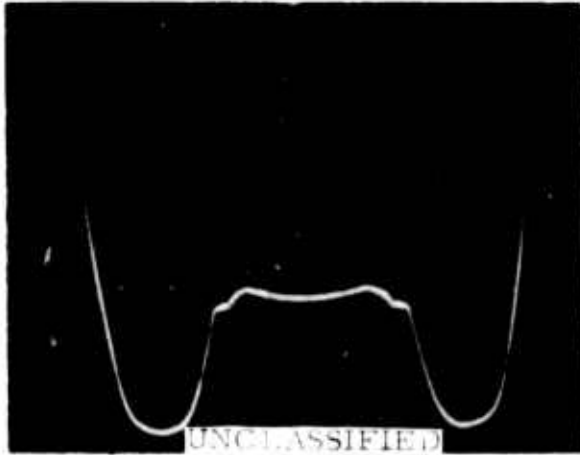
Composition B-Octol
1" Dia x 6" Long
Steel Barrier
1/8" Thick
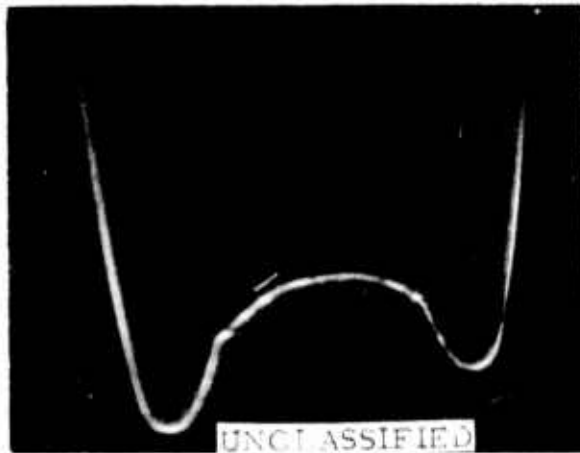
Composition B-Octol
1" Dia x 6" Long
Aluminum Barrier
0. 135" Thick

Composition B-Octol
1" Dia x 6" Long
No Barrier

Figure 9.   (Continued)

34

Baratol-A2
1" Dia x 4" Long
Phenolic Barrier
1/16" Thick
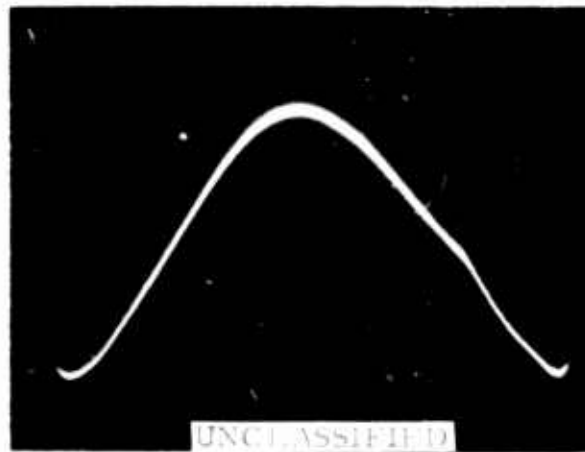
Baratol-A2
1" Dia x 4" Long
Phenolic Barrier
1/8" Thick

Baratol-A2
1" Dia x 4" Long
Phenolic Barrier
1/4" Thick

Figure 9.   (Concluded)

35
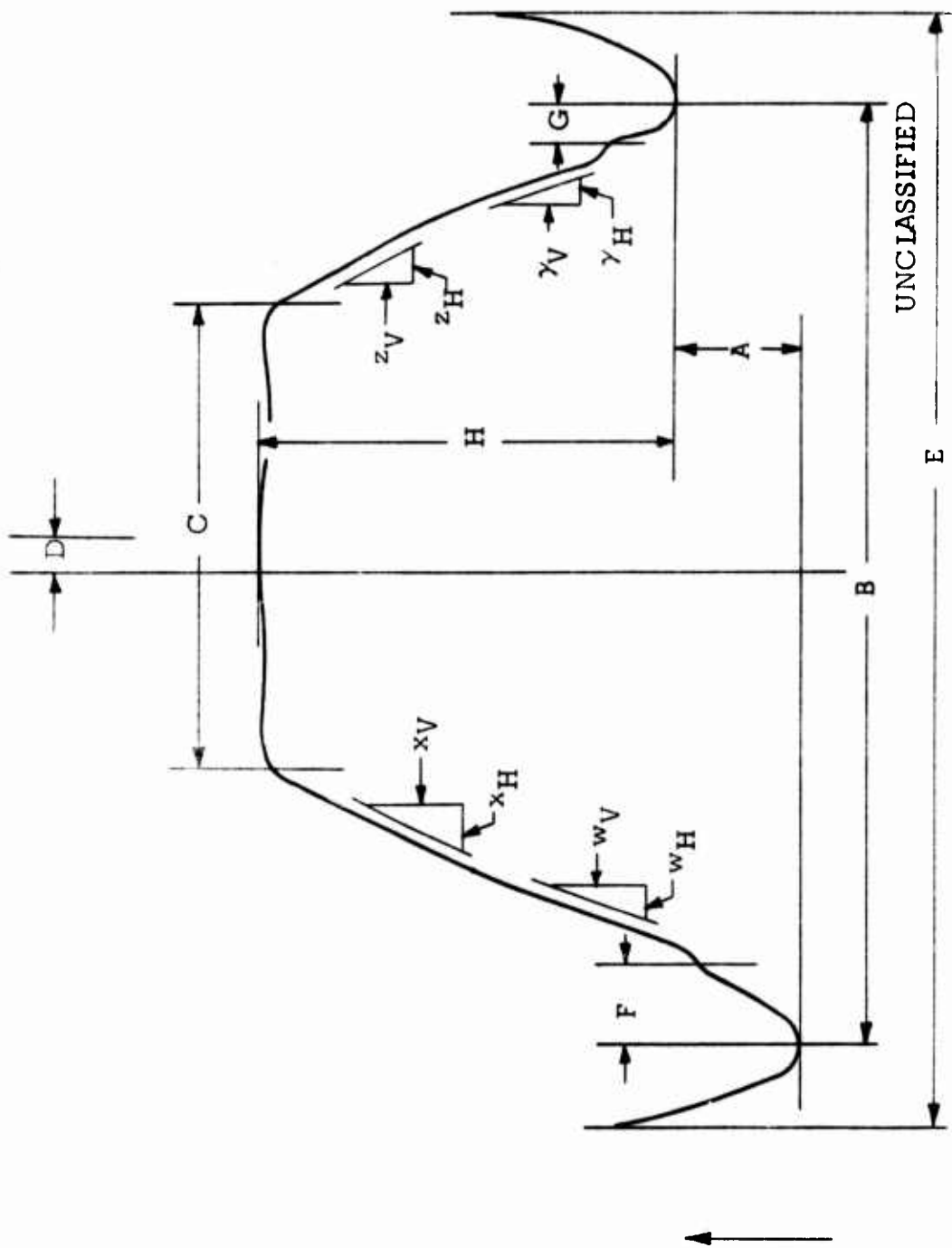
Figure 10. Critical Measurements on Representative Streak Record

UNCLASSIFIED

36

(U)   From the time dimension measurements we compute

        Actual time span = (measured value) (PROD. 1)

where

$$\text{PROD. 1} = \frac{(0.500 \text{ in.})}{(CINT)(CTIME)}$$

(U)   From the distance dimension measurements we compute

        Actual horizontal distance = (measured value)(PROD. 2)

where

$$\text{PROD. 2} = \frac{(0.500 \text{ in.})(FCHART)}{(CINT)(FPOL)}$$

(U)   From the measured slope components we compute, as
in Appendix B

$$\text{Actual Slope} = \left(\frac{\text{measured vertical comp.}}{\text{measured horizontal comp.}}\right) \cdot \text{PROD. 3}$$

where

$$\text{PROD. 3} = \frac{(39.37 \text{ in/m})(10^{-6} \text{ sec/usec})(VEL)(FPOL)}{(FCHART)(CTIME)}$$

(U)   Since the purpose of these experiments is to provide a basis
for correlating the results with the Mach wave theory, an important
quantity is the ratio of the width of the Mach wave to the diameter of
the inner explosive, or "tube diameter" which is expressed as r/r_o.

(U)   The other important experimental results whose correlation with
the theory are to be studied is the incident and transition angles.

(U)   Prior to locating these angles on the tracings, the barriers and
explosive interfaces were sketched on the original tracings. With the
actual diameters and thicknesses known, the scaling process was
similar to that used to analyze the horizontal (distance dimension)
measurements.

(U)   The slopes corresponding to the incidence angles were computed
as indicated previously. The angles are found from the relationship

$$\theta = \text{Arc cot (slope)}$$

The pair of angles, θ_1 and θ_2 for each case, were averaged and θ_O tabulated.

(U)   The slopes corresponding to the transition angles were similarly computed, and θ_O was again determined using the relationship

$$\theta = \text{Arc cot (slope)}.$$

4.   COMPARISON OF THEORY AND EXPERIMENT

(U)   An approximate theory for conically convergent shock and detonation waves was presented in section 1. The experimental plan was presented in section 2., and the methods of data reduction and the reduced sults were given in section 3.

(U)   In this section, a comparison is made of the theory and the experimental results. A short discussion is given for each of the three experimental parameters that relate directly to the theory, i.e., (a) the initial angle of the shock or detonation wave as it enters the inner explosive; (b) the charge length required to permit formation of the Mach wave in the inner explosive; and (c) the diameter of the Mach region in relation to the diameter of the inner explosive.

(U)   These parameters are then interpreted in terms of particular explosive configurations, of which there were four.

        1. Inner explosive - TNT, outer explosive - A2 sheet explosive
        2. Inner explosive - TNT, outer explosive - Octol
        3. Inner explosive - Baratol, outer explosive - A2 sheet explosive
        4. Inner explosive - Comp B, outer explosive - Octol.

(U)   The experimentally determined values of the ratio of Mach radius to inner charge radius, and the initial wave angles for these explosive configuration are given in Table III.

(U)   Finally, there is provided a discussion of additional implications of the theory.

        a. Initial Angles

(U)   The initial angle (θ_O) of the detonation wave in the inner explosive at the interface between the inner and outer explosive can be theoretically calculated from the equation

$$\theta_O = \text{Arc sin} \frac{D_I}{D_O} \tag{38}$$

38

TABLE III. RATIO OF MACH RADIUS (r) TO CHARGE RADIUS (r_o) AND INITIAL ANGLES (θ_1 & θ_2) FOR VARIOUS EXPLOSIVE CONFIGURATIONS AND BARRIERS

Inner Explosive: TNT
Outer Explosive: A-2
Calculated: $\theta_o = 62.1°$

Test No.	Barrier Material	Inner Expl. Diameter (inches)	Inner Expl. Length (inches)	Barrier Thickness (inches)	r/r_o	θ_1	θ_2	Average $\frac{\theta_1 + \theta_2}{2} = \theta_o$
6	Phenolic	1	4	1/8	----	----	----	----
7	Phenolic	1	4	1/8	.2756	47°17'	46°40'	46°59'
8	Phenolic	1	4	1/8	.4255	51°11'	58°20'	54°46'
26	Phenolic	1	6	1/16	.5759	59°51'	61°20'	60°36'
27	Phenolic	1	6	1/16	.4403	57°7'	62°39'	59°53'
28	Phenolic	1	6	1/16	.4072	63°36'	59°48'	61°42'
35	Phenolic	1	6	1/8	.5811	48°46'	52°47'	50°47'
37	Phenolic	1	6	1/8	.4574	43°1'	48°23'	45°42'
29	Phenolic	1	6	1/4	.5374	43°14'	38°3'	40°39'
30	Phenolic	1	6	1/4	.5194	39°55'	38°3'	38°59'
31	Phenolic	1	6	1/4	.5814	34°44'	33°21'	34°3'
32	Steel	1	6	.120	.6719	26°12'	28°48'	27°30'
33	Steel	1	6	.120	----	----	----	----
34	Steel	1	6	.120	.6542	29°11'	33°17'	31°14'
38	Aluminum	1	6	.135	.7433	25°12'	32°10'	28°41'
39	Aluminum	1	6	.135	.7260	30°30'	26°58'	28°44'
40	Aluminum	1	6	.135	.8299	16°37'	22°53'	19°45'
68	None	1/2	6	----	.4800	80°40'	72°31'	76°36'
14	None	1	2	----	----	81°30'	79°24'	80°27'
15	None	1	2	----	----	73°36'	81°47'	77°42'
16	None	1	2	----	----	74°28'	63°20'	68°54'
17	None	1	6	----	.4153	67°38'	57°51'	62°45'
18	None	1	6	----	.4747	67°37'	66°19'	66°58'

TABLE III. (Continued)

Inner Explosive: TNT
Outer Explosive: A-2
Calculated: $\theta_o = 62.1°$

Test No.	Barrier Material	Inner Expl. Diameter	Inner Expl. Length	Barrier Thickness	r/r_o	θ_1	θ_2	Average $\dfrac{\theta_1 + \theta_2}{2} = \theta_o$
19	None	1	6	----	.4870	70°8'	69°49'	69°59'
59	None	2	6	----	.3471	44°5'	47°49'	45°57'
60	None	2	6	----	.2692	43°27'	48°32'	45°55'
61	None	2	6	----	.3113	47°15'	42°13'	44°44'

Inner Explosive: TNT
Outer Explosive: Octol
Calculated: $\theta_o = 52.9°$

Test No.	Barrier Material	Inner Expl. Diameter	Inner Expl. Length	Barrier Thickness	r/r_o	θ_1	θ_2	Average $\dfrac{\theta_1 + \theta_2}{2} = \theta_o$
62	Phenolic	1	6	1/8	.5038	57°36'	48°21'	52°59'
63	Phenolic	1	6	1/8	.5127	55°7'	56°19'	55°43'
64	Phenolic	1	6	1/8	.5193	58°18'	58°36'	58°27'
65	Phenolic	1	6	1/8	.4557	55°25'	60°39'	58°2'
66	None	1	6	----	.5009	60°17'	61°5'	60°41'
67	None	1	6	----	.4691	53°18'	62°32'	57°55'

Inner Explosive: Baratol
Outer Explosive: A-2
Calculated: $\theta_o = 43.6$

Test No.	Barrier Material	Inner Expl. Diameter	Inner Expl. Length	Barrier Thickness	r/r_o	θ_1	θ_2	Average $\dfrac{\theta_1 + \theta_2}{2} = \theta_o$
10	Phenolic	1	4	1/16	----	51°31'	50°46'	51°9'
9	Phenolic	1	4	1/8	----	50°14'	48°23'	49°19'
11	Phenolic	1	4	1/8	----	51°12'	45°12'	48°12'
12	Phenolic	1	4	1/4	----	41°32'	37°29'	39°31'

TABLE III. (Concluded)

Inner Explosive: Comp B
Outer Explosive: Octol
Calculated: $\theta_o = 68.3°$

Test No.	Barrier Material	Inner Expl. Diameter (inches)	Inner Expl. Length (inches)	Barrier Thickness (inches)	r/r_o	θ_1	θ_2	Average $\dfrac{\theta_1 + \theta_2}{2} = \theta_o$
41	Phenolic	1	6	1/8	.5660	78°0'	71°30'	74°45'
42	Phenolic	1	6	1/8	.5205	78°0'	80°51'	79°26'
43	Phenolic	1	6	1/8	.7595	61°39'	75°41'	68°40'
44	Phenolic	1	6	1/4	----	----	----	----
45	Phenolic	1	6	1/4	----	----	----	----
50	Phenolic	1	6	1/16	----	78°21'	72°24'	75°23'
51	Phenolic	1	6	1/16	----	80°21'	80°33'	80°27'
52	Phenolic	1	6	1/16	----	70°27'	75°44'	73°6'
49	Steel	1	6	.120	.7038	66°33'	58°1'	62°17'
56	Steel	1	6	.120	.9066	----	----	----
57	Steel	1	6	.120	.6098	73°21'	74°5'	73°43'
58	Steel	1	6	.120	----	51°35'	55°2'	53°19'
46	Aluminum	1	6	.135	----	72°35'	78°48'	75°40'
47	Aluminum	1	6	.135	----	83°2'	84°59'	84°1'
48	Aluminum	1	6	.135	----	----	77°11'	77°11'
24	None	1	6	----	.9315	75°34'	76°2'	75°48'
25	None	1	6	----	.9032	81°45'	83°42'	82°44'

41

where D_I and D_O are the detonation velocities of the inner and outer explosives respectively. The presence of a barrier between the inner and outer explosive can alter the angle of the wave in the inner explosive, especially if the barrier is an effective attenuator so that the pressure wave that passes into the inner explosive is appreciably weaker than that needed to cause detonation. In this case the above equation becomes

$$\theta = \text{Arc } \sin \frac{S_I}{D_O} \tag{39}$$

where S_I is the shock velocity in the inner explosive corresponding to the induces pressure.

(U)   If the shock entering the inner explosive is powerful enough to cause immediate detonation of the inner explosive, then the wave angle in the interior explosive at the interface between the two explosives will correspond to that given by Eqn. (38). The assumption is made that the detonation waves have traveled far enough to reach a steady state configuration. There will also be a lag between the detonation fronts in the two explosives as a result of the deviation of the shock in the barrier. Of the angles calculated for the four explosive configurations given in Table III, the cases most pertinent to the computed initial angle are those in which the charge is 1 inch in diameter and 6 inches in length.

b. Charge Length Needed to Form Mach Waves

(U)   In section 1.d the theoretical treatment of convergent shock waves gave guidelines to estimate the charge length needed to form the steady state mach wave. The critical variable was the ratio of the two detonation velocities.

(U)   This ratio was calculated for all the cases in the experimental plan. The experimental configurations correspond to a case somewhere between case A and B in Figure 6, but somewhat closer to case A especially where there is a barrier. The detonation velocity ratio is given with the corresponding results taken from case A on the graph.

c. Mach Diameter Calculations

(U)   One of the major predictions of the theory presented in section 1. was the size of the Mach region in relation to the diameter of the inner explosive and the ratio of the detonation velocities of the inner and outer explosives.

42

(U)   It was possible, in many of the experiments performed, to obtain a measurement of a central region with roughly the shape characteristics of a Mach region. It should be noted here that the presence in the center of a wave pattern of a flat or shallow curve is not a priori proof of the presence of a Mach wave. It can be seen from Figure 5 that such structures occur in the transient period before Mach wave formation. In the following portions of this section, the various explosives configuration will be discussed separately.

(1) TNT - A2 Charges

(U)   Photographs 2, 3 and 5 of Figure 9 show the progression of wave forms obtained for a 1 inch diameter x 6 inch long charge within a cylindrical phenolic barrier of three different thicknesses, each of which was wrapped in a sheet of A2 explosive. Figure 6 indicates that for a combination of TNT-A2 in the most severe case, namely Case A, an L/R_0 ratio of 13 would be required to generate a Mach disc. Thus, a Mach wave would be expected in this case.

(U)   The following points are evident when comparing the series of photographs.

      (a) The center pattern of the wave form falls further behind the side portion of the record made by the outer explosive, as the barrier thickness increases. This reflects the delay of the wave as it passes through the barriers.

      (b) The initial angle of the wave at the outer surface of the inner explosive also decreases as the barrier thickness increases.

(U)   This would indicate that no detonation occurs through a phenolic barrier thicker than approximately 1/16". The angle calculated for the case of instantaneous detonation at the interface is 62.1°. The most likely configuration of the TNT-A2 combination required to obtain a stationary Mach wave is that of the 1 inch diameter x 6 inch long inner charge with no barrier between it and the outer charge as shown in photograph no. 9 of Figure 9. Table III gives the initial angles obtained for this configuration and the average angles are close to but slightly larger than 62.1°, the largest being between 12 and 13% greater than the theoretical angle. This trend is followed by all the explosive combinations where the configuration is such as to be optimum for obtaining a steady-state Mach configuration, i.e., 1"x6" inner charge either with no barrier or a thin phenolic barrier between it and the outer charge. The initial angles for the 1"x6" charges with phenolic barriers

43

average less than the theoretical value becoming smaller as the barrier thickness increases. The records for the configurations in which the barrier was either aluminum or steel, also show smaller initial angles than the theoretical value, as computed from Eqn. (38). If the initial angle (θ_o) is appreciably smaller than that obtained from Eqn. (38), the wave entering the TNT must be a shock wave rather than a detonation wave. In this case, Eqn. (39) applies and knowledge of the non-reactive Hugoniot of TNT permits calculation of initial shock wave angles in TNT for various shock pressure, as shown in Table IV.

TABLE IV. SHOCK ANGLE VS PRESSURE IN TNT

Initial Angle (θ_o) (Degrees)	Shock Pressure (kilobars)
20	~ 5
30	~ 40
40	~ 100
50	~ 150

The values in Table IV can be used in conjunction with Table III to estimate the shock pressures in TNT for the configurations with barriers.

(c) Where the initial wave into the inner explosive is a shock rather than a detonation wave, the theory predicts that an abrupt, but not discontinuous transition to the wave angle corresponding to a detonation wave will occur. However the shock patterns of the TNT-A2 tests, in which the initial angle is less than one would expect for detonation at the inner explosive interface, shows a distinct and sharp turning and leveling out in the middle portion of the record without transition to another angle compatible with the onset of detonation. It seems improbable that a detonation is not present, since in the actual tests complete detonation of the entire charge occurs.

44

(U)   Thus, it appears that transition to detonation and to the Mach structure occur at the same radius for the TNT-A2 configuration. There also appears in the center of the test record for all the TNT-A2 tests an additional pattern distinguished by a curved horizontal line preceeded by a high-lighting effect in the record. It is not known at present why this pattern occurs. It is believed however that the high-lighting is indicative of a very high pressure region. The intensity of this pattern also seems to decrease with increasing barrier thicknesses. In contrast to this, the records obtained for a 2" x 6" inner charge of TNT surrounded with A2 in direct contact show that the initial angles in these cases are around 45°. However, a transition point does occur and the pattern is consistent with that predicted by the theory.

(d)   The measured width of the Mach region is presented in Table III. The edges of the Mach region were considered to be defined by the points at which the wave form made the sharp horizontal turn. It was not always possible to obtain a sharp reading on some of the configurations. However, enough measurements could be made to obtain meaningful data.

(U)   The most relevant configurations with respect to the theoretical model are those configurations in which there is no barrier material and the diameter to length ratio is such as to optimize the probability of a steady state Mach structure. The closest configuration to these requirements is the 1" x 6" charges with no barrier. The ratio of the Mach width (r) to the original diameter (r_o) as a function of the average initial angle (θ_o) is plotted in Figure 11, where the theoretical lines are drawn for a value of K varying from .3 to 1.0. The observed points are arranged approximately around the line corresponding to K = .7. If the results from the 1/2" x 6" and the 2" x 6" configurations are added to the graph, the points are clustered around the line corresponding to K = .4 and K = 1.0, respectively. The data in Table III shows that the scatter in θ_o is generally larger than 10%. The 2" x 6" test gives a larger Mach region than would be derived directly from the initial angle. However, a transition to detonation occurs in this case so the result could be understood as follows. The width of the Mach region is greater than would ordinarily be expected from an initial angle of 45° without a transition. However it is less than what would be expected for the case where the initial angle indicates detonation. The observations for the cases involving barriers do not appear to fit with the theoretical predictions. The deviation from theory becomes even greater at the thickness of the phenolic, aluminum and steel barriers increases. As a possible explanation of these deviations, there may be a preshocking effect which does not show up on the records but which causes turning of the wave prematurely in comparison to what would be expected from the observed initial angles in terms of the theory.

45

Figure 11. Graph of Ratio of Experimentally Determined Mach Wave Radius to Charge Radius vs Observed Initial Wave Angle in Inner Explosive for the Inner-Outer Explosive Combination of TNT - A2. Theoretical Lines are Drawn in for K Values from .3 to 1.0 Where K is the Convergence Pressure Magnification Exponent.

(2) TNT-Octol Charges

(U) The (r/r_O) vs θ_O points for the 1" x 6" TNT-Octol charges with no barriers, is plotted in Figure 12 and gives points along the line corresponds to $K = 1.0$. As indicated in the previous section, the imposition of a barrier causes a decrease in the initial angle and (r/r_O) is larger than would be predicted by the theory from the initial angle.

(3) Baratol-A2 Charges

(U) It is not possible to distinguish a definite Mach region in these tests. The initial angles decrease with increasing barrier thickness as noted in previous cases.

(4) Composition B-Octol Charges

(U) The angles, θ_O, obtained for all cases, with the possible exception of the steel case, are essentially the same. From this it would appear that detonation occurs immediately in the Comp B at the interface. This is reasonable since the detonation threshold for Comp B is approximately equal to that of TNT. However, as can be seen in Figure 13, the pressure generated in a steel barrier from an Octol surround is about 60 kilobars higher than that from an A2 surround. There are also the factors that the Octol surround was thicker than the A2 and that the density of the Comp B explosive is higher than that of TNT, thereby providing a slightly better impedence match with the steel. The (r/r_O) ratios vary widely but, taking the case with no barrier as the most relevant to the theory, the results give points above the $K = 1.0$ curve, as shown in Figure 14.

(5) Conclusions Regarding the Comparison of Theory and Experiment.

(U) The initial angles measured experimentall show appreciable scatter within each group. However, the barrier effects are large enough, when they are present, to show trend differences between the different groups.

(U) A comparison of the calculated values and the experimental values of θ_O shows that they are fairly close, with the experimental values usually slightly larger. Considering only the charges with barriers which are 6 inches long, it can be seen that the initial angles for the TNT-A2 tests are all smaller than these found when there is no barrier. Generally, the thicker the barrier (for a phenolic barrier) the smaller the initial angle is found to be, when compared to the situation with no barrier.
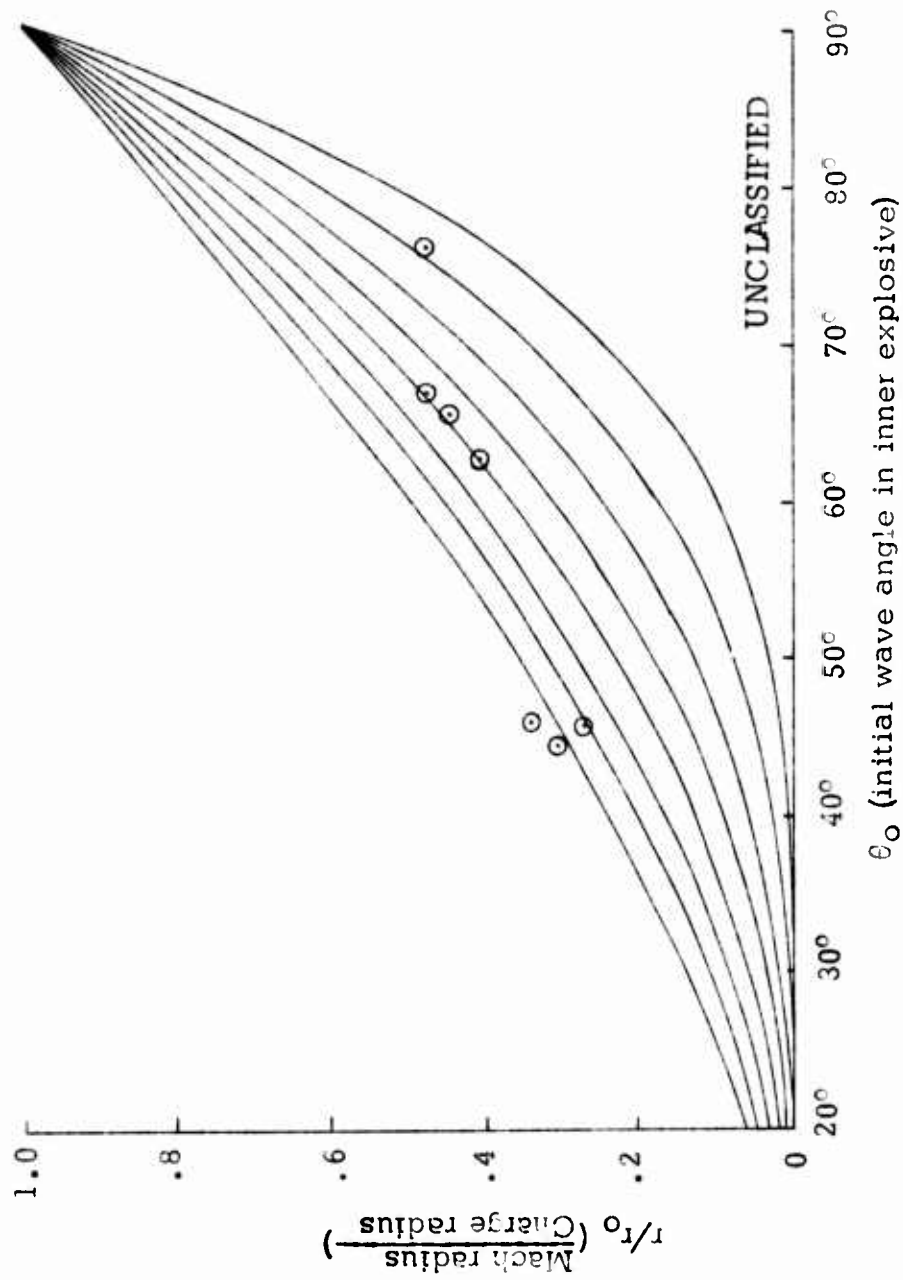
47

Figure 12. Graph of Ratio of Experimentally Determined Mach Wave Radius to Charge Radius vs Observed Initial Wave Angle in Inner Explosive for the Inner-Outer Explosive Combination of TNT - Octol. Theoretical Lines are Drawn in for K Values from .3 to 1.0 Where K is the Convergence Pressure Magnification Exponent.

48

Figure 13. Graph of Pressure vs Turning Angle in Steel to Obtain Pressure in Steel from Lateral Detonation of Several Explosives as Computed from the Method in Appendix I

49

θ_O (initial wave angle in inner explosive)

UNCLASSIFIED
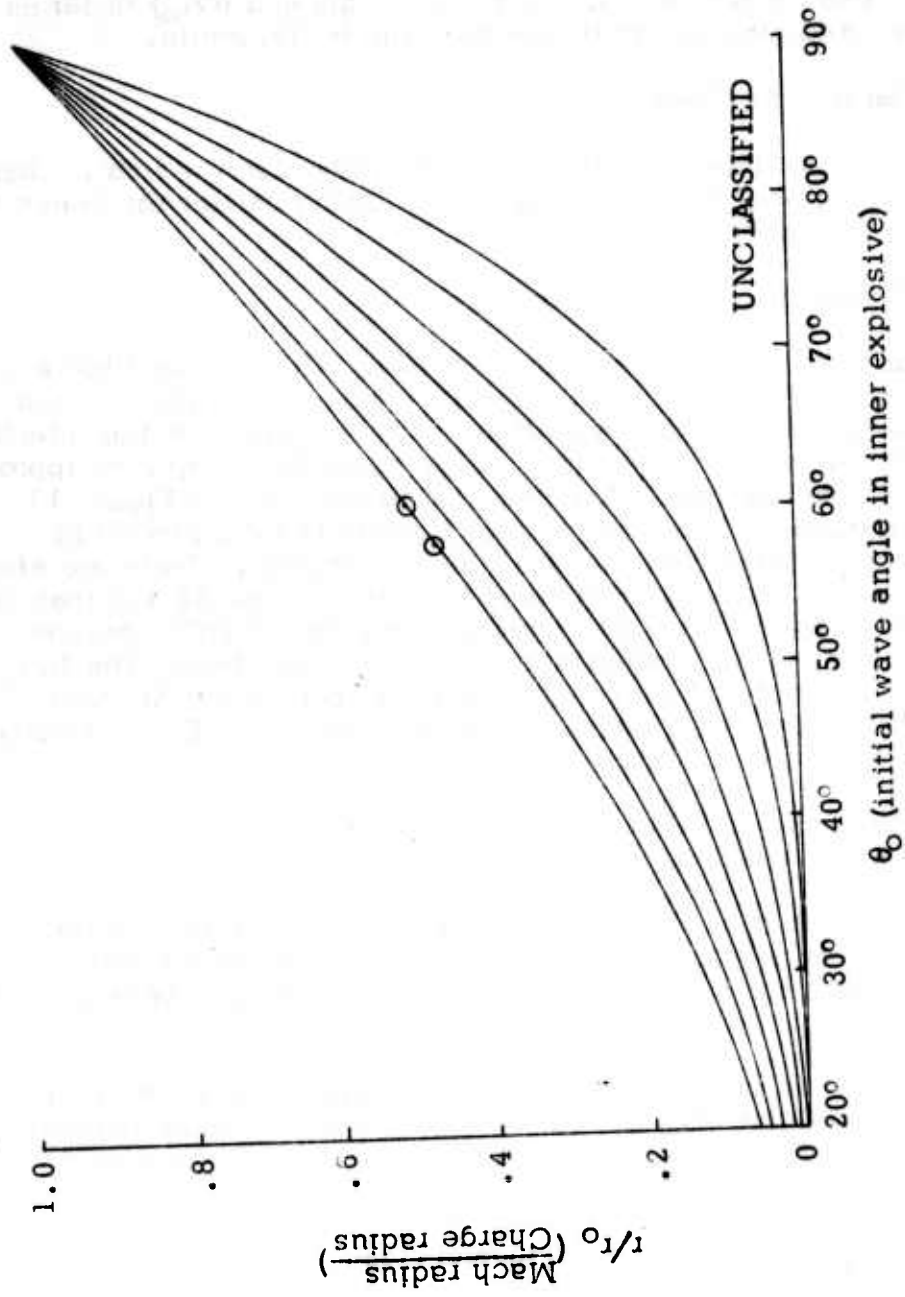
Mach radius / Charge radius (r/r_O)

Figure 14.   Graph of Ratio of Experimentally Determined Mach Wave Radius to Charge Radius vs Observed Initial Wave Angle in Inner Explosive for the Inner-Outer Explosive Combination of Comp B - Octol.   Theoretical Lines are Drawn in for K Values from .3 to 1.0 Where K is the Convergence Pressure Magnification Exponent.
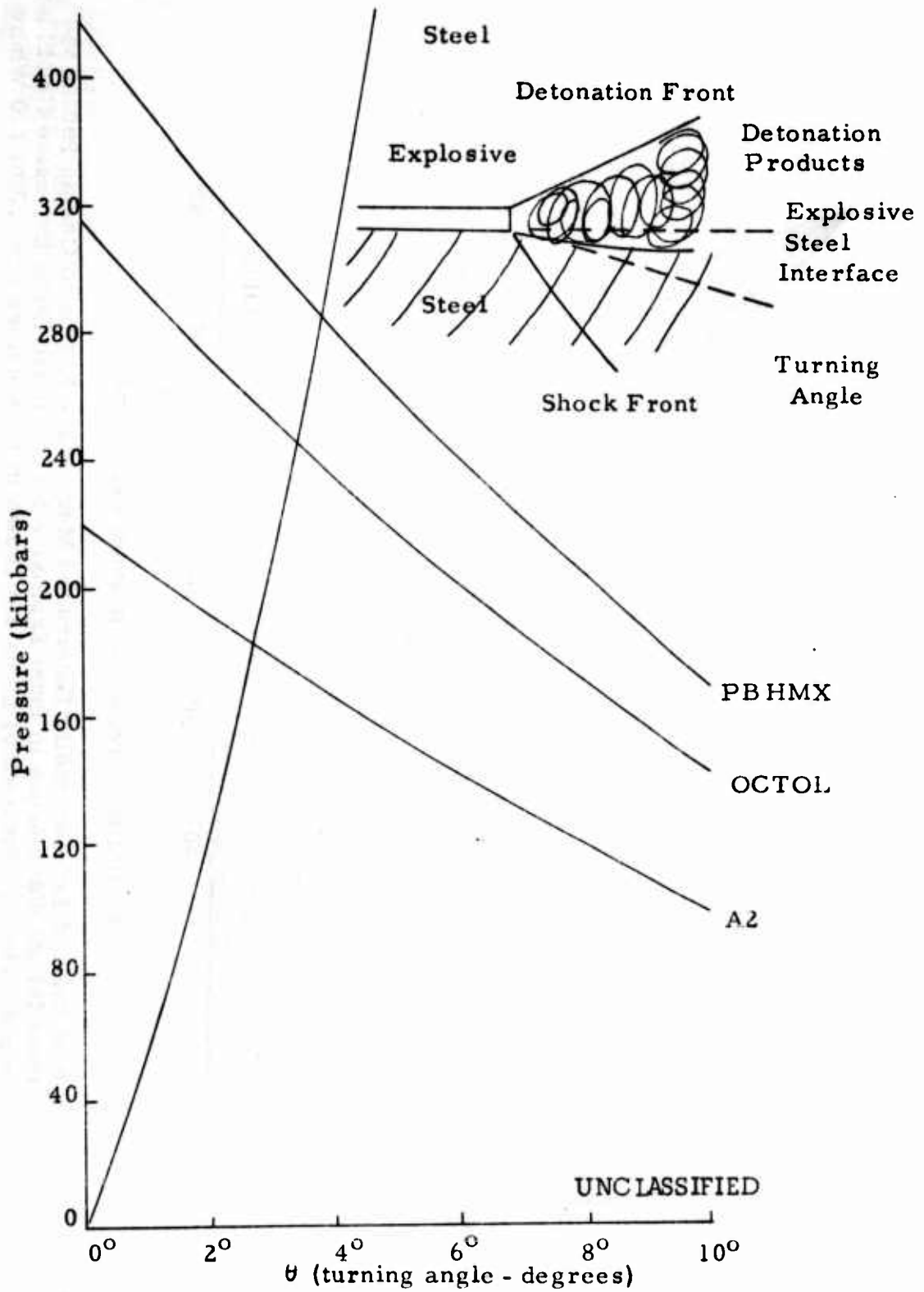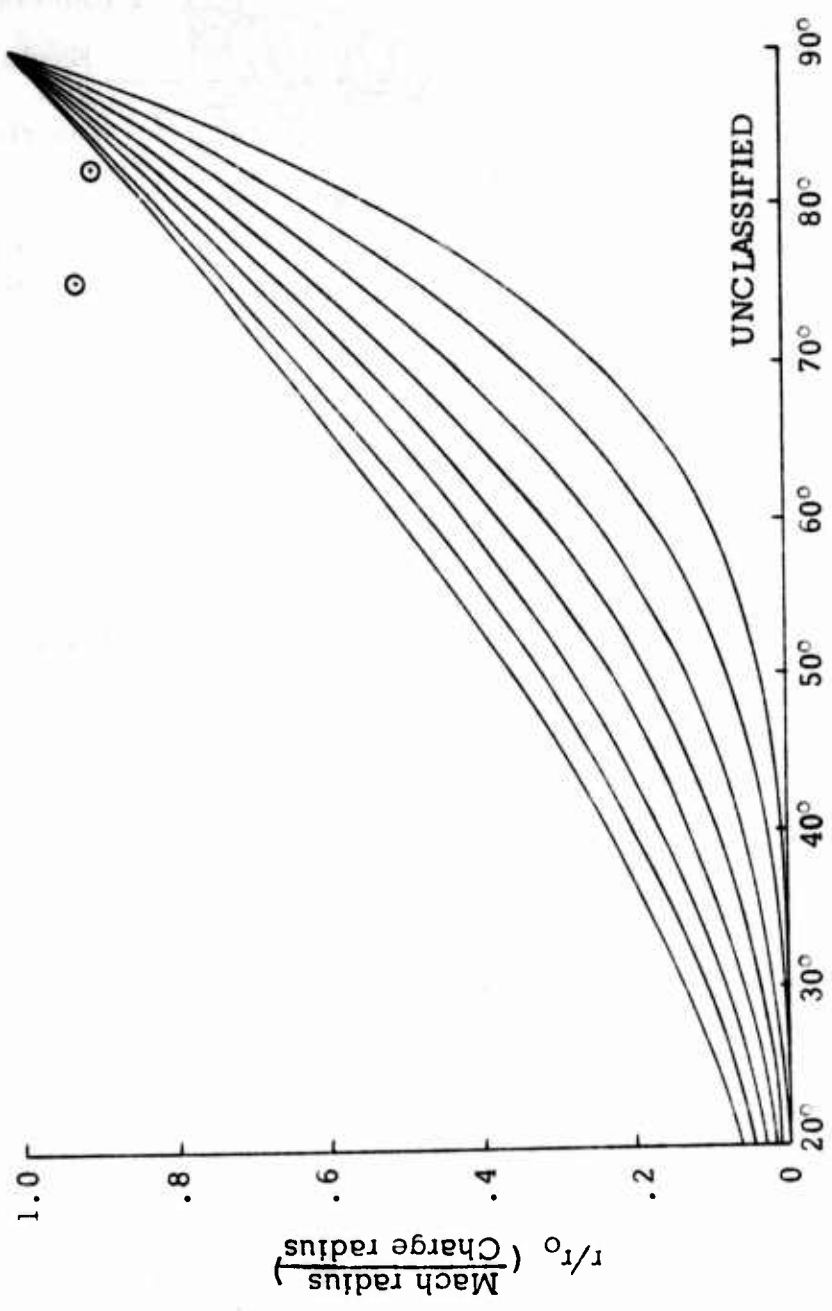
50

(U)   The metal barriers show the smallest initial angles. This indicates that detonation does not occur immediately in the TNT charge as the shock from the A-2 passes through the barrier. Therefore the initial angle must be calculated by means of Eqn. (39).

(U)   The results obtained when Comp B is the inner explosive and Octol is the outer charge, are entirely different. Nearly all of the initial angles are equal to or greater than the calculated angle. This indicates that detonation in the Comp B occurs immediately when the shock enters from the barrier.

(U)   This result is very plausible when it is considered that the threshold for initiation of detonation in the two explosives is very nearly the same, namely, approximately 100 kilobars. However, the Octol outer explosive for the Comp B-Octol experiments was significantly more powerful than the A-2 used for the TNT tests. Furthermore, A-2 explosive can be obtained in thin sheets while the Octol must be cast in place. Hence, the thickness of the Octol was several times that of the A-2.

(U)   When TNT is tested with Octol as the outer charge, it can be seen in Table III that the experimental initial angles both with and without a barrier are larger than the theoretical value and approximately equal to each other.

(U)   The most important general prediction of the theory, namely that the size of the Mach region varies in proportion to the initial angle, seems to hold fairly well for the cases in which no barrier is used. The appropriate K value appears to lie between .5 and 1.0.

     d. Additional Predictions of the Theory

(U)   The theory developed here permits estimation of the Mach system characteristics which may be useful in predicting the behavior of Mach driven explosives in such applications as the projection of metal plates. The following discussion assumes that a steady state Mach wave is present and that detonation of the inner explosive begins immediately at its interface with the outer explosive. The results are expressed in terms of the ratio of the detonation velocity of the inner explosive to that of the outer explosive, i.e. (D_I/D_O). No account is taken of the thickness of the Mach wave. It was merely assumed that the thickness is sufficient to provide nearly constant conditions over the interval of interest.

(U)   The interesting Mach parameters which may be estimated from the present theory include the pressure ratio, P/P_{cj}, the particle velocity ratio, U/U_{cj}, the detonation velocity ratio, D/D_{cj}, and the Mach disc area ratio $(r/r_o)^2$. The symbols without subscripts refer to the Mach parameter. Those with the subscript cj refer to the normal detonation. It is of interest to show how some of these ratios vary as a function of

51

the ratio of detonation velocities of the inner and outer explosives. Figure 15 shows the variation of P/P_{cj} as a function of $/D_I/D_O)$.

(U)   A measure of the force available to accelerate a metal plate can be obtained by computing the parameter $P/P_{cj} (r/r_O)^2$. This is shown in Figure 16. A measure of the relative momentum in the Mach wave $(P/P_{cj})_x (U/U_{cj})$ vs (D_I/D_O) is given for TNT and Comp B in Figures 17 and 18.

(U)   The same momentum ratio parameter multiplied by $(r/r_O)^2$ provides a number reflecting the effect of the smaller diameter of the Mach wave. This parameter is given in Figures 19 and 20. It is apparent from these graphs that the wave parameters in the Mach wave increases significantly as the ratio (D_I/D_O) decreases.

52
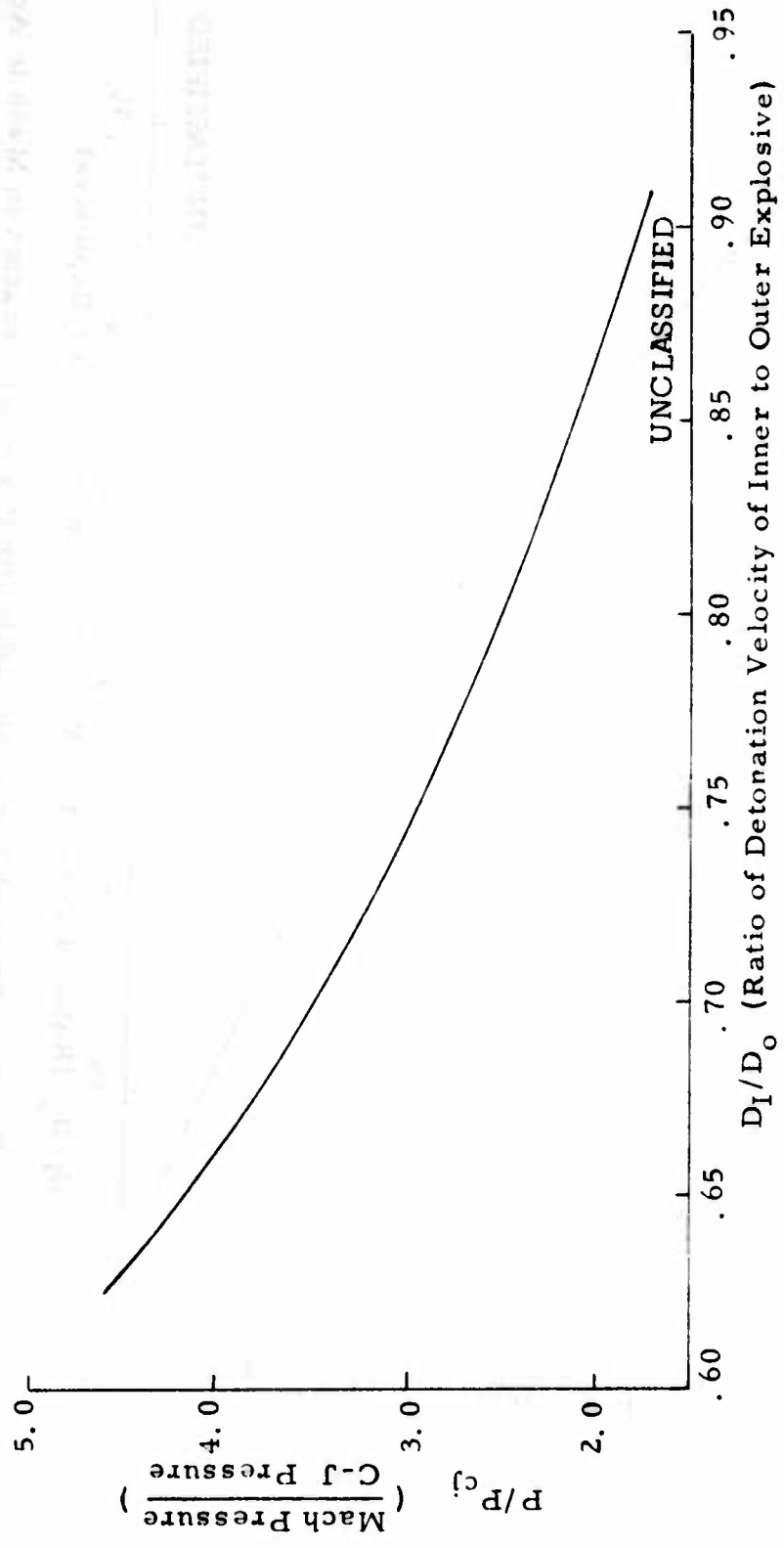
Figure 15. Graph of Ratio of Mach Wave Pressure to C-J Pressure vs Ratio of Detonation Velocities of Inner to Outer Explosive for Any Explosive as Inner Explosive

53
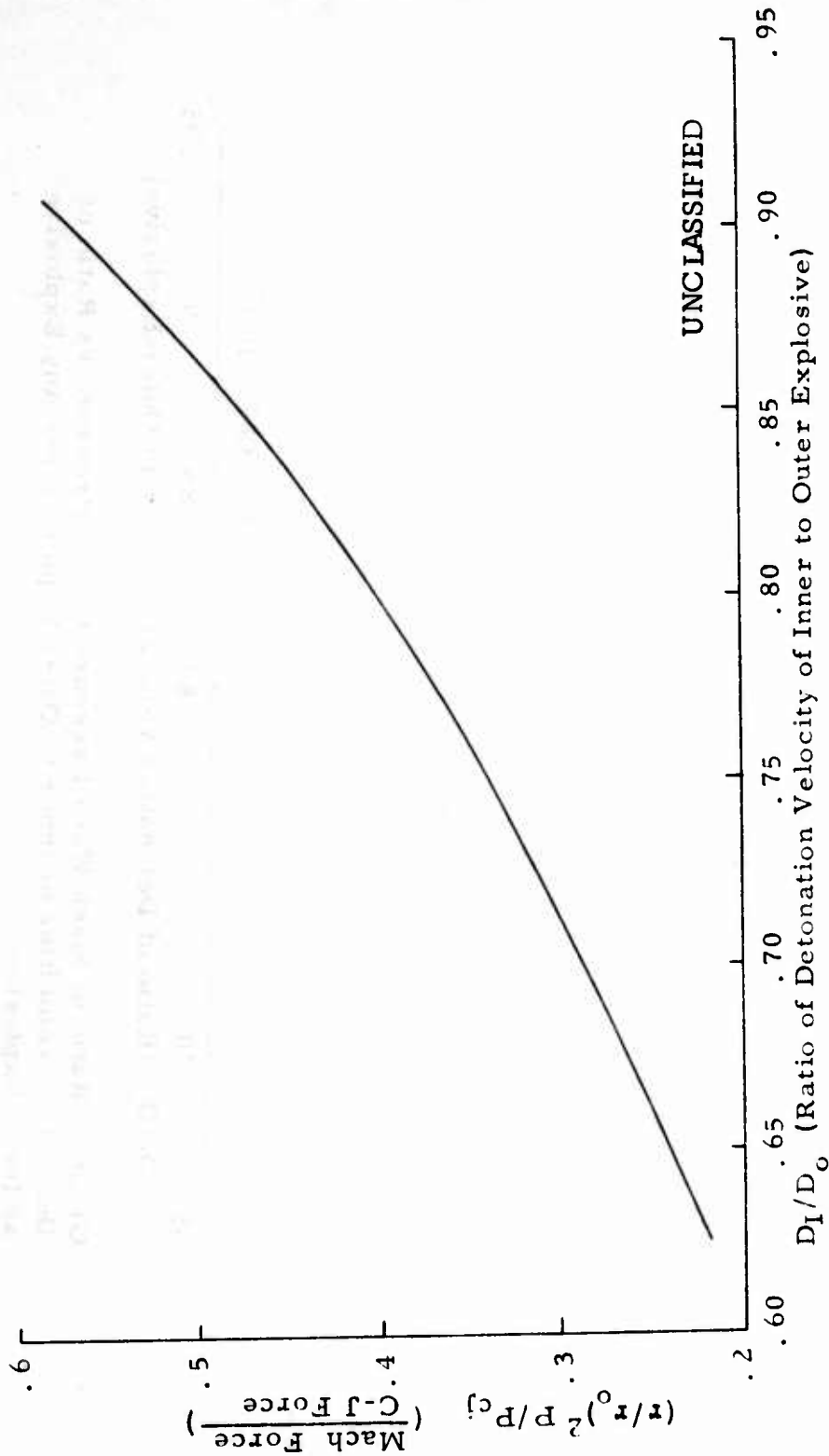
Figure 16. Graph of Ratio of Force Available for Plate Acceleration in Mach to Acceleration Force Available from C-J Wave Over Entire End Area of Charge vs Ratio of Detonation Velocity of Inner to Outer Explosive for Any Explosive as Inner Explosive

54
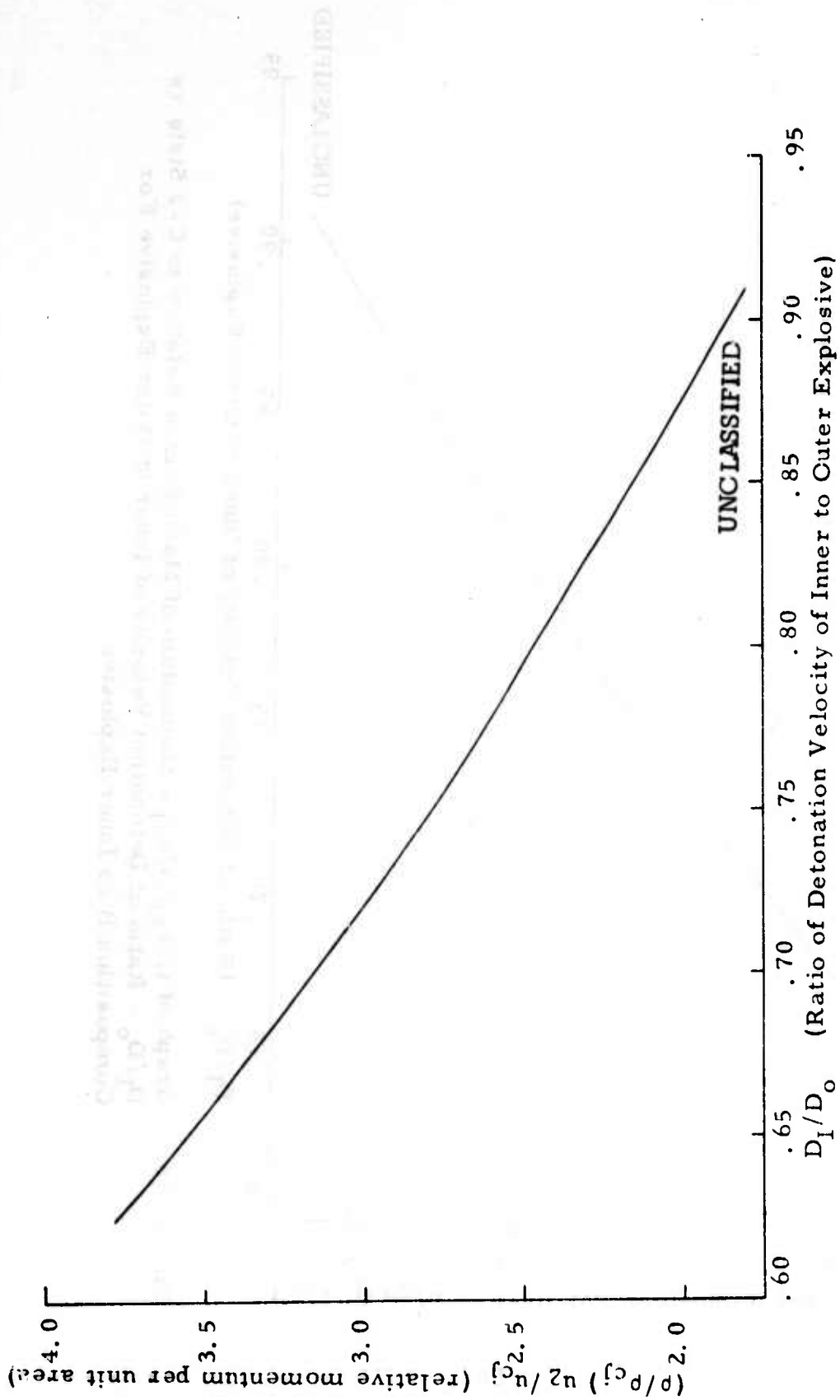
Figure 17. Graph of $(\rho/\rho_{cj})\, u/u_{cj}$ - Momentum of Mach Region Relative to C-J State vs D_I/D_o - Ratio of Detonation Velocity of Inner to Outer Explosive for TNT as Inner Explosive
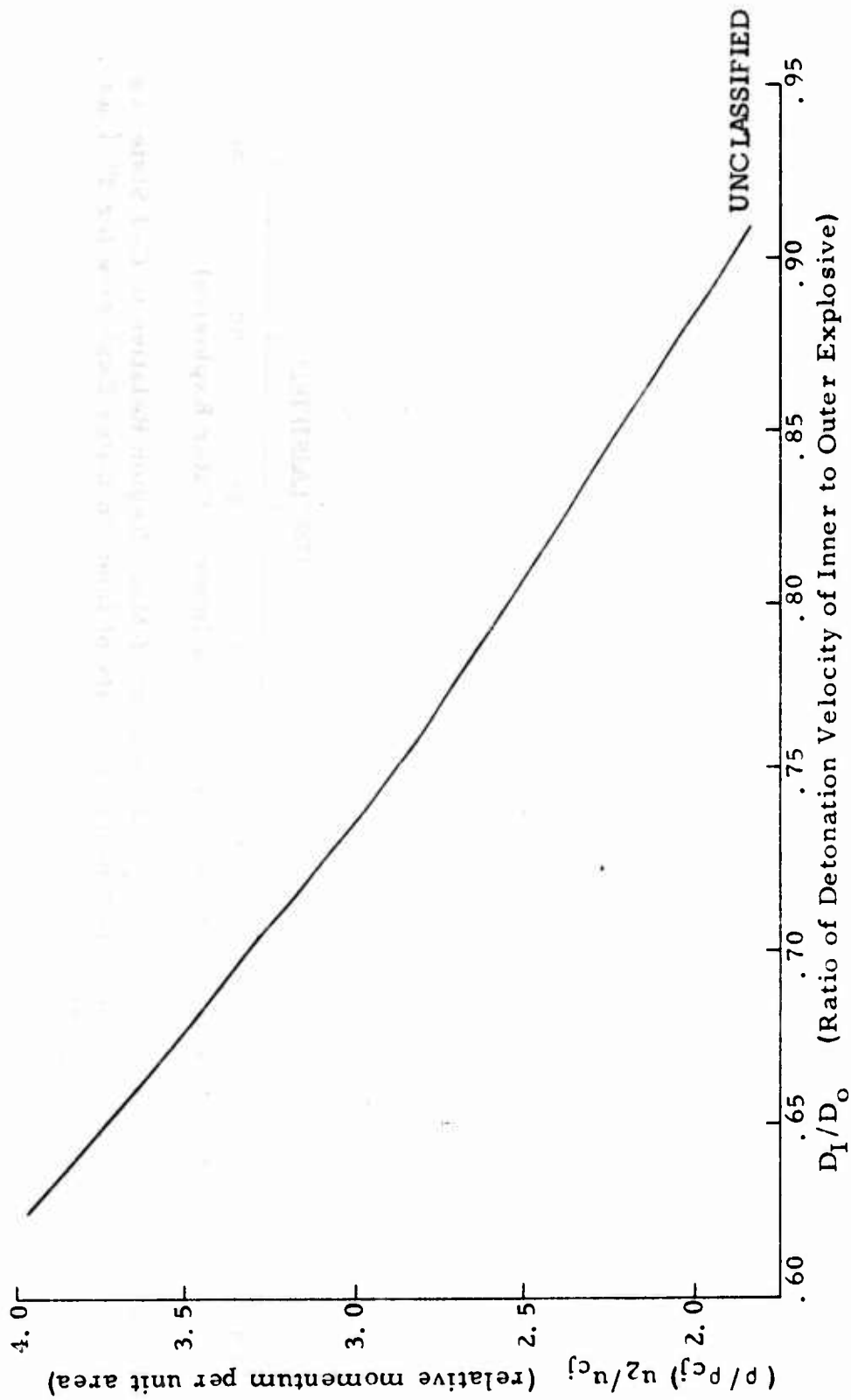
Figure 18. Graph of (ρ/ρ_{cj}) u/u_{cj} - Momentum of Mach Region Relative to C-J State vs D_I/D_o - Ratio of Detonation Velocity of Inner to Outer Explosive For Composition B as Inner Explosive
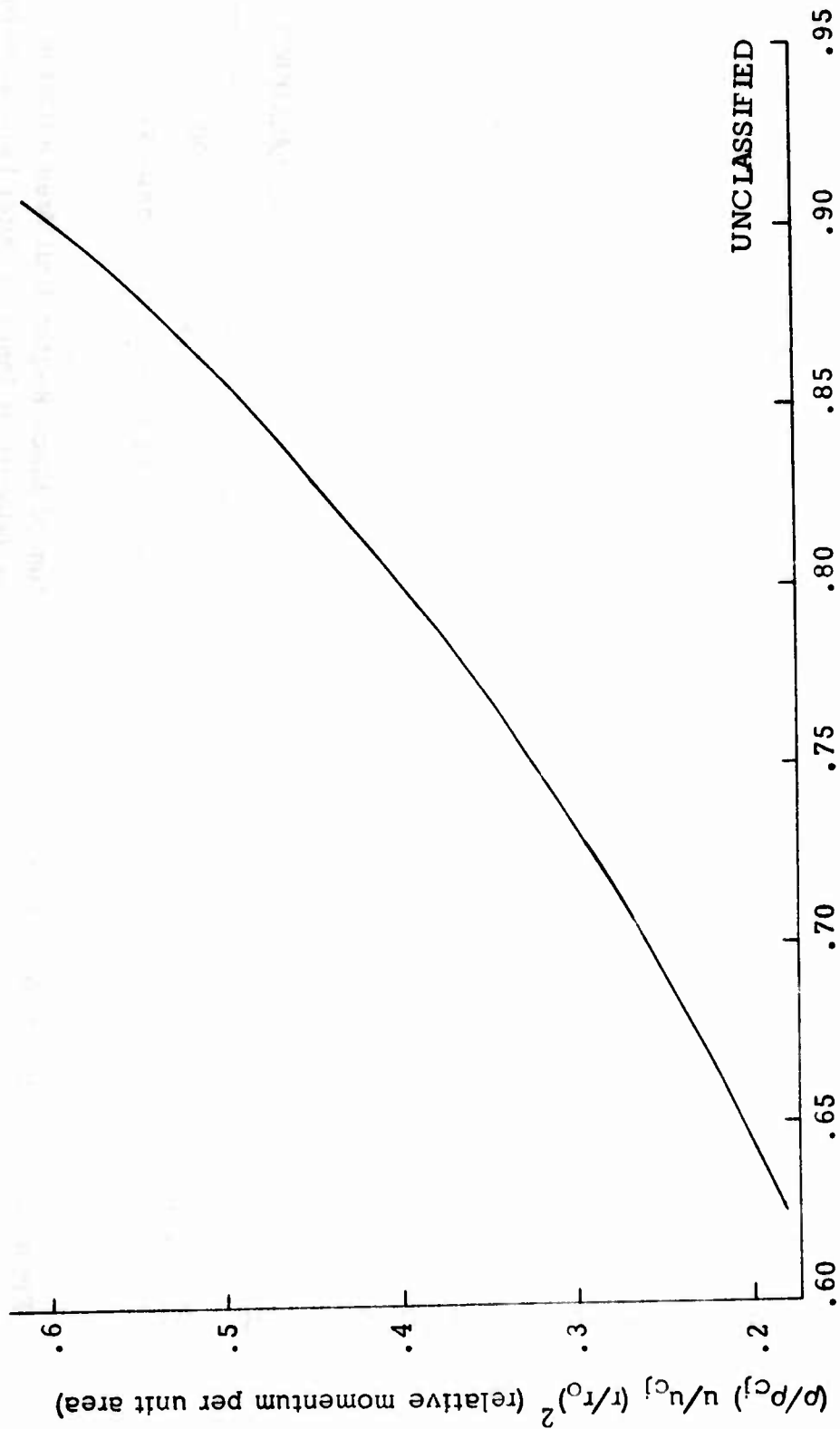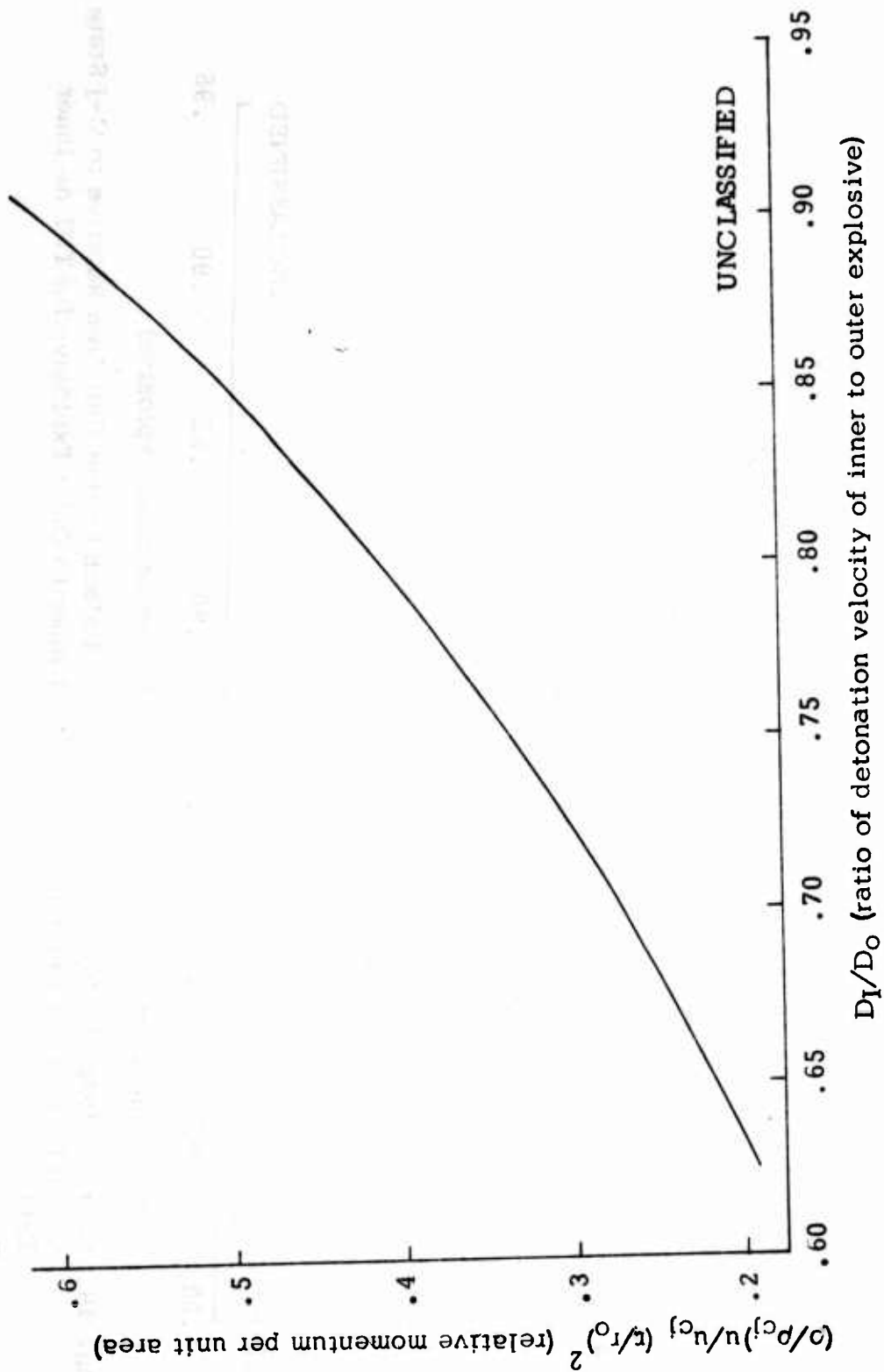
Figure 19. Graph of $(\rho/\rho_{cj})\, u/u_{cj}\, (r/r_o)^2$ Momentum of Mach Region Unit Area Relative to C-J State vs D_I/D_O Ratio of Detonation Velocity of Inner to Outer Explosive for TNT as Inner Explosive.

D_I/D_O (ratio of detonation velocity of inner to outer explosive)

$(\rho/\rho_{cj})\, u/u_{cj}\, (r/r_o)^2$ (relative momentum per unit area)

UNCLASSIFIED

57

Figure 20. Graph of (ρ/ρ_{cj}) u/u_{cj} $(r/r_o)^2$ Momentum of Mach Region Unit Area Relative to C-J State vs D_I/D_O Ratio of Detonation Velocity of Inner to Outer Explosive for Comp B as Inner Explosive.

Axis labels:

X-axis: D_I/D_O (ratio of detonation velocity of inner to outer explosive)

Y-axis: $(\rho/\rho_{cj})u/u_{cj}(r/r_o)^2$ (relative momentum per unit area)

UNCLASSIFIED

58

SECTION III

INITIAL SHAPED CHARGE SCREENING EXPERIMENTS -
NON PRECISION ASSEMBLIES

(U)   In a set of initial screening experiments, a study of the potential application of the convergent wave techniques to shaped charges was undertaken.

(U)   The copper cones used were conventional drawn cones and the bodies used were either steel or plastic, made from commercial stock tubing. These cone and body combinations were assembled with the proper care required for shaped charge assemblies. Machined mandrels were used to align the cones within the bodies and precautions were taken to maintain concentricity of the entire assembly. Thus, while the components used were not precision machined, the assembly operations followed the proper careful practices.

(U)   Two sizes of cones, two body materials and two inner explosive charges were selected for the basic shaped charge assemblies in order to explore a useful range of parameters. The cone and body details are shown in Figures 21 and 22 . Experiments were carried out with and without the outer annular charge. In all cases the outer annular charge was Detasheet A-2 having an areal density of 2 gms/in^2. This assembly is shown in Figure 23.

(U)   The particular selections of basic shaped charge combinations used on the experiments are shown in Table V . It should be noted that all cast charges were X-rayed prior to use. If significant defects were observed, the charges were discarded. The target consisted of a stack of 1/4" thick flat mild steel plates (hardness Rb 64). The standoff range extended from one to seven cone diameters.

(U)   Table V summarizes both the experimental configurations used and the experimental results obtained. The experimental penetration-standoff data for these screening experiments is shown in Figures 24a and 24b.

1.   CONCLUSIONS DRAWN FROM THE SCREENING EXPERIMENTS

(U)   Analysis of the data given in Table V provides the following conclusions:

> 1. Without an annular Detasheet A-2 surround, TNT
> loaded into 1.0" diameter 1/32" wall steel bodies,
> or into 1.0" diameter 1/8" wall phenolic bodies is
> in a marginally subcritical diameter condition and
> fails to propagate the detonation.

59

42°

t = .030 nominal

1.0"

1" Dia. Cone

60°

t = .044 nominal

.25"

1.3"

UNCLASSIFIED

1.3" Dia. Cone
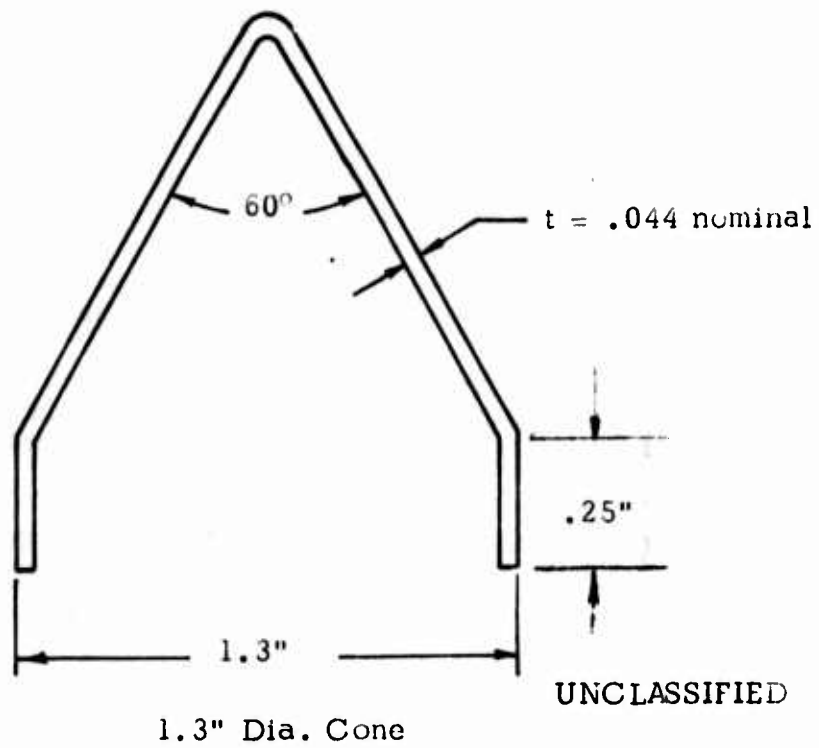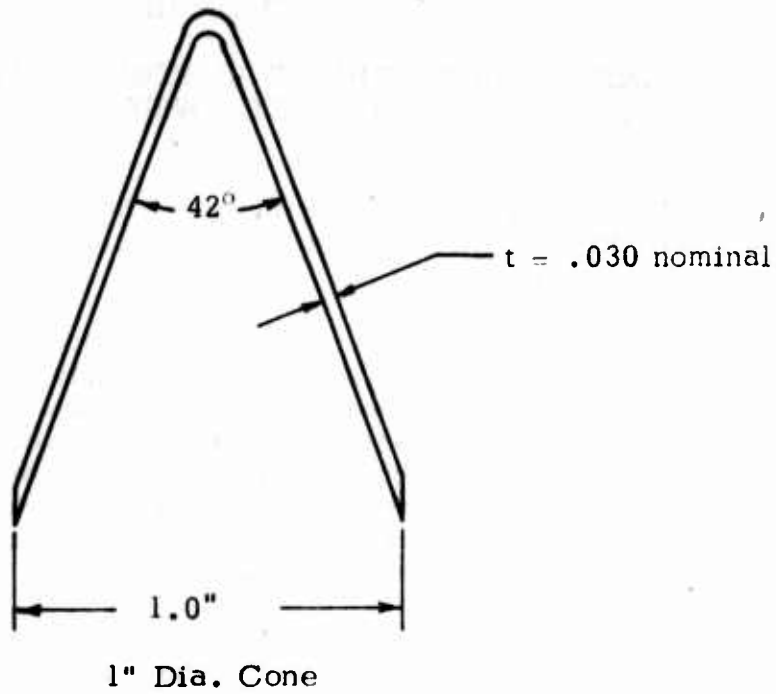
Figure 21.   Nominal Dimensions of Shaped Charge Cones Used
in Screening Experiments.

60

TNT or Comp B

UNCLASSIFIED
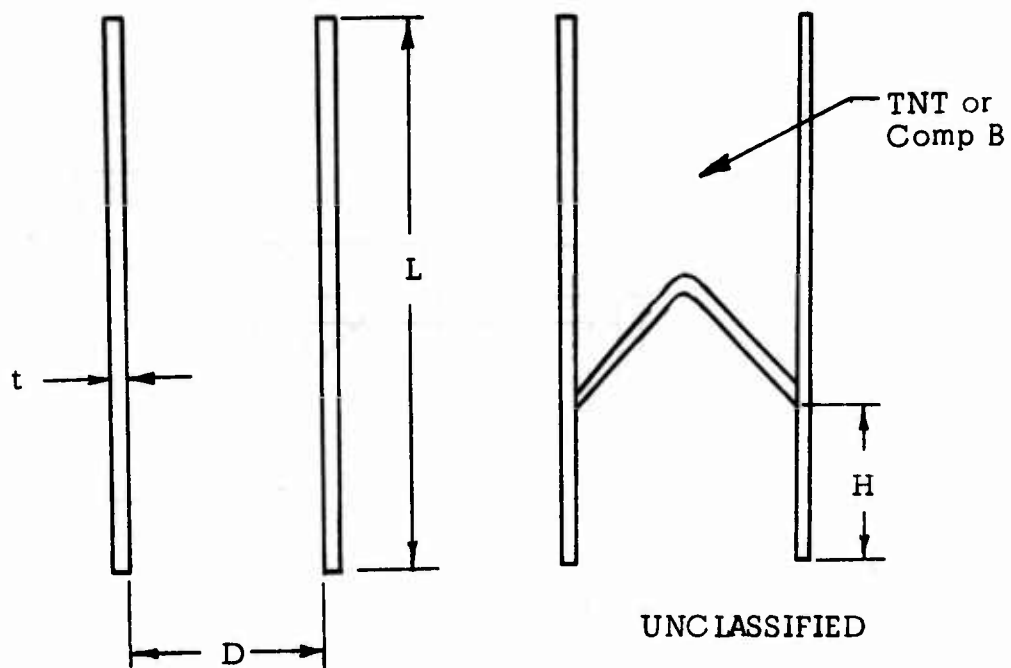
Nominal Cone Parameters	Body Material	Dimension - inches			
		D	H	L	t
1.0" 42°	Steel	1.0	1.06"	4"	1/32"
	Phenolic	1.0	1.06"	4"	1/8"
1.3" 60°	Steel	Not Used In Screening Experiments			
	Phenolic	1.3	1.31"	5.5"	1/16"

UNCLASSIFIED

Figure 22. Description of Bodies and the Basic Shaped Charge Assembly Used in the Screening Shaped Charge Experiments.

61
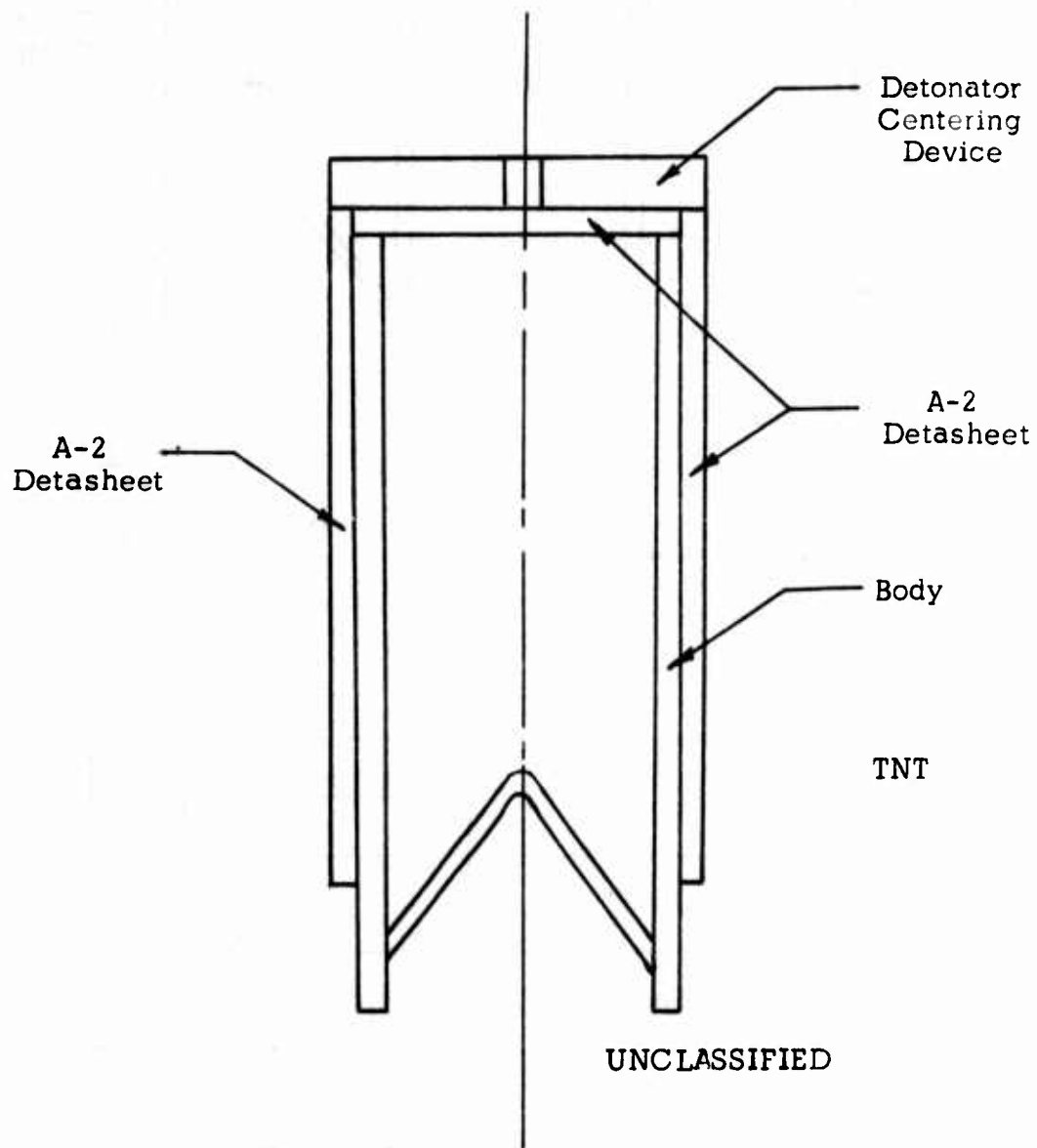
Figure 23. Charge Configuration Used When Adding the Annular A-2 Detasheet Explosive in the Screening Shaped Charge Experiments.

TABLE V. SUMMARY MATRIX OF SHAPED CHARGE EXPERIMENTAL DATA

Inner Explosive Charge	Cone Diameter* 1.0"	1.3"	Casing of Inner Charge — Steel Wall Thickness	Phenolic Plastic Wall Thickness	Outer Charge None	A-2	Cone Diameter Standoff 1D	2D	3D	5D	7D	Average Penetration P inches
TNT	5		1/32"		x		x					**
TNT	2			1/8"	x		x					**
TNT	3		1/32"			x	x					3.20
TNT	3			1/8"		x	x					3.75
TNT		2		1/16"	x		x					**
TNT		3		1/16"		x	x					5.42
TNT		3		1/16"		x			x			6.25
TNT		3		1/16"		x				x		5.33
TNT		3		1/16"		x					x	4.92
Comp B	3		1/32"		x		x					4.04
Comp B	3			1/8"	x		x					4.20
Comp B	2		1/32"			x	x					3.56
Comp B	2			1/8"		x	x					3.25
Comp B		12		1/16"	x		x					4.75
Comp B		10		1/16"	x			x				5.80
Comp B		3		1/16"		x	x					4.58
Comp B		3	1/8"			x	x					4.08
Comp B		2	1/8"			x	x					4.25
Comp B		3		1/16"	x				x			5.58
Comp B		3		1/16"	x					x		5.83
Comp B		3		1/16"	x						x	2.67

* No. of tests for each cone diameter are listed in these columns.

** Subcritical explosive diameter, incomplete detonation - negligible penetration.

63
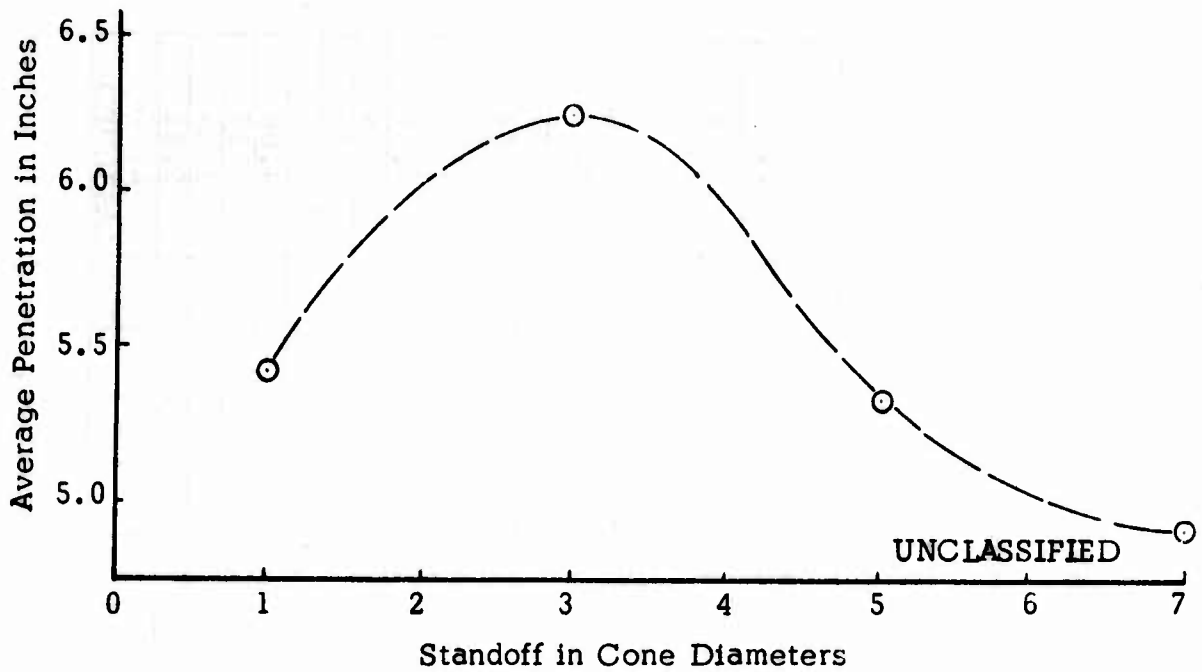
Figure 24a. Penetration Standoff Curve for TNT-A2
Combination in 1/16" Phenolic Body
Cone Diameter 1.3" Nominal.
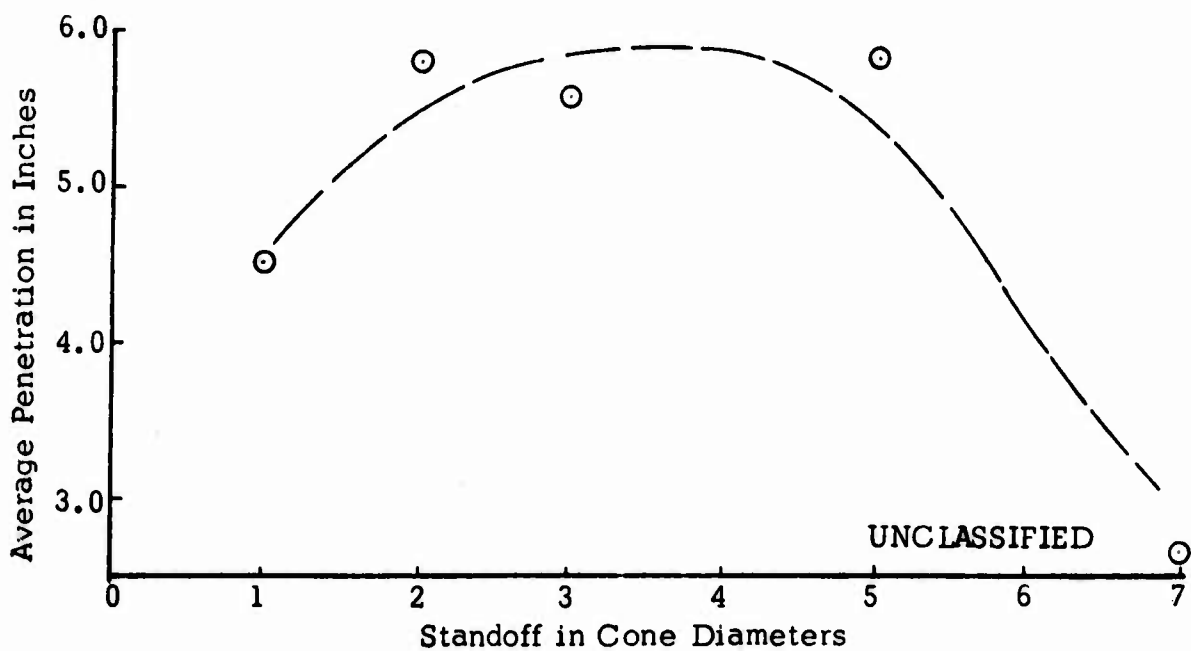
Figure 24b. Penetration Standoff Curve For Simple
Comp B Loaded Shaped Charge in 1/16"
Phenolic Body Cone Diameter 1.3" Nominal.

Figure 24. Standoff-Penetration Curves Comparing TNT Loaded Non-
Precision Shaped Charges Overdriven with A2 Detasheet,
And Similar Simple Comp B Loaded Non-Precision
Shaped Charges.

64

2. TNT when loaded into 1.3" diameter phenolic bodies with a 1/16" wall is also marginally subcritical and fails to propagate the detonation.

3. When provided with the annular Detasheet A-2 both sizes of TNT loaded charges detonate completely and generate penetrating shaped charge jets.

4. Composition B, when loaded into the 1.0 steel bodies with a 1/32" wall and into the 1.3" phenolic bodies with a 1/16" wall, detonates completely, indicating that in both cases, the Composition B is at a supercritical diameter.

5. The penetration-standoff curves generated, show somewhat more than the expected scatter but provide the general form of the relationships which were desired as an output of these screening experiments.

6. The significant comparison evaluates the performance of the TNT charges with the annular A-2 Detasheet relative to the performance of the Composition B charges without the Detasheet. It is evident that the TNT-A-2 charge combination at 3 cone diameters standoff performs at least as well as the Comp B alone. This is very unusual since TNT is appreciably less energetic than Comp B.

7. The initial tentative conclusion drawn from this comparison, is that either the converging wave system or the extra explosive weight (i.e. the added weight of A-2 Detasheet) is responsible for the improvement.

8. Check experiments were therefore carried out using an A-2 surround with the Composition B charges. It was found that the performance of the Composition B was in fact deteriorated by the extra explosive. The conclusion one reaches therefore is that the TNT-A-2 combination must perform better because of the converging wave effects, since Detasheet A-2 has a higher detonation velocity than TNT but a lower detonation velocity than Comp B.

9. The final conclusion reached from these screening experiments was that the proper pursuit of these performance enhancement effects should be carried out with precision assemblies.

10. In addition, it appeared reasonable to expect
that if a proper explosive material could be provided,
having a higher detonation velocity than Comp B,
one might expect to enhance the performance of the
Comp B so that it's penetration would be increased
to a point comparable to that which analogously
might be expected with a much more energetic
explosive than Comp B.

SECTION IV

EXPERIMENTS USING PRECISION SHAPED CHARGE ASSEMBLIES

(U)   Following the initial screening experiments, plans were made to confirm the performance enhancement effect with TNT loaded precision shaped charge assemblies in order to provide better resolution of the results obtained with the Detasheet A-2 outer driver explosive. In addition, a program was planned to attempt to exploit the performance improvement with a Composition B main charge, using PBX 9404 as the faster outer driver explosive.

(U)   The comparative detonation velocity data for the combinations of TNT and A-2 Detasheet, and for the Comp B-PBX9404 combination planned for these experiments is given in the table below.

TABLE VI DETONATION VELOCITIES AND RATIOS FOR THE EXPLOSIVE COMBINATIONS

Combination No.	Explosive	Relative Detonation Velocity	Detonation Velocity (m/sec)	Ratio V_F/V_S
1	TNT	Slow	6784	1.13
	A-2	Fast	7630	
2	Comp B	Slow	7848	1.12
	PBX-9404	Fast	8800	

UNCLASSIFIED

(U)   The precision liner and body assemblies, which were used in the following experiments were specially fabricated for this program by the Marquardt Corporation, to very high precision. They were also assembled to retain the precision in terms of very low eccentricity in the assembly.

(U)   The fabrication drawings of the cones and bodies are shown in Figures 25 and 26 . The cones were machined down from the same basic drawn copper cones originally provided by Picatinny Arsenal and used in the screening experiments without modification.

67

Basic Preform Data

UNCLASSIFIED
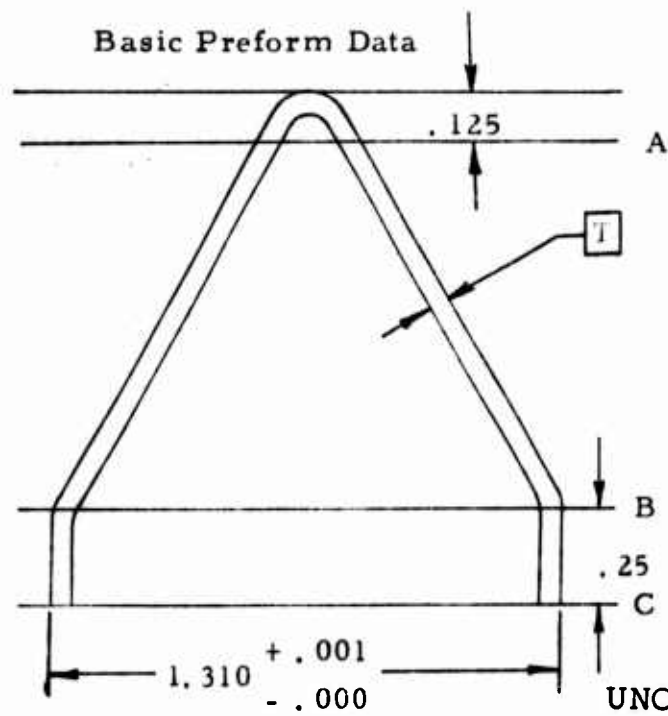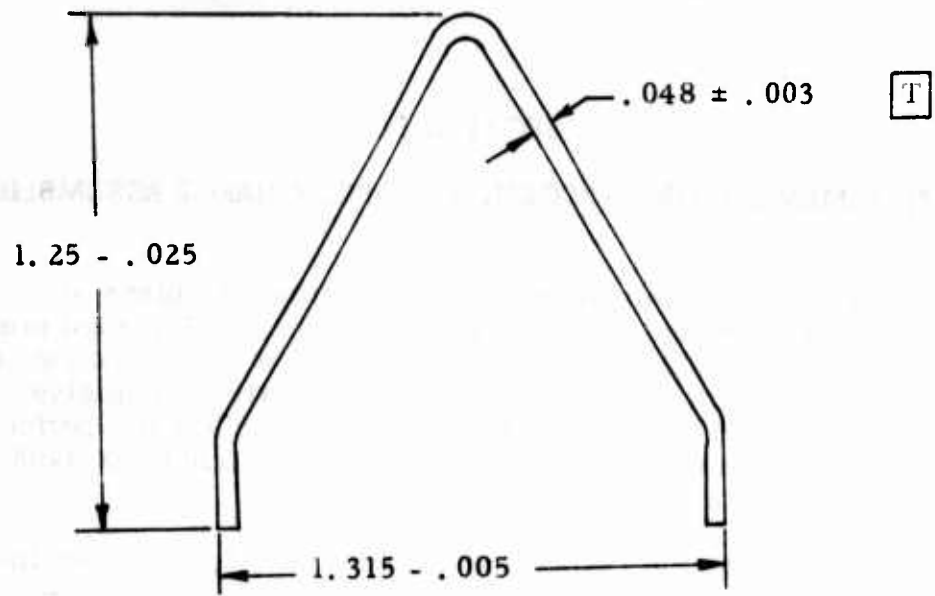
$\boxed{T}$ = .044 ± .0002 over 360° region defined
between planes A and B. For portions
outside of defined region, T = .004 ± .001.

Final Precision Cones

Figure 25. Basic Preform Data and Final Precision Cone Dimensions
and Tolerances

68
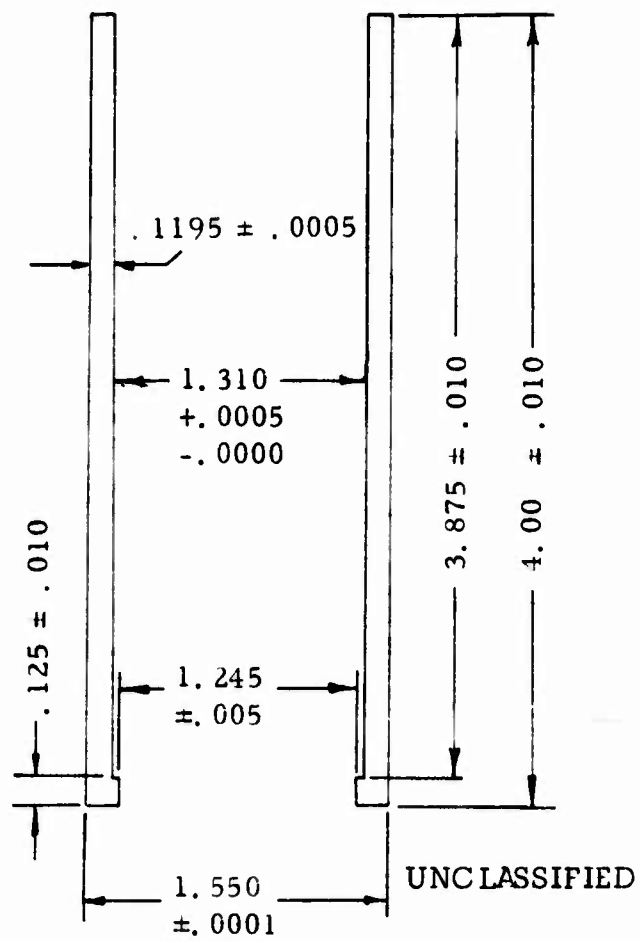
Figure 26. Dimensions and Tolerances for Precision Steel Bodies

(U)   The cone-body assemblies were very carefully assembled and
checked for eccentricity after assembly. The measured eccentricity
between the external surface of the precision cone and the internal sur-
face of the precision body, at the locations shown in Figure 27 was
checked to be less than ± .0005".

(U)   The precision assemblies were melt loaded with TNT and with
Composition B. In all cases, the charges were X-rayed following
loading and any charges showning significant deviation from good
quality casting were not used in the experiments.

1.   PERFORMANCE EVALUATION OF BASIC SHAPED CHARGE
ASSEMBLIES

(U)   The basic shaped charge assemblies loaded with TNT, even
when assembled in the heavier precision steel bodies, showed marginal
propagation performance and yielded very poor penetration data, indica-
ting either lack of jet formation or a fading detonation.

(U)   The charges loaded with Composition B showed excellent per-
formance. The standoff penetration curve obtained with the Comp B
loaded precision charges is shown in Figure 28 as the solid line.

2.   EVALUATION OF THE TNT-A2 COMBINATION WITH
PRECISION ASSEMBLIES

(U)   The crucial experiments to verify the improved performance of
the TNT loaded precision assemblies with the A-2 Detasheet external
driving explosive were also carried out. The results obtained were
even better than those observed in the screening experiments. The
penetration-standoff data at 3 different standoffs, for the TNT-A2 com-
bination (Fig. 29) is shown superimposed on the Comp B curve in Figure
28. It is evident that the TNT, which as previously noted, doesn't even
detonate properly in the basic configuration, has been overdriven by the
external A-2 explosive driver to the point where it not only detonates
completely but also generates shaped charge jets whose performance is
at least as good as those from Comp B loaded charges. In view of
the large differences in detonation energy and the even larger differences
in detonation pressure, this represents a very unusual performance. A
flash X-ray of a typical shaped charge jet obtained with the TNT charges
overdriven with A-2 Detasheet is shown in Figure 30.

a. Attempts to Overdrive Comp B

(U)   The successful verification of the performance enhancement with
the overdriven TNT precision shaped charges, naturally led to the
experiments aimed at obtaining a comparable improvement by over-
driving Composition B loaded shaped charges.

70
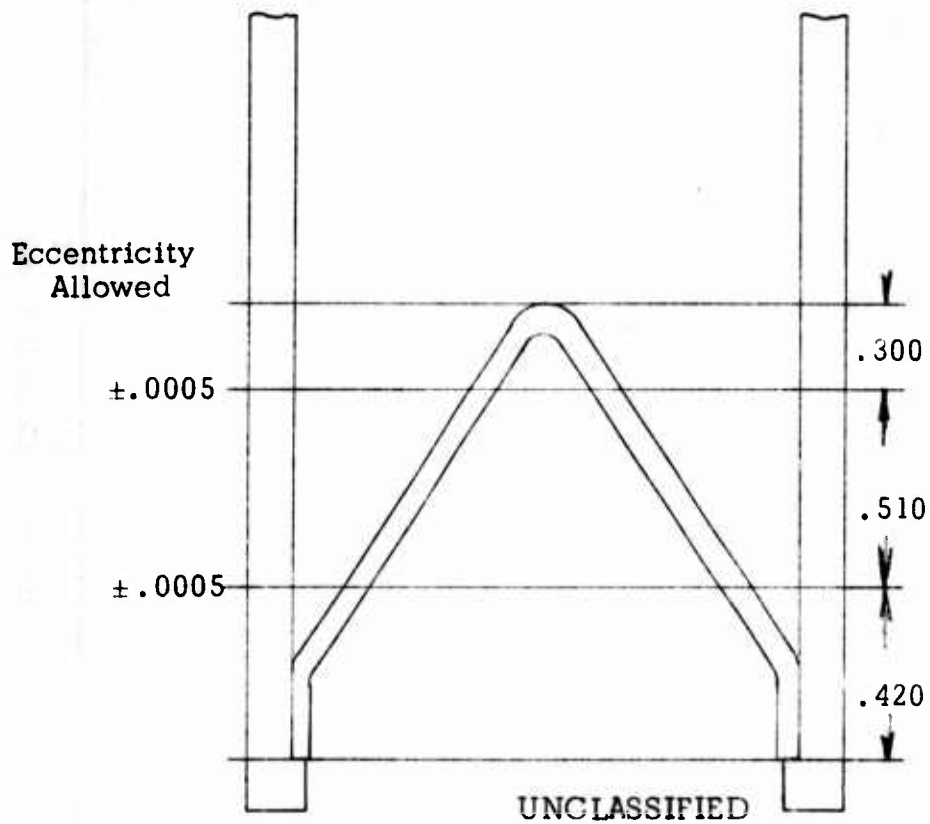
Figure 27. Maximum Eccentricity Permitted Between Assembled
Body and Cone at Planes Indicated, For Precision
Shaped Charge Assemblies
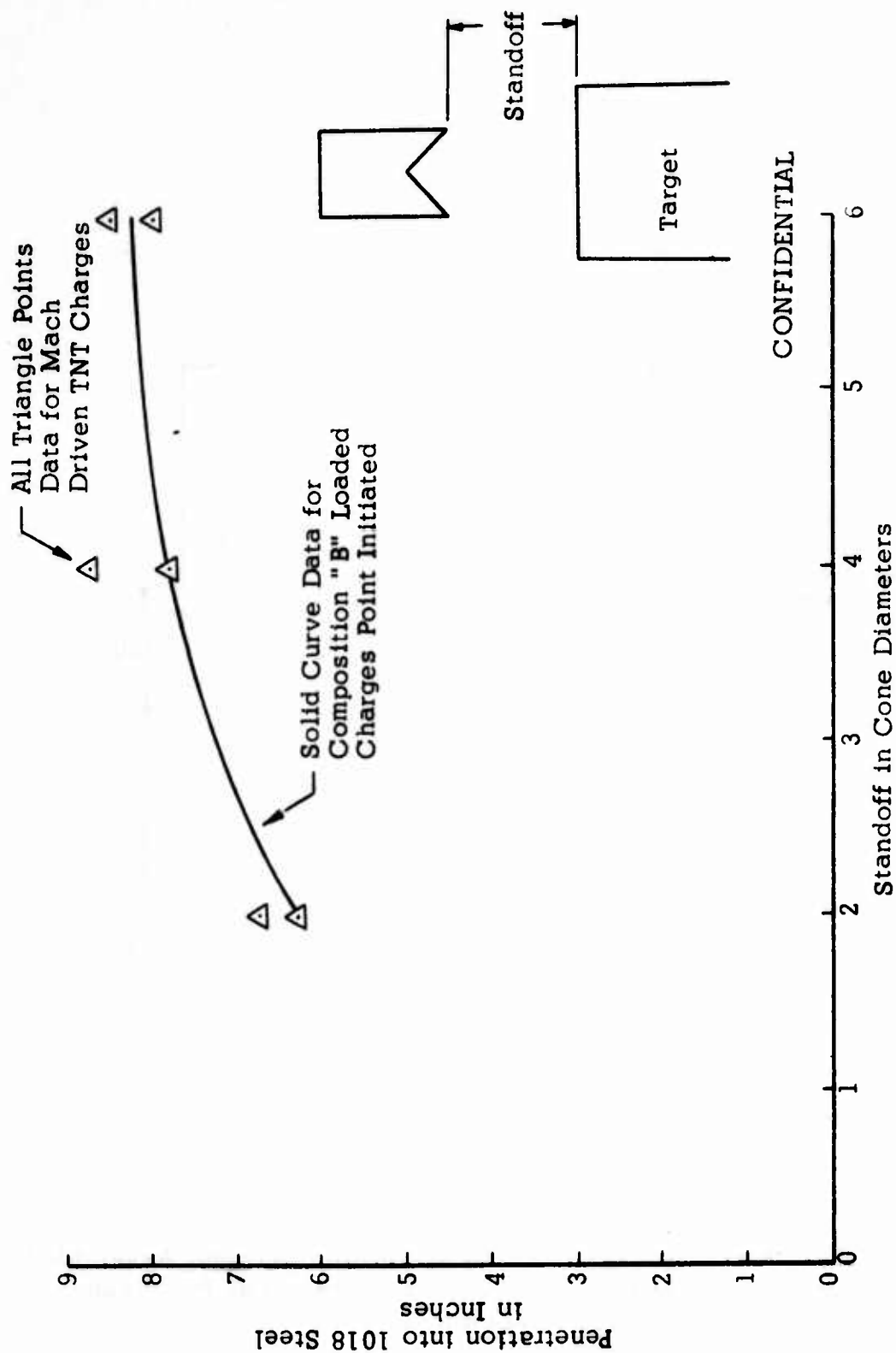
Figure 28. Comparison of Penetration Performance of Precision Shaped Charges Loaded with Comp "B" and Mach Driven TNT.
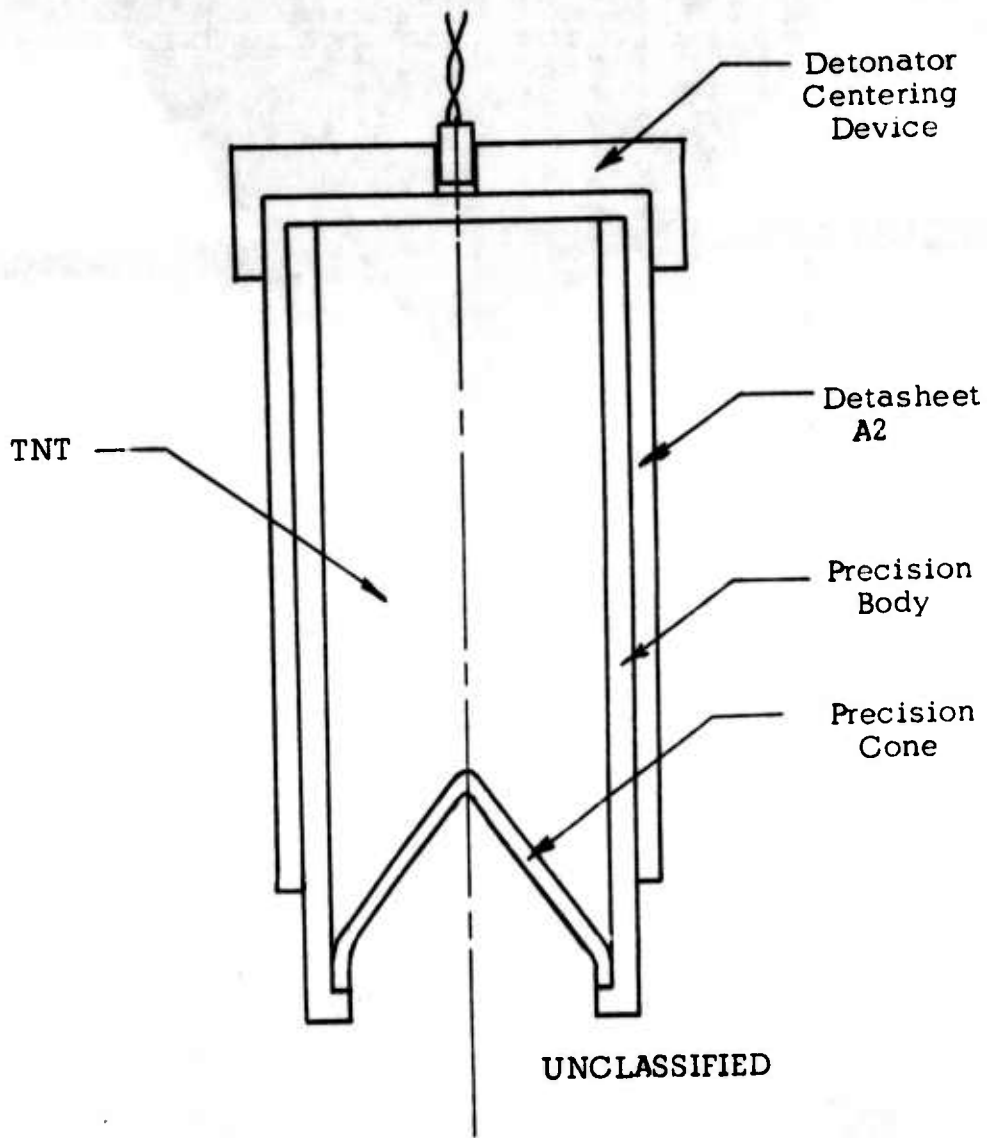
Figure 29. The Experimental Configuration Used for Obtaining the TNT-A2 Overdriven Standoff-Penetration Performance with Precision Assemblies.
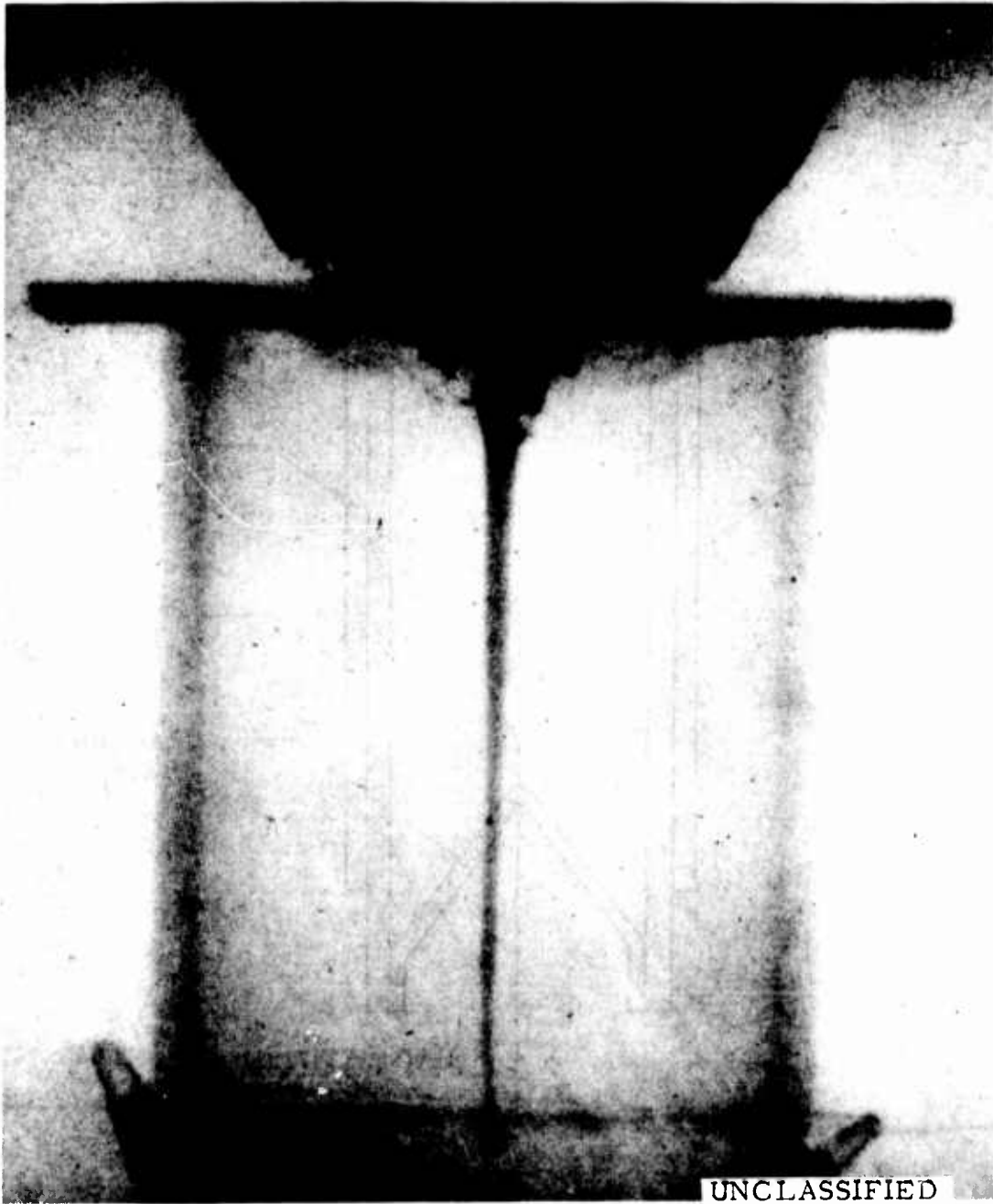
Figure 30. Flash Radiograph of Jet Obtained From TNT
Loaded Shaped Charge Overdriven with
Detasheet A-2.

(U)   Annular charges of PBX-9404 were designed and submitted to Picatinny Arsenal which undertook to fabricate them. The annular charge drawing is shown in Figure 31.

0.25"

4.00"

1.556"

2.056"
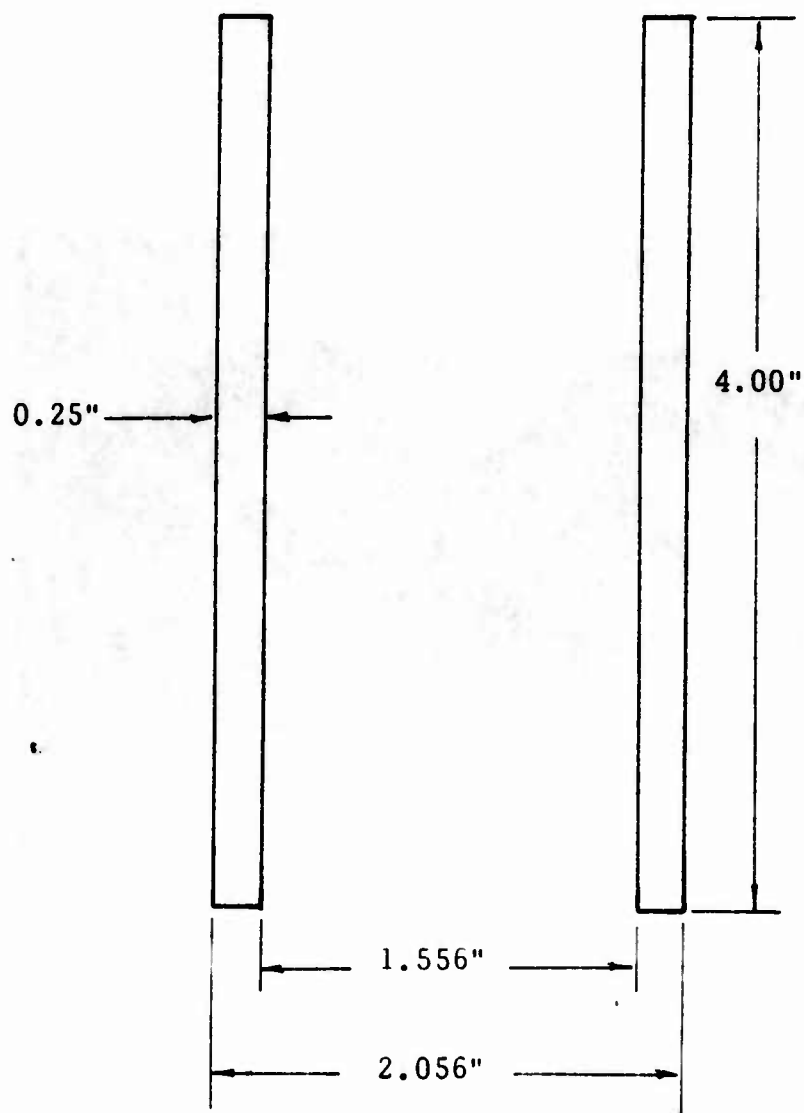
UNCLASSIFIED

Figure 31.   Annular Charge of PBX-9404 Used in Converging Wave Experiments with Precision Shaped Charge Assemblies.

(U)   When the 9404 annular charges arrived, they were X-rayed and found to be quite uniform.

(U)   It was therefore very dissappointing to find that the penetration performance of the 9404 driven Composition B charges was poorer and more erratic than the performance obtained with the basic Composition B loaded charges. The target plates showed evidence of jet dispersion as shown in Figure 32.

Figure 32. Target Evidence of Jet Dispersion for Composition B Shaped Charges Overdriven by PBX 9404

(U)   Typical penetration performance data with the annular 9404 charge overdriving the Composition B, is shown in Table VII.

    b. Flash Radiography of Jets from Comp B
        Overdriven by PBX-9404

(U)   In view of these poor results, a flash X-ray investigation of these jets was undertaken, in order to ascertain whether any specific structural peculiarities could be observed.

TABLE VII. PENETRATION PERFORMANCE OF COMPOSITION B LOADED PRECISION SHAPED CHARGES OVERDRIVEN WITH PBX-9404

Round No.	Standoff (cone dia.)	Penetration (inches)
1	2	4.0
2	2	5.25
3	2	6.50
4	2	5.00
5	2	5.5
6	4	5.5
7	4	7.25
8	4	1.75
9	4	4.50
10	4	1.25
11	4	2.25
12	4	2.00
13	4	5.00
14	6	8.00
15	6	5.25 UNCLASSIFIED

(U)   The experimental set-up used for the flash X-ray investigation is shown in Figures 33 to 36. Two types of flash X-ray observations were made. The first, was a two flash observation without a target. This turned out to be less useful than the single flash experiment with a target for obtaining penetration data. The experimental set-up for two flash technique is shown in Figure 33 and the associated electronic circuitry is shown in Figure 34. The experimental set-up for single flash observation with a target, is shown in Figure 35 and the associated electronic circuitry is shown in Figure 36.

1/2" Plywood

Film Holder

1/2" Plywood

5/8" Celotex

Charge

Heavy Protection

Foil Switches to
Trigger X-Rays

Heavy Protection
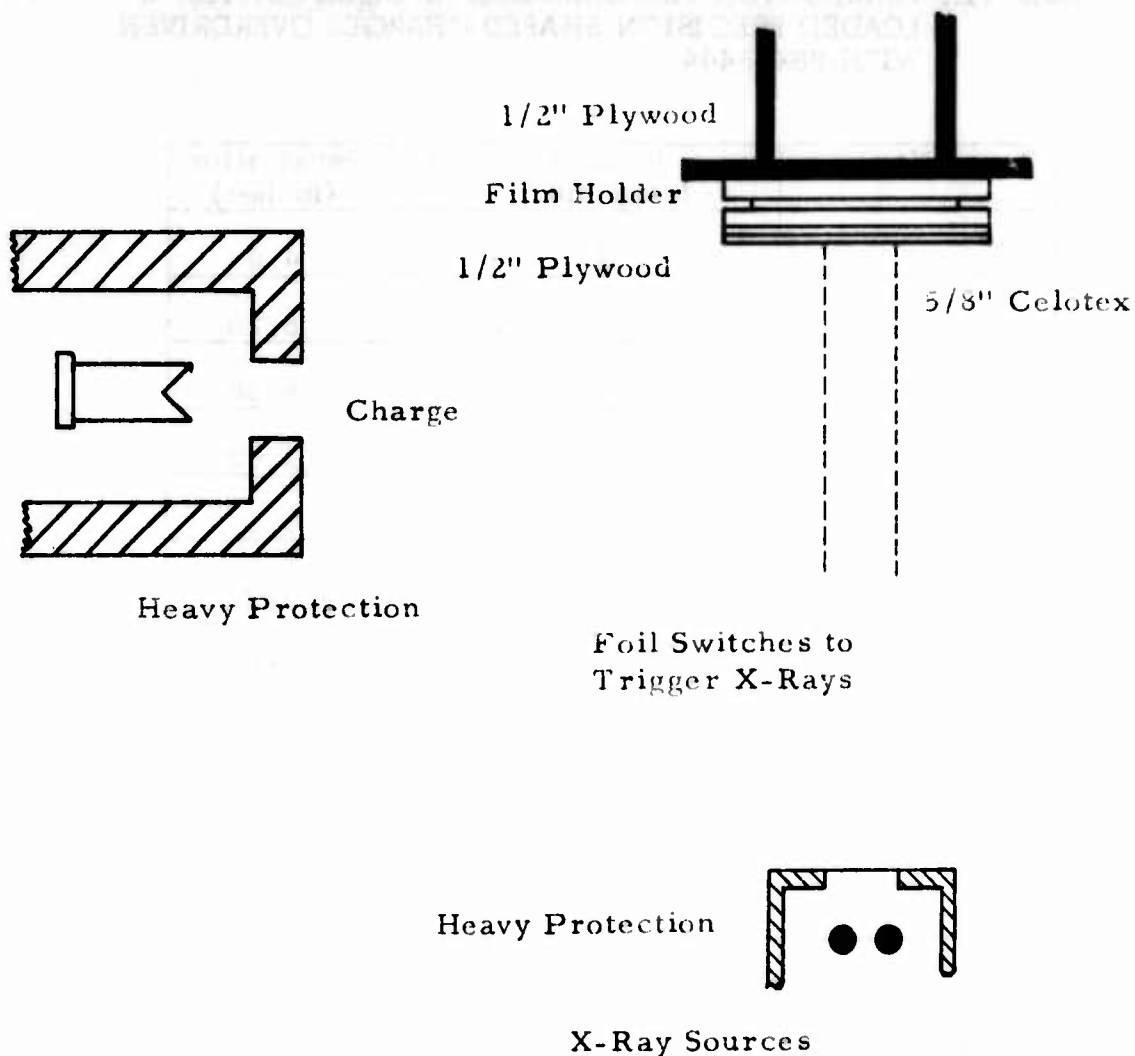
X-Ray Sources

Figure 33. Charge, Film, X-Ray Source and Protection Configuration
Employed in the Double Flash Radiograph of Jet at Long
Standoff

(U)   The flash X-ray study of the jets from Composition B charges
overdriven with PBX-9404 indicated very clearly that the jet was being
disrupted shortly after leaving the collision region on the axis. The
difference is shown very dramatically when a comparison is made of
the jets from a basic Comp B charge and the jet from an overdriven
Comp B charge. This comparison is shown in Figures 37 and 38 for
short standoffs and in Figures 39 and 40 for long standoffs.

(U)   The striking characteristics observed in these comparisons
are:

(1) The disruption occurs primarily over the
forward portion of the jet, being evident
immediately at short standoff.

78
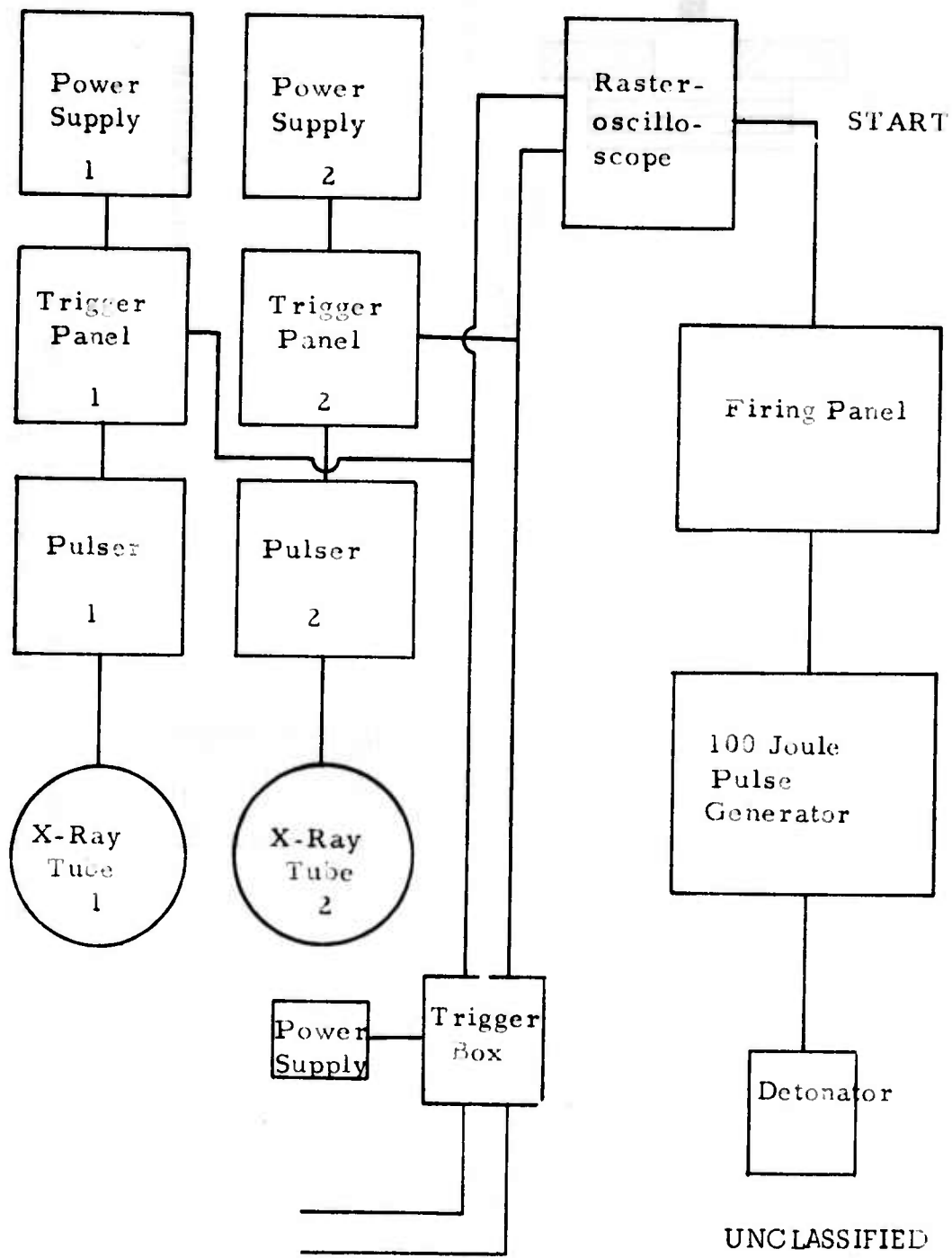
Figure 34.   Electronic Configuration Employed in
Double Flash Radiographs

79

X-Ray Source

1" Steel

4 - 1/4" Aluminum Projection

Charge

Foil Switch

Target Stack 1/4" Steel Plates

1-1/2" Steel

Film Holder   1/3" Glass

Sponge Rubber

1" Steel Box

UNCLASSIFIED

80
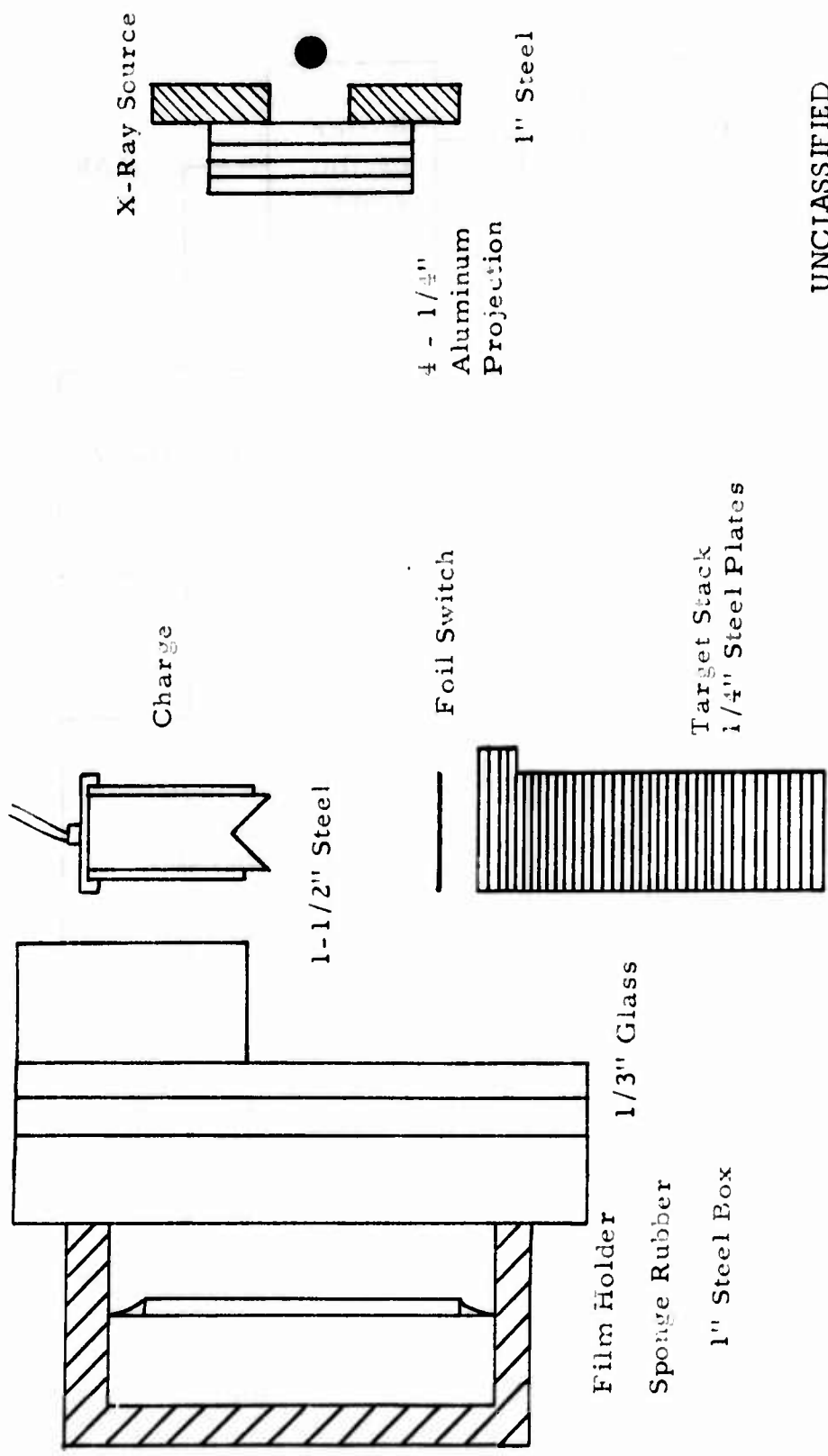
Figure 3c.   Configuration of Charge, Film, Protection and X-Ray Source Employed in Single Flash Radiographs
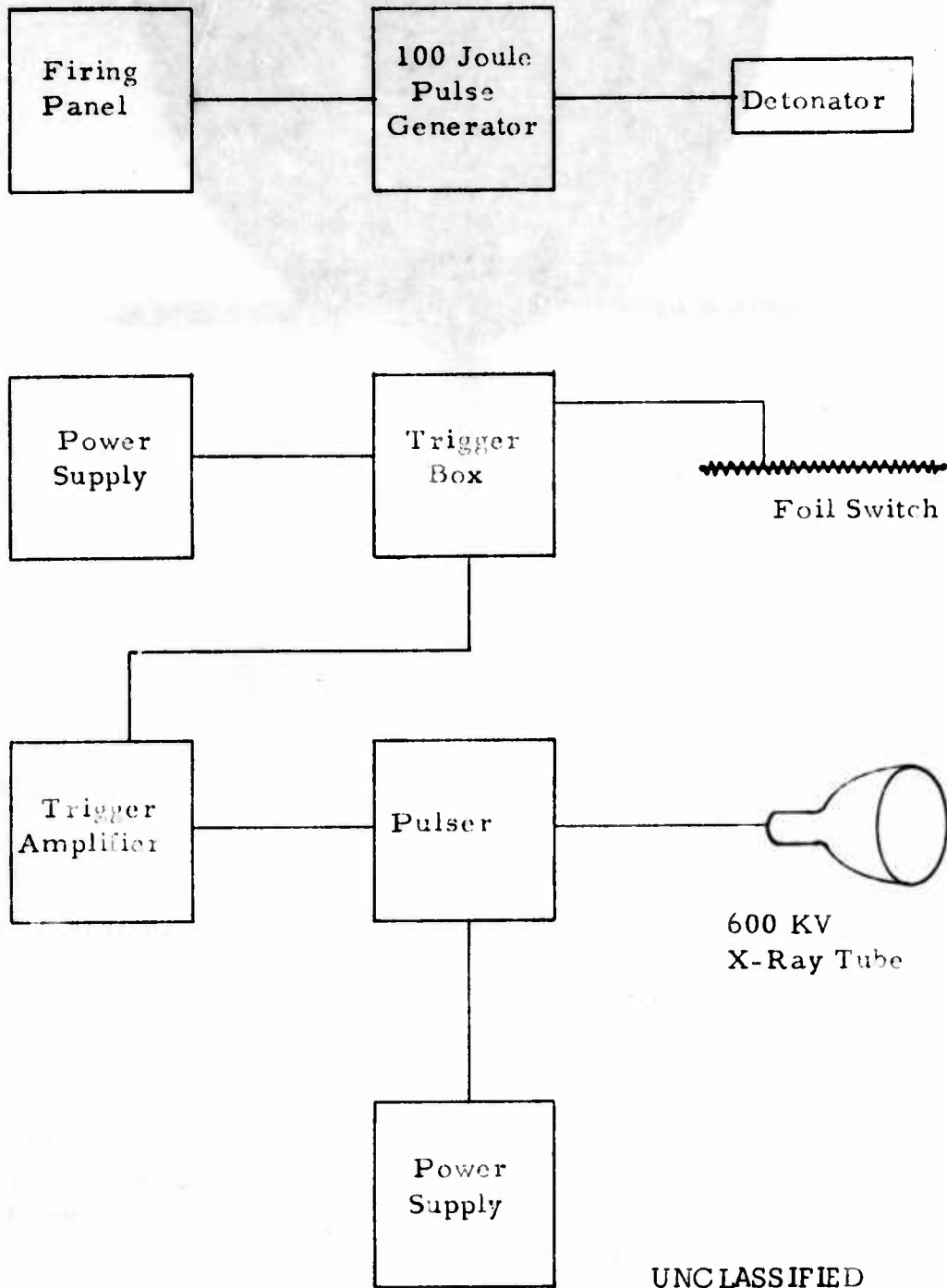
Figure 36. Electronic Configuration Employed in Single Flash Radiographs

81

UNCLASSIFIED
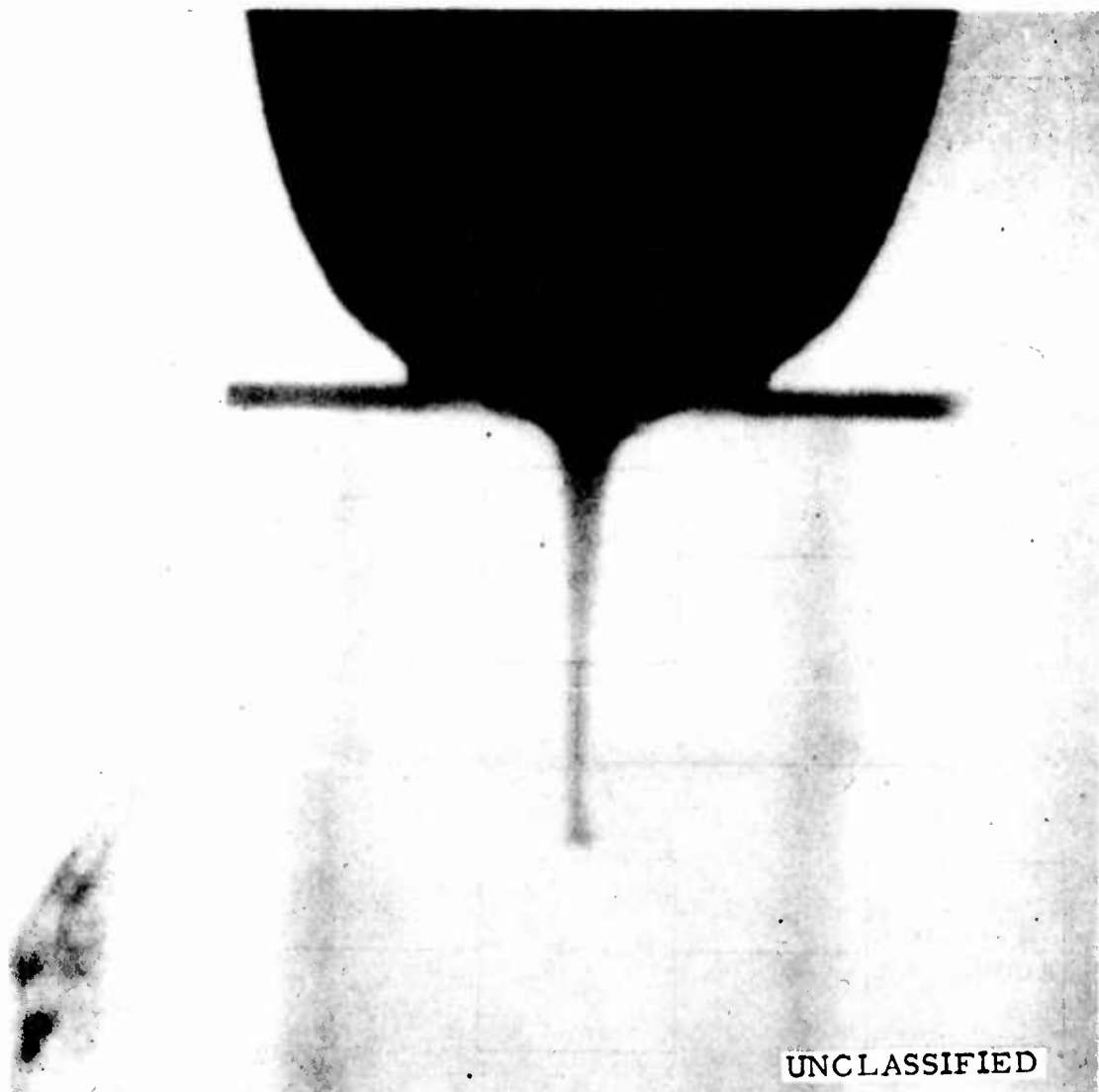
Figure 37.   Flash Radiograph of Jet Obtained at Short Standoff From
A Precision Shaped Charge Assembly With A Simple
Composition B Charge. There was no External Over-
Driving Charge Used.   Note the Well Formed Undisturbed
Jet in Contrast With Figure 38.

UNCLASSIFIED

Figure 38. Flash Radiograph of Jet Obtained at Short Standoff
From A Precision Shaped Charge Assembly With
A Composition B Charge Overdriven by An External
PBX 9404 Driver. Note that the Jet is Straight But
Badly Disrupted Over the Forward Half, in
Contrast With Figure 37.

UNCLASSIFIED

Figure 39.   Flash Radiograph of Jet Obtained at Long Standoff
From a Precision Loaded Shaped Charge Assembly
With A Simple Composition B Charge.   There was
no External Charge.   Note the Well Formed,
Straight Jet With Gradual Taper.

Figure 40. Flash Radiograph of Jet Obtained at Long Standoff From Precision Shaped Charge Assembly with a Composition B Charge Overdriven by an External PBX 9404 Driver. Note that Jet is Straight But Disrupted Over the Forward Half.

85

(2) At long standoff, the rear end of the jet seems
to be hardly affected, while the disrupted for-
ward portion still shows evidence of the dis-
turbance.

It is this set of observations that led to the formulation of the hypo-
thesis which suggests a possible explanation.

3. DECOMPRESSION DISRUPTION HYPOTHESIS

a. Basis for the Hopothesis

(U)   In seeking to understand the reasons for the observed jet dis-
ruption at the forward end, and the apparent lack of disturbance at the
rear, the high pressures generated in the cone collapse collision
region by an overdriven detonation represented a possible mechanism.

(U)   The data shown in Table VIII below indicates the higher pres-
sures one would expect to generate by overdriving a given explosive
by means of another explosive having a higher detonation velocity. The
overdriven pressures for TNT and Comp B are estimated for external
drivers of A-2, Octol and PBX-9404.

TABLE VIII. OVERDRIVEN PRESSURES ESTIMATED FOR TNT
AND COMP B, OVERDRIVEN BY A-2, OCTOL
AND PBX 9404

Explosive	Normal Detonation Velocity (m/sec)	Normal Detonation Pressure (kilobars)	Overdriven Detonation Pressure Overdriven Explosive		
			A-2	Octol	9404
TNT	6784	182	336 kb	455 kb	502
Comp B	7848	292	N. A. A-2 slower	499	533
Octol	8476	343			
PBX 9404	8800	390			UNCLASSIFIED

(U)   It is clearly evident from this table that the successful combin-
ation of explosives, i.e. TNT and Detasheet A-2 show the lowest
overdriven pressure, namely 336 kb. It is also evident that both Octol
and PBX-9404 which have been used successfully as single charge
loadings for shaped charges, also show normal detonation pressures
under 400 kilobars. However, all other combinations show overdriven

86

pressures in excess of 450 kilobars. Even Octol, when overdriving TNT, generates an estimated overdriven pressure of 455 kb.

(U)   The Decompression Disruption Hypothesis suggests that the higher overdriven detonation pressures, result in a correspondingly higher pressure in the collision region on the cone axis from which the jet finally emanates.

(U)   The jet undergoes "decompression" upon leaving the collision region. If the internal energy stored in the jet material by compression in the collision region, exceeds the cohesive energy of the jet material, under decompression, the jet will be expected to come apart, as noted in the radiographs. The effect is expected to be most severe for the highest cone collapse velocities and to become less severe as the collapse velocity decreases. This consequence is also consistent with the observation that the forward end of the jet is primarily affected while the rear portion is not.

b. Further Experimental Checks on the Hypothesis

(U)   As a further indirect check of this hypothesis, flash X-ray observations were carried out with Composition B overdriven by Octol, and with TNT overdriven by Octol. In accordance with Table VIII both combinations would be expected to exceed the 336 kb overdriven pressure listed for TNT-A2. In fact, the overdriven pressures would be expected to be 499 kb and 455 kb respectively. Hence, one would expect in both of these cases, to see jet behavior similar to that observed with Comp B overdriven by PBX-9404. Figures 41 and 42 confirm this expectation. These additional data points suggest that the critical overdriven pressure is below 450 kb. Therefore one can tentatively conclude that the critical overdriven pressure lies between 390 kb which characterizes PBX-9404 alone, and 450 kb which is the overdriven pressure for TNT-Octol.

4.   OPTICAL OBSERVATIONS OF POSSIBLE ASYMMETRY IN DETONATION

(U)   While it appeared clear that jet disruption was a major factor in impairing the performance of the Comp B charges overdriven with PBX-9404, a separate investigation was undertaken to determine to what extent detonation asymmetry could also be contributing to the problem.

(U)   The experimental set-up which was used is shown in Figure 43 In principle, an argon gap is provided just forward of the cone, by inserting a transparent plastic fixture with a carefully controlled spacing. As the detonation wave strikes the back surface of the cone, it sends a shock into the cone. This shock emerges into the argon gap and causes it to become illuminated. The diameter of the forward end of the plastic insert to the shaped charge is viewed with time resolution by means of the slit of a streak camera.

87
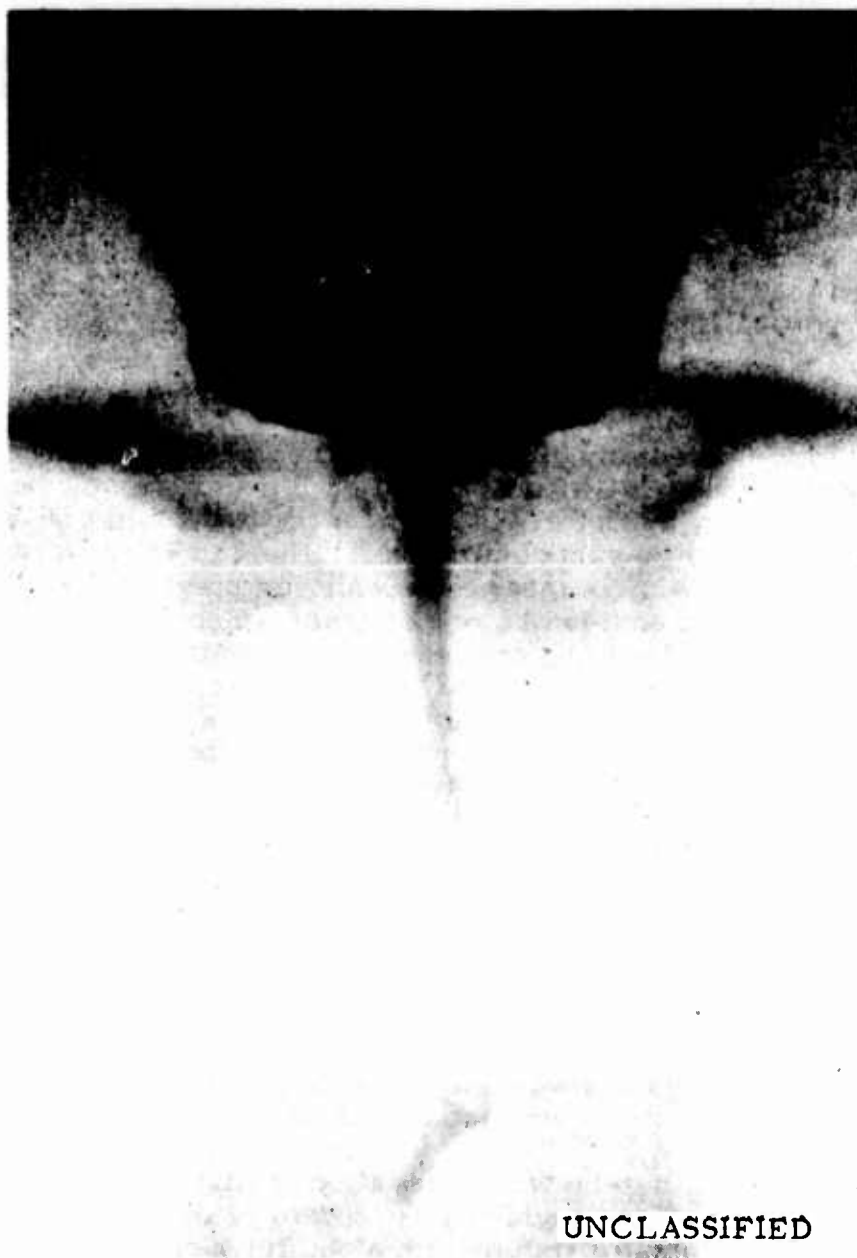
Figure 41.   Flash Radiograph of Jet Obtained From Precision
Shaped Charge Assembly With A Composition B
Charge Overdriven by an External Octol Driver.
Note Disruption of Forward Half of Jet.

88
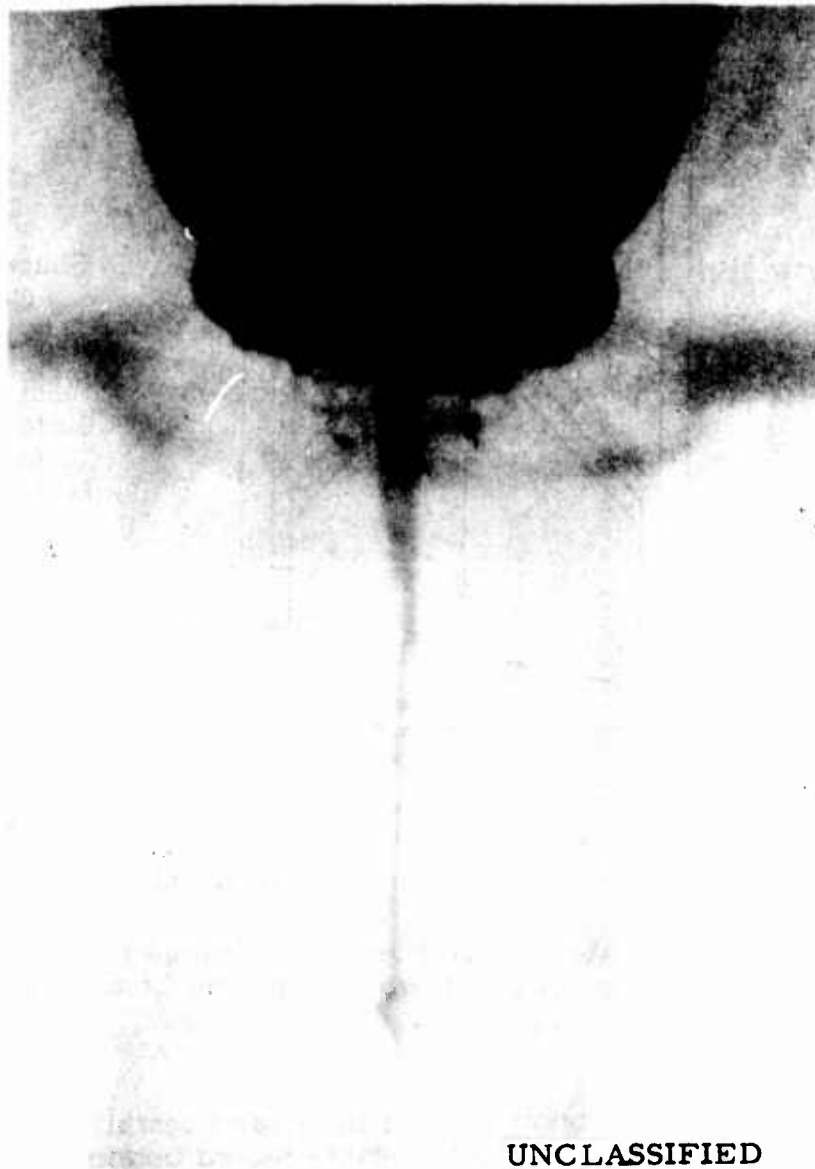
Figure 42. Flash Radiograph of Jet Obtained From Precision Shaped Charge Assembly With TNT Charge Over-Driven by External Octol Driver. Note that Jet is Straight but Forward Portion is Disturbed.
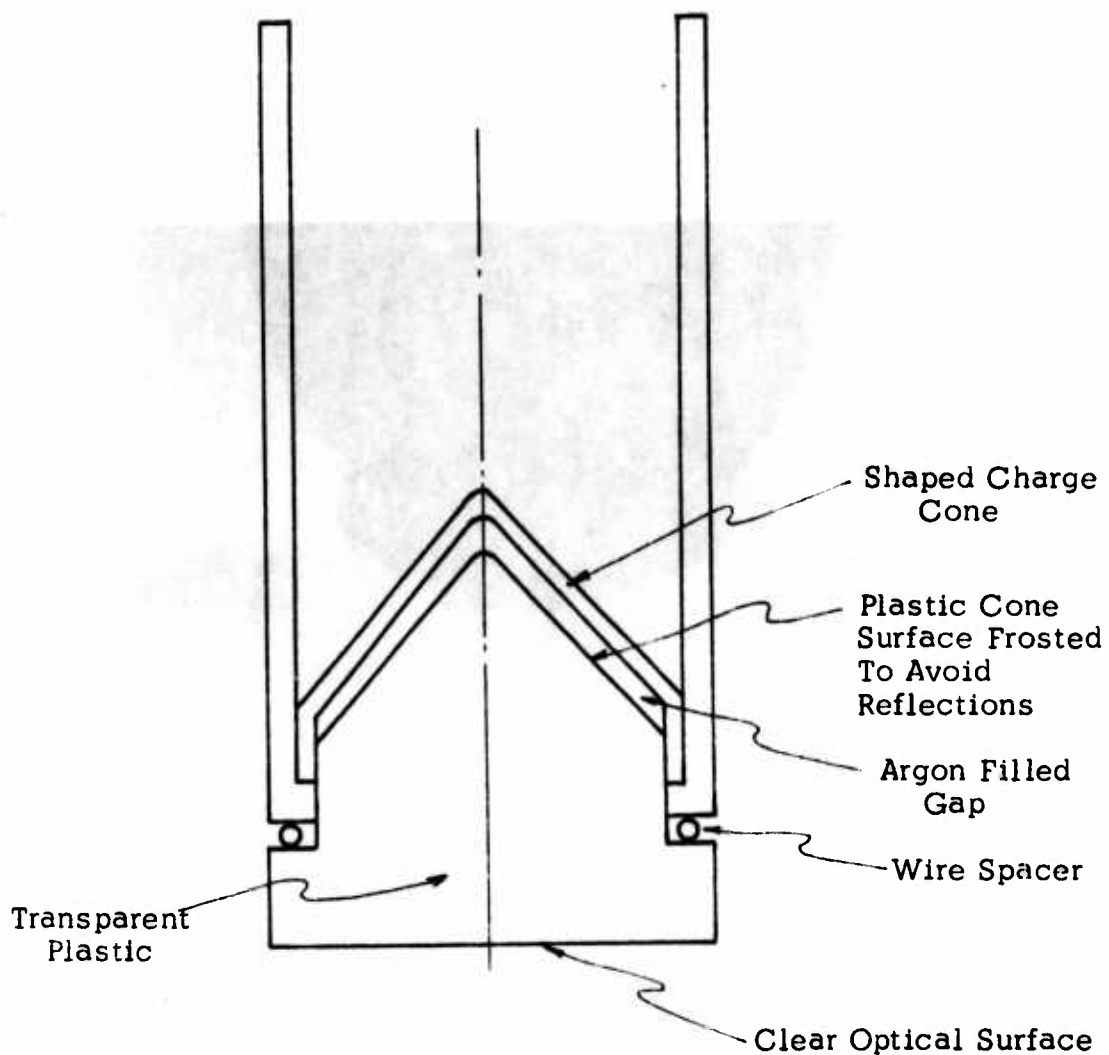
Figure 43. Schematic of Experimental Technique for Observing
Symmetry of Shock Wave Emerging from Shaped Charge
Cone.

(U) Figure 44 is a photograph of the experimental components and
Figure 45 shows a typical streak camera record obtained with a Comp B
charge having a PBX-9404 external explosive driver.

   a. Summary of Optical Observations of Asymmetry

(U) Three experiments were carried out and the data reduced. The
results may be summarized as follows.

Figure 44. Assembled Shaped Charge and Optical Fitting Just Prior
            to Assembly for Streak Camera Observation of Wave
            Symmetry.

(U)   There was observable asymmetry in some of the emerging shock
waves for the case of the Comp B overdriven by the PBX-9404 driver.
There was also some observed asymmetry in the emerging shock wave
for the basic Composition B charges, for which the flash X-rays showed
straight jets. The observed asymmetry could account for deviated jets
which were occasionally observed with the flash X-ray. However, the
flash radiographs showing early and late jet disruption are in most cases
quite straight and essentially undeviated. Hence, the asymmetry can-
not be considered to be an important contributor to the disruption
process.

The observational technique used to obtain this
emerging shock wave record, is illustrated in
Figures 43 and 44.

Figure 45.　Typical Streak Camera Photograph of the
Shock Wave Emerging From the Shaped
Charge Cone in a Precision Assembly with
Composition B and PBX 9404

SECTION V

CONCLUSIONS

(U)   The most significant conclusions concern the behavior of the convergent wave initiation and overdriving systems upon the detonation and shaped charge performance of the charges which they overdrive.

1. A very important and useful effect of a convergent wave system is its ability to fully detonate explosive charges which are either at sub-critical or marginally critical diameters.

2. The shaped charge penetration performance of TNT loaded charges, when overdriven by the convergent wave system generated by an external A-2 driver charge, matches or exceeds the penetration performance of the identical shaped charges loaded with Composition B.

3. The large differences in normal detonation velocity and detonation pressures of TNT and Comp B, as well as their substantial detonation energy differences make this a very unusual and significant result.

4. This effect cannot be attributed to the added external driver explosive charge, because in parallel experiments in which the external A-2 driver was used with Composition B loaded charges, their penetration performance was seriously degraded.

5. The analogous increase in penetration performance of Composition B loaded charges, overdriven with faster external driver explosives like PBX-9404 and Octol, has not been observed.

6. Instead, a jet breakup phenomenon has been observed by means of flash X-ray observation of the jets.

7. A "Decompression Disruption" hypothesis has been offered as an explanation of the observed jet break-up phenomenon.

8. The "Decompression Disruption" hypothesis is based upon the concept of compressional energy exceeding cohesive energy, so that on release, the jet material is unable to sustain the stresses and is disrupted.

93

9. The experimental evidence indicating that the break-up occurs over the forward portion of the jet, is consistent with the hypothesis offered, because the axial collision zone pressures are highest during the first stages collapse of the conical liner and decreases as the collapse progresses.

10. The optical asymmetry observations confirm that while some asymmetry exists, it cannot be the major factor accounting for the jet breakup.

11. The observations reported here are applicable to the specific copper cone of 58.5° included angle and specific thickness, used in there experiments, since the collapse velocity, the collision zone pressures and the cohesive energy are all dependent upon the geometry and the material of the cone. These considerations are in fact the ones that appear to be most appropriate for future study aimed at further exploitation of the interesting and useful phenomena observed.

APPENDIX I

APPROXIMATE CALCULATION OF THE INTERFACE ANGLE (θ) AND SHOCK ANGLE (ɸ) FROM THE LATERAL DETONATION OF AN EXPLOSIVE ALONG THE SURFACE OF A METAL OR PLASTIC

(U)   The solution of the problem requires finding the pressure-expansion angle (A) for the explosive and matching it to the pressure-compression angle (θ) of the metal or plastic, see Figure I-1.

I-1.   Pressure-Expansion Angle for Explosive

(U)   The expansion of the explosive at the interface is approximated as the expansion of a high pressure gas that is at rest with respect to the direction perpendicular to the interface in its initial state. The calculation is made in the x-t plane only and no attempt is made to take into account the rarefaction arising at the free surface of the explosive since only the initial turning angle is being sought.

(U)   The detonation products of the explosive are assumed to obey the polytropic equation of state.

$$P = A\rho^{\gamma} \tag{I-1}$$

where

   P is pressure

   ρ is density

   A and γ are constants.

The value of γ for detonation products is taken to be three. If u is the particle velocity,

$$w = \int_{\rho_1}^{\rho_2} \frac{C}{\rho} \, dp \tag{I-2}$$

and c is the sound velocity, then the quantity

$$u + w \tag{I-3}$$

is invariant across the characteristics so that

$$u + w = u_1 + w_1 \tag{I-4}$$

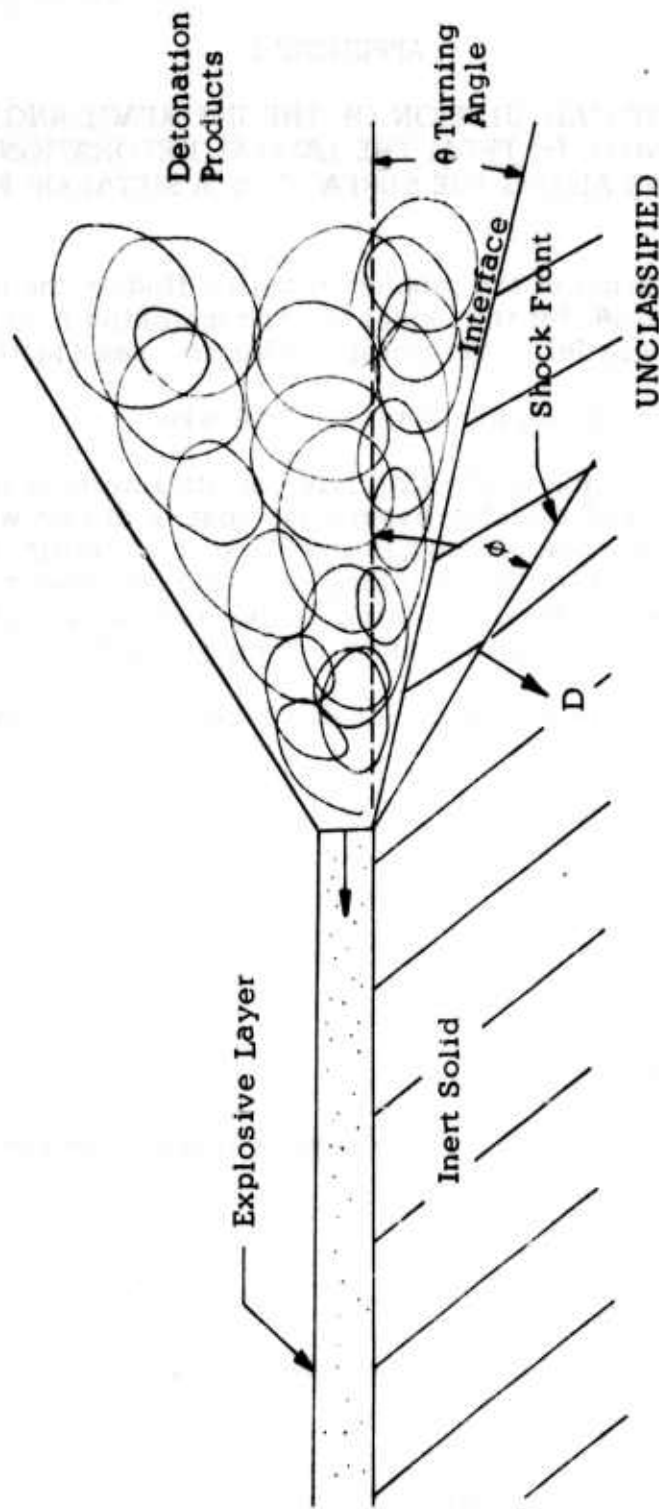where the subscript 1 denotes the initial values. It was assumed that

95

Figure I-1. Geometry for the Turning Angle of the Interface Between a Solid and an Explosive for a Lateral Detonation

$$u_1 = 0 \tag{I-5}$$

Therefore

$$u = w_1 - w \tag{I-6}$$

Now,

$$c^2 = \left(\frac{\partial P}{\partial \rho}\right)_s = A\gamma \rho^{(\gamma-1)} \tag{I-7}$$

Thus,

$$w = \frac{2\sqrt{A\gamma}}{(\gamma-1)} \rho^{(\gamma-1)/2} = \frac{2A^{1/2\gamma}\sqrt{\gamma}}{(\gamma-1)} P^{\gamma-1/2\gamma} \tag{I-8}$$

or

$$u = \frac{2\sqrt{\gamma}}{(\gamma-1)} A^{1/2\gamma} (P_1^{\gamma-1/2\gamma} - P^{\gamma-1/2\gamma}) \tag{I-9}$$

from Eqns. (I-1), (I-7) and (I-8)

$$C = \sqrt{\gamma} \, A^{1/2\gamma} P^{\gamma-1/2\gamma} \tag{I-10}$$

or,

$$A^{1/2\gamma} = \frac{C}{\sqrt{\gamma} \, P^{\gamma-1/2\gamma}} \tag{I-11}$$

(U)   Since Eqn. (I-1) holds for the detonation front, the constant A can be computed from the Chapman-Jouguet values for the explosive, i.e.,

$$A^{1/2\gamma} = \frac{C_{cj}}{\sqrt{\gamma} \, P_{cj}^{\gamma-1/2\gamma}} \tag{I-12}$$

Also since $P_1 = P_{cj}$, Eqn. (I-9) becomes

$$u = \frac{2C_{cj}}{(\gamma-1)} \left(1 - \left(\frac{P}{P_{cj}}\right)^{\gamma-1/2\gamma}\right) \tag{I-13}$$

The value C_{cj} is related to the detonation velocity (D_{cj}) and the particle velocity behind the detonation front, in the direction perpendicular to the front (u_{cj}), i.e.

$$C_{cj} = D_{cj} - u_{cj} \tag{I-14}$$

Hence Eqn. (I-13) becomes

$$u = \frac{2 (D_{cj} - u_{cj})}{(\gamma - 1)} (1 - (\frac{P}{P_{cj}})^{\gamma - 1/2\gamma})$$ (I-15)

D_{cj} and u_{cj} can be related by

$$u_{cj} = \frac{D_{cj}}{\gamma + 1}$$ (I-16)

or

$$u = \frac{2 P_{cj}}{(\gamma - 1)} (1 - \frac{1}{\gamma + 1})(1 - (\frac{P}{P_{cj}})^{\gamma - 1/2\gamma})$$ (I-17)

or

$$u = \frac{2\gamma}{(\gamma^2 - 1)} D_{cj} [1 - (\frac{P}{P_{cj}})^{\gamma - 1/2\gamma}]$$ (I-18)

If u is considered as the expansion velocity of a particle on the inter-
face in a direction perpendicular to the undisturbed interface, then the
expansion angle (θ) can be calculated from

$$\tan \theta = \frac{u}{D_{cj}}$$ (I-19)

or from Eqn. (I-18)

$$\theta = \text{Arc tan} \{\frac{2\gamma}{(\gamma^2 - 1)} [1 - (\frac{P}{P_{cj}})^{\gamma - 1/2\gamma}]\}$$ (I-20)

2.   Pressure-Compression (or Turning) Angle for an Inert Solid

(U)   If u is the particle velocity in the solid behind the shock,
which moves at velocity D, then application of the conservation equa-
tions of mass and momentum gives

$$\tan \theta = \frac{(u/D) \tan \phi}{1 + [(D-u)/D] \tan^2 \phi}$$ (I-21)

98

where ϕ is the angle that the shock in the solid makes with the line of the original interface.

(U)   The Hugoniot of the solid can be expressed as,

$$D = Au + B \tag{I-22}$$

where A and B are constants. Since

$$P = \rho_o \, Du \tag{I-23}$$

where ρ_o is the uncompressed density of the solid, both D and u can be computed as a function of the pressure (P). The angle ϕ can be found from the expression

$$\sin \phi = \frac{D}{D_{cj}} \tag{I-24}$$

(U)   Since D_{cj} is a known constant and D is a function of P, then ϕ is a function of P. Likewise, since u, D, and ϕ are functions of P, then from Eqn. (I-21), θ is a function of P. If this function is represented by

$$\theta = \text{Arc tan } F(P) \tag{I-25}$$

then, the initial shock pressure induced in the inert solid is the solution of the equation.

$$F(P) - \left\{ \frac{2\gamma}{(\gamma^2 - 1)} \left[1 - \left(\frac{P}{P_{cj}}\right)^{\gamma - 1/2\gamma} \right] \right\} = 0 \tag{I-26}$$

P can be found from the above equation and hence θ and ϕ can be computed.

APPENDIX II

RELATION BETWEEN ANGLE OBSERVED ON STREAK PHOTOGRAPH
AND THE TRUE ANGLE OF THE WAVE FRONT

(U)   Let the wave front be time invariant and moving at a constant velocity, V, towards the detecting plane, see Figure II-1. If, at any time, t_o, y is the distance from the plane to the wave front above the place at point x, then

$$t(x) - t_o = \frac{y(x)}{V}$$ (II-1)

where $t(x)$ is the time at which the part of wave front corresponding to the point x, arrives at the detecting plane. Then

$$\frac{dt}{dx} = \frac{1}{V} \frac{dy}{dx}$$ (II-2)

This relates the slope at any point in the streak record to the actual physical slope of the wave front.

(U)   The velocity used should correspond to the detonation velocity of the outer explosive.
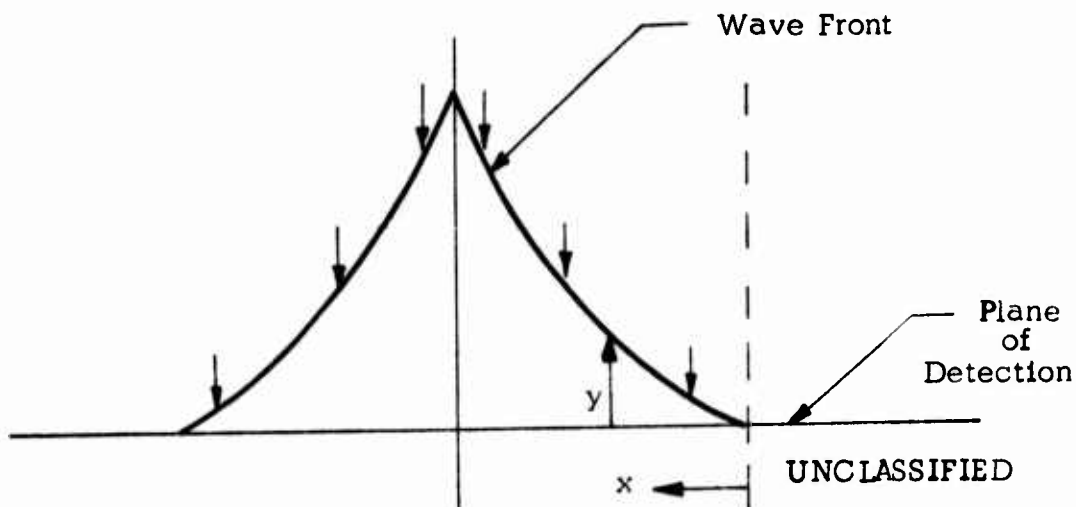

Figure II-1. Wave Configuration as the Wave Front
Reaches the Detection Plane

REFERENCES

1. W. Bleakney and A. H. Taub, Rev. Mod. Phys. 21, 584 (1949).

2. G. Birkhoff and J. M. Walsh, Publ. Sci. Min. Air. (France) (1954).

3. T. Y. Thomas, Plastic Flow and Fracture in Solids, Academic Press, New York (1961).

4. G. R. Fowles and W. M. Isbell, J. Appl. Phys. 36, 1377 (1965).

5. R. W. Perry and A. Kantrowitz, J. Appl. Phys. 22, 878 (1951).

6. R. F. Chisnell, J. Fluid Mech. 2, 286 (1957).

7. Y. B. Zeldovich, JETP 36, 550 (1959).

8. I. C. Skidmore and S. Hart "Preprints Fourth Symposium Detonation, U. S. Naval Ordnance Lab, White Oak, Maryland, October 1965.

DOCUMENT CONTROL DATA - R & D

(Security classification of title, body of abstract and indexing annotation must be entered when the overall report is classified)

1. ORIGINATING ACTIVITY *(Corporate author)*	2a. REPORT SECURITY CLASSIFICATION
Shock Hydrodynamics Incorporated 15010 Ventura Boulevard Sherman Oaks, California 91403	CONFIDENTIAL
	2b. GROUP 4

3. REPORT TITLE

STUDY AND APPLICATION OF MACH WAVE TECHNIQUES (U)

4. DESCRIPTIVE NOTES *(Type of report and inclusive dates)*

Final Report - June 1966 through December 1967

5. AUTHOR(S) *(First name, middle initial, last name)*

Nikolai A. Louie   Richard P. Randall
Arthur L. Mottet, Jr.   Louis Zernow
Irving Lieberman

6. REPORT DATE	7a. TOTAL NO. OF PAGES	7b. NO. OF REFS
May 1968	110	8

8a. CONTRACT OR GRANT NO. AF08(635)-5999	9a. ORIGINATOR'S REPORT NUMBER(S)
b. PROJECT NO.	SHI C-1016
c.	9b. OTHER REPORT NO(S) *(Any other numbers that may be assigned this report)*
d.	AFATL-TR-68-60

10. DISTRIBUTION STATEMENT In addition to security requirements which must be met, this document is subject to special export controls and each transmittal to foreign governments or foreign nationals may be made only with prior approval of the Air Force Armament Laboratory (ATWT), Eglin AFB, Florida 32542.

11. SUPPLEMENTARY NOTES	12. SPONSORING MILITARY ACTIVITY
Available in DDC	Air Force Armament Laboratory Air Force Systems Command Eglin AFB, Florida 32542

13. ABSTRACT

(U) A theoretical and experimental study of convergent wave initiation and detonation techniques has been carried out. This included analytical and experimental studies of wave shapes and Mach discs in cylindrical explosive charges overdriven by concentric external faster explosives. The techniques were also applied to shaped charge systems. The results indicate that it is possible to overdrive TNT loaded shaped charges so that they perform as well as Composition B loaded charges. A depressurization disruption mechanism has been postulated to explain the jet breakup seen in flash X-ray and penetration observations, made when similar overdriving methods were applied to more energetic explosive systems like Composition B overdriven by PBX-9404.

DD _{FORM} **1473**
1 NOV 65

14.		LINK A		LINK B		LINK C	
KEY WORDS		ROLE	WT	ROLE	WT	ROLE	WT
FLASH X-RAY							
MACH WAVES							
OVERDRIVEN DETONATION							
SHAPED CHARGE							
WAVE SHAPING							